E.O. Paton Electric Welding Institute of the National Academy of Sciences of Ukraine

International Scientific-Technical and Production Journal

The Paton WELDING JOURNAL

November 2014
No.11

Published since 2000

English translation of the monthly «Avtomaticheskaya Svarka» (Automatic Welding) journal published in Russian since 1948

Founders
E.O. Paton Electric Welding Institute
of the NAS of Ukraine,
International Association «Welding»

Publisher
International Association «Welding»

Translators
A.A. Fomin, O.S. Kurochko,
I.N. Kutianova
Editor
N.A. Dmitrieva
Electron galley
D.I. Sereda, T.Yu. Snegiryova

Address
E.O. Paton Electric Welding Institute,
International Association «Welding»
11, Bozhenko Str., 03680, Kyiv, Ukraine
Tel.: (38044) 200 60 16, 200 82 77
Fax: (38044) 200 82 77, 200 81 45
E-mail: journal@paton.kiev.ua
www.patonpublishinghouse.com

State Registration Certificate
KV 4790 of 09.01.2001
ISSN 0957-798X

Subscriptions
$348, 12 issues per year,
air postage and packaging included.
Back issues available.

CONTENTS

ELIMINATION OF LOCAL DEFORMATIONS OF BUCKLING TYPE BY MEANS OF ELECTRODYNAMIC TREATMENT

L.M. LOBANOV, N.A. PASHCHIN, O.L. MIKHODUJ and **T.G. SOLOMIJCHUK**
E.O. Paton Electric Welding Institute, NASU
11 Bozhenko Str., 03680, Kiev, Ukraine. E-mail: office@paton.kiev.ua

Non-uniform heating of hull structures in welding of longitudinal-transverse framing promoted appearance of residual local deformations (buckling) in form of alternating bulges and indentations at adjacent sections of a panel. They have negative effect on service properties and appearance of the structure as well as hydrodynamic characteristics of ships, reducing their speed to 10 %. Traditional methods of buckling removal such as thermal and cold straightening have series of disadvantages (noise, vibration, significant consumption of energy carriers). Development of new methods of buckling straightening based on minimum energy consumption is a relevant task. Electrodynamic treatment is one such methods. Aim of present work is a study of effect of electrodynamic treatment on reduction of local deformations of buckling type in welded joints from aluminum alloys and low-carbon steels. Square samples of tee welded joints from AMg6 alloy and low-carbon steel St3 were used for simulation of buckling with different sign and deflection value. Mode of treatment corresponded to energy accumulated by storage, not exceeding 800 J. Effect of distribution of electrodynamic impacts, namely spot, circular and spiral ones, over sample surface on change of buckling form was investigated. Spot scheme has the lowest efficiency, and circular and spiral ones can be compared by efficiency. Comparative analysis showed that consumption of energy in electrodynamic treatment is significantly lower than in use of traditional methods of straightening. 10 Ref., 1 Table, 7 Figures.

Keywords: *local deformations, buckling, low-carbon steel, aluminum alloy, electrodynamic treatment, treatment scheme, pulse energy, traditional straightening methods*

Non-uniform heating of hull structures in welding of longitudinal-transverse framing promoted appearance of residual local deformations (buckling) in form of alternating bulges and indentations at adjacent sections of a panel. They have alternating nature and are directed to framing as well as in opposite direction. It is a well-known fact [1] that buckling of structure takes place as a result of loss of panel stability between framing under effect of compressive stresses and has negative effect on working capacity, service characteristics and appearance of structure as well as hydrodynamic characteristics of ships, reducing their speed to 10 %. At that, number of welded sheet hulls are designed with such combination of elements, at which appearance of buckling of more than allowable level is inevitable. Straightening is the main method for reduction of deformations in such structures [2].

Straightening of buckling using local heating with dynamic impact has found the widest distribution in shipbuilding. It is related with application of rough labor, high level of noise (120–140 dB) and structure vibration. Taking into account that straightening in the closing stages of welding works is mainly carried out at ship-way, when large number of operating personnel is engaged in assembly and completion, it promotes for rough labor conditions, results in extension of completion period and, in separate cases, promotes unallowable damages of surface being treated.

Application of thermal straightening eliminates noise and vibration, but being related with negative thermal effect on operating personnel, significant overexpenditure of heat building gas mixtures during heat sink into environment and technological equipment. Besides, application of heat in straightening of structures from aluminum alloys is insufficiently effective in series of cases due to their high heat conduction. Indicated disadvantages are also typical for thermal straightening by «idle» rolls using welding arc heating.

Using of enumerated straightening methods is connected with sufficiently noticeable damages of surface of welded structures, caused by dynamic impact of mechanical tool as well as thermal-deformation cycles as a result of welding heating.

Application of cold straightening with stretching benches for buckling removal is limited by geometry peculiarities of this type of change of form, among which are their localizing and significant dimensions of structure, as well as high cost of equipment.

Therefore, development of novel methods of buckling straightening, based on minimum energy consumption and providing minimum damage to surface to be treated, is sufficiently relevant. Treatment of structures using pulse electric and magnetic fields [3–6] can be referred to them. Electrodynamic treatment (EDT) is its variety.

Earlier the investigations were carried out in relation to effect of EDT on regulation of longitudinal and transverse buckling of butt welded joints from aluminum alloys and structural steels [7]. Perspective of application of EDT for reduction of such types of buckling was confirmed by work results.

Aim of the present work is a study of EDT impact on reduction of local deformations of buckling type in welded joints from aluminum alloys and low-carbon steel used in shipbuilding.

Samples with tee welded joints from aluminum alloy AMg6 and low-carbon steel St3 were used for investigations and simulation of bucking with deflection f (Figure 1). They represent itself a plate with four stiffeners welded by fillet welds. Size of plate and stiffeners are given in Figure 1, *a*. Change og form of samples from AMg6 alloy with plates of equal thickness δ and stiffeners of two dimension-types, corresponding to δ = 2 and 4 mm, and steel St3 (δ = 2 mm) of one dimension-type was investigated. At that, deflection of plate f in direction to stiffeners was taken with sign «+» and that with sign «–» in direction from stiffeners. Deflection in samples from AMg6 alloy (δ = 4 mm) was set in direction to stiffeners as well as from them, and that in samples from AMg6 alloy and steel St3 (δ = 2 mm) was taken only in direction to stiffeners.

It can be assumed, based on [8], providing parametric characteristics of pressure pulses at electrodynamic impacts, as well as data from [9], showing that metal at outer contact surface with electrode is subjected to compression in radial direction in sheet plane, that EDT application is reasonable for zones with maximum curvature of buckling, and direction of electrodynamic impact application should be turned to f reduction.

Fillet welds of samples from AMg6 alloy were carried out by manual TIG welding in argon at 130 A current and 1.3 mm/s speed using 3 mm diameter filler rod of SvAMg6 grade. Geometry characteristics of change of buckling form, corresponding to different f signs, were provided with the help of different combinations of bead deposition. Joining of samples from St3 steel was performed by manual welding using coated electrode of Monolit RTs grade of 3 mm diameter at 120 A current and 1.5 mm/s speed.

EDT (Figure 2) was carried out with the help of flat inductor equipped by electrode from M1

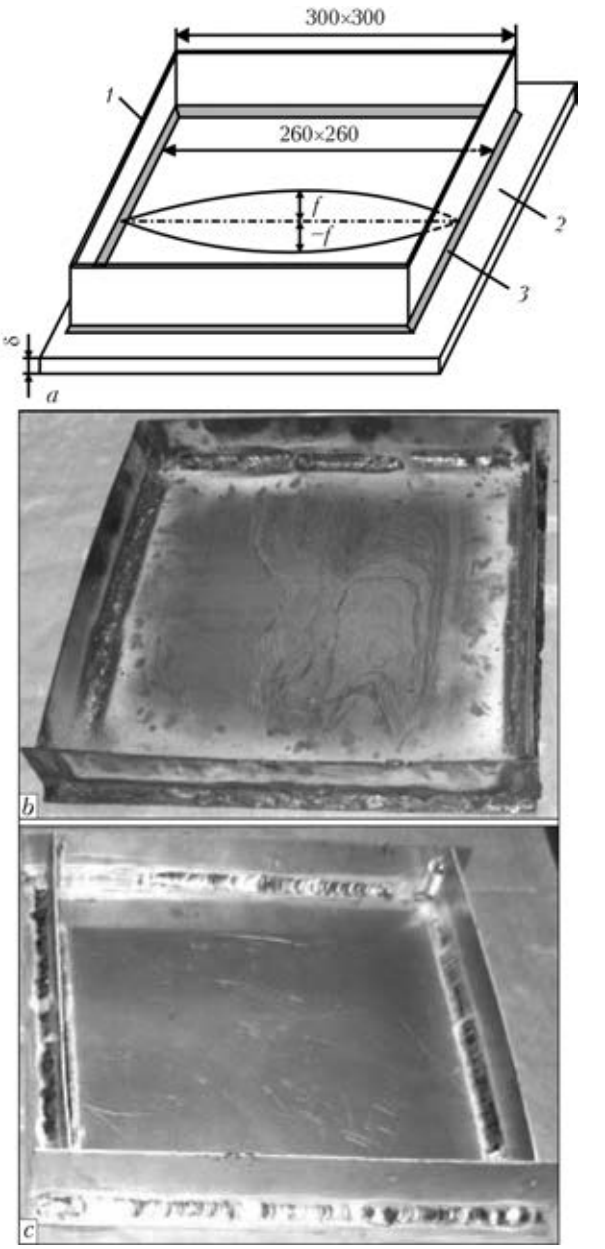

Figure 1. Scheme of samples of welded joints with buckling type deformation (*a*: *1* — stiffener; *2* — plate; *3* — fillet weld) and appearance of samples from steel St3 (*b*) and alloy AMg6 (*c*)

grade copper with semi-spherical tip, and capacitor storage was used as a pulse generator [6]. EDT mode corresponded to energy accumulated by capacitor storage E_{k1}, necessary for realizing of single electrodynamic impact (n = 1), not exceeding 800 J. Value of accumulated energy E_{EDT}, necessary for realizing of series from n electrodynamic impacts, was calculated from expression

$$E_{EDT} = E_{k1}n. \quad (1)$$

Distance between the zones of electrodynamic impacts was varied from 10 (for St3) to 30 mm (for AMg6), that provided stable results of straightening on length of treated section of sample surface.

Figure 2. EDT of AMg6 alloy samples with buckling (δ = = 2 mm)

Influence of different schemes of distribution of electrodynamic impacts over sample surface on change of buckling form was investigated. Deflections f in cross-section of the samples were controlled by standard procedure using ruler and caliper. Three schemes of EDT of sample surface, i.e. spot, circular and spiral in direction from center to edges, were investigated using samples from AMg6 alloy with δ = 4 mm.

Spot EDT was realized by means of application of series from five electrodynamic impacts (n = 5) in plate center, where initial bucking had typical deflection form with maximum initial value f_{max} = −5 mm (Figure 3, curve *1*) in direction from the stiffeners. Figure 3 represents change of buckling form in sample, where EDT zone corresponds to x = 100 mm coordinate on abscissa axis. As can be seen, maximum efficiency of EDT takes place at n = 1, that corresponds to f = −4 mm (Figure 3, curve *2*) and monotonously decreases to f = −2 mm at n = 5 (Figure 3, curves *3*–*5*). Change of typical form of deflection takes place at n = 3–5 mm, that is accompanied by decrease of f values in zone of treatment and their increase outside the zone, in sections of corresponding coordinates x = 75 and 125 mm.

This can be explained based on theory of normal contact of inelastic bodies [9] for the case of interaction of semi-spherical indenter (in our case — electrode) with elasto-plastic media. It is shown that wrought metal at contact interactions is displaced by indenter to free surface behind the contact zone. At that, plastic flow of the displaced material takes place along the indenter edges. EDT cycle, corresponding to n > > 3, includes this mechanism, which is characterized by metal displacement behind the treatment zone and local distortion of buckling surface in sections corresponding to x = 75 and 125 mm coordinates (see Figure 3). Repeated plastic flow in zone of electrode contact, observed at n = 4–5, takes place under conditions of constrained deformation and its effect on surface profile is insignificant, that can be seen from similarity of curves *4* and *5* in Figure 3.

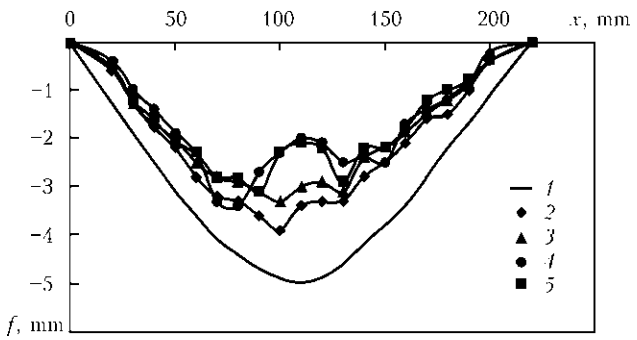

Figure 3. Change of buckling form f in sample from AMg5 alloy (δ = 4 mm) after EDT of plate center: *1* — initial f_{max} values; *2* — f after EDT at n = 1; *3* — same, n = 2; *4* — n = 3; *5* — n = 4 and 5

Besides work [10] shows that EDT of AMg6 alloy promotes significant increase of $\sigma_{0.2}$ value, and interaction of buckling with electrode at treatment cycles, corresponding to n > 3, proceeds to elastic stage without significant residual change of form. Thus, scheme of local multiple application of electrodynamic impact to selected section on sample surface allows for not more than 60 % reduction of f initial values.

This EDT scheme is not efficient, since allowable f values should correspond to the following condition, according to norms of local deformation, for example OST 5.9079–72:

$$f = a/80, \qquad (2)$$

where a is the size of spacing (distance between the stiffeners).

The allowable f value should not exceed 3.75 mm for samples considered in this work, which is close to curve *5* in Figure 3, and being maximum allowable for spot EDT. An advantage of given scheme is the minimum (in comparison with other schemes) quantity of accumulated energy E_{EDT} of capacity storage, necessary for change of form, shown in Figure 3, which does not exceed 4000 J at n = 5 according to (1).

Circular scheme of EDT was realized by means of application of three series of electrodynamic impacts in form of concentric circumferences with different radius R on sample surface (Figure 4, *a*) with initial buckling, form and f_{max} value of which (Figure 4, *b*, curve *1*) were similar to considered in Figure 3. R values were equal 15, 50 and 90 mm, and n and E_{EDT} values (according to (1) for EDT of set circumferences made 8, 30, 55 and $6.4 \cdot 10^2$, $2.4 \cdot 10^4$, $4.4 \cdot 10^4$ J, respectively.

As can be seen from Figure 4, *b*, f values steadily reduce with rise of R, which is accompanied by change of deflection sign and gradual change of its form from typical to wave-like. Using of R = 15 mm provides for f values (Figure 4, *b*, curve *2*) and change of buckling form close to shown in Figure 3 for spot EDT at n = 1–3, that is explained by low R value. Form of deflection

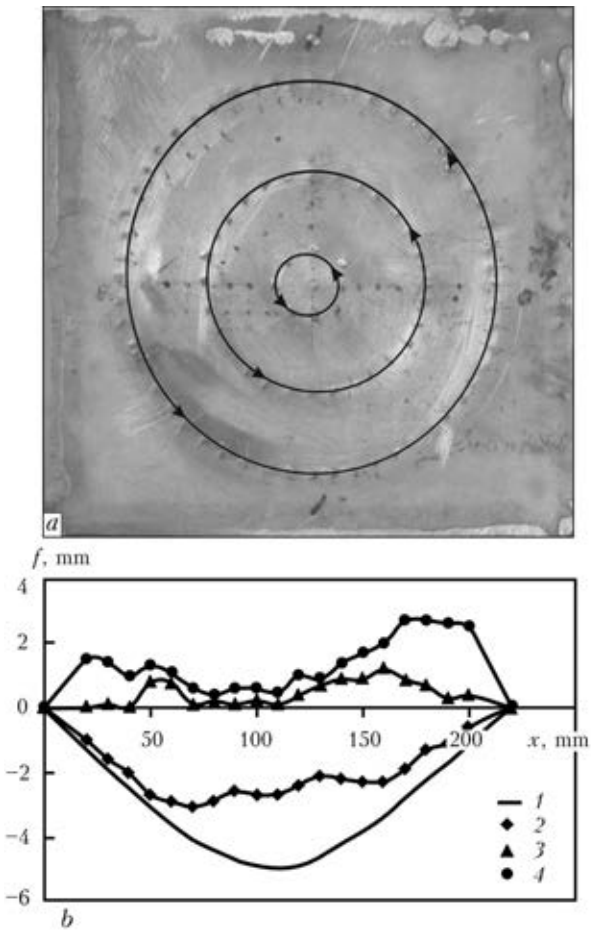

Figure 4. Appearance (*a*) and change of buckling form (*b*) in AMg6 alloy sample (δ = 4 mm) after circular EDT at change of radius *R*: *1* — initial f_{max} values; *2* — *f* after EDT at *R* = = 15 mm; *3* — same, *R* = 50 mm; *4* — *R* = 90 mm

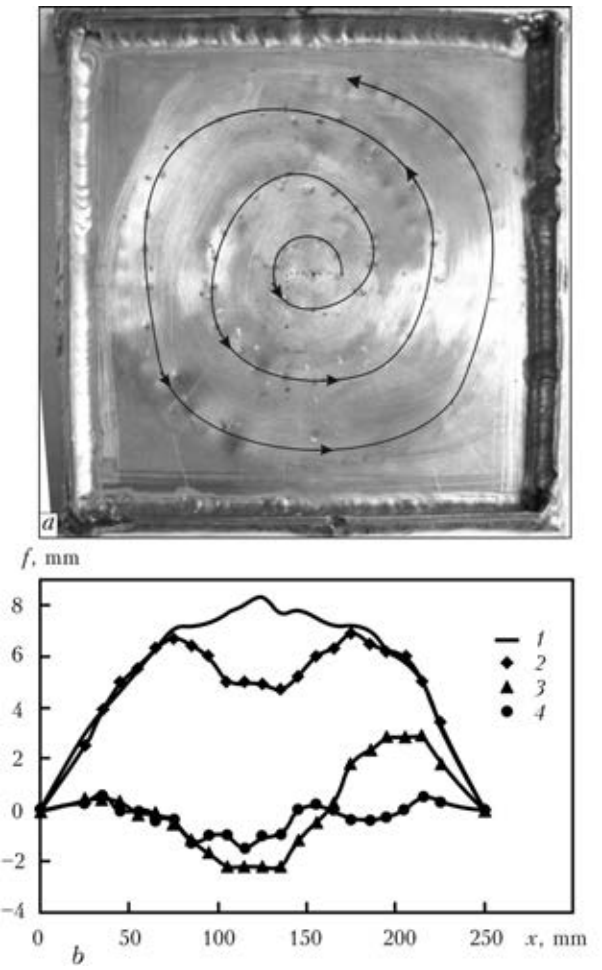

Figure 5. Appearance (*a*) and change of buckling form (*b*) in AMg6 alloy sample (δ = 4 mm) after spiral EDT at change of radius *R*: *1* — initial f_{max} values; *2* — *f* after EDT at *R* = 15 mm; *3* — same, *R* = 50 mm; *4* — *R* = 90 mm

is close to wave-like at sign change with rise of *R* up to 50 mm (Figure 4, *b*, curve *3*), that corresponds to central part of plate, and *f* value achieves 1 mm. EDT at *R* = 90 mm (Figure 4, *b*, curve *4*) was carried out for investigation of possibility of buckling removal, f_{max} of which exceed indicated in Figure 4, *b*. Using of scheme of concentric circumferences at discrete increase of *R* value allows for virtually complete elimination of local deformation as well as application of given scheme at increased f_{max}.

It can be concluded, based on analysis of data from Figure 4, *b*, that EDT of central part of plate is supposed to be the most efficient at *R* = = 50 mm in comparison with *R* = 15 and 90 mm. At the same time, considering data of Figure 3, it can be deduced that EDT in wide range of *R* values can rise the efficiency of electrodynamic impact at increased initial *f* values and area of surface to be treated.

Evolution of two previous schemes is a spiral EDT, realized by means of application of electrodynamic impacts to treated surface in form of spiral with alternating radius *R*, which spreads from center to sample edges (Figure 5, *a*). At that, parabolic form of initial buckling was set in stiffener direction and f_{max} value (Figure 5, *b*, curve *1*) achieved 8 mm. Change of *f* was registered at *R* = 15, 50 and 90 mm for comparison with circular EDT, shown in Figure 4. Values of *n* and E_{EDT} (1) for EDT at *R* = 15, 50 and 90 mm made 8, 30, 22 and $6.4 \cdot 10^2$, $2.4 \cdot 10^4$, $1.7 \cdot 10^4$ J, respectively.

As can be seen from Figure 5, *b*, nature of form changing and *f* values is close to circular EDT scheme without consideration of deflection sign. *f* values (see Figure 5, *b*, curve *2*) reduce in central zone of the buckling from 8 to 5 mm with preservation of deflection sign in achievement of *R* = 15 mm. Change of form at EDT of middle part of the buckling, corresponding to increase of *R* up to 50 mm (see Figure 5, *b*, curve *3*), varies the nature from parabolic to sine-shaped, that is accompanied by steady growth of values of negative half-wave of amplitude *f* from 0 to −2 and positive one from 0.5 to 3.0 mm. Asymmetry of form changing, presented in Figure 5, *b*, curve *3*, is removed at EDT under conditions of *R* growth up to 90 mm (curve *4*),

Values of f_0 and f_{EDT} deflections and ΣE_k energy at different types of straightening of AMg6 alloy and St3 steel

Number of item	Metal	δ, mm	Types of EDT straightening	f_0, mm	f_{EDT}, mm	ΣE_k, kJ	$\Sigma E_k/\Delta f$, kJ/mm
1	AMg6	4	Spot	–5	–3	4.0	2
2	Same	4	Circular	–5	1	74.4	12
3	»	4	Spiral	8	–1	47.4	5,2
4	»	2	Same	8	–1	31.2	3
5	»	2	»	8	–2	115	11.5
6	St3	3–5	Impact with preheating	N/D		41,160 [1]	N/D
7	AMg5	3–5	Heat	Same		15,876 [1]	Same

at which sine curve becomes symmetric with excursion to 2 mm, and its positive half-wave does not exceed 0.5 mm. This is significantly lower than allowable f values at used spacing a = = 300 mm according to (1).

The most efficient from point of view of f reduction, the same as for circular scheme, is EDT of central part of the plate at R growth to 50 mm (see Figure 5, *b*, curve *3*) in comparison with R = = 15 (curve *2*) and 90 mm (curve *4*). It should be noted that application of EDT in compressive stress zone near the stiffeners (R = 90 mm) can provide corrective impact, directed at local straightening of sections of buckling surface.

Comparison of EDT schemes, given in Figures 3–5, allows concluding that spot scheme is the least efficient and energy consuming, and circular and spiral ones can be matched in efficiency, however the latter one requires lower E_k value for realizing. Thus, spiral EDT scheme is supposed to be the most relevant for straightening of local buckling deformations.

EDT of samples from AMg6 alloy (δ = = 2 mm) and St3 steel (δ = 2 mm) was carried out using spiral scheme, similar to shown in Figure 5. Receiving of indices of f_{max} reduction, close to presented in Figure 5, required lower E_k value for AMg6 samples in comparison with 4 mm ones in contrast to St3 samples, where E_k value is significantly higher.

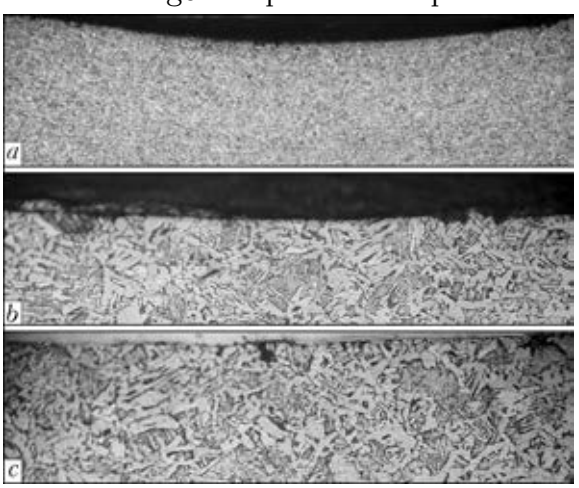

Figure 6. Microstructure of steel St3 after EDT with insert from M1 copper 0.5 mm thick: *a* — general appearance of indentation (×50); *b* — center of indentation (×200); *c* — St3 in initial condition (×200)

Compared data on EDT impact on initial f_0 and residual f_{EDT} deflections at different configurations of EDT schemes as well as corresponding to schemes ΣE_k values after full cycle of treatment are represented in the Table. Absolute values of deflection change $\Delta f = If_0 - f_{EDT}I$ and specific energy efficiency $\Sigma E_k/\Delta f$ at different EDT schemes were determined based on f_0 and f_{EDT} data. Besides, the Table also shows ΣE_k values at heat and impact straightening with preheating of surface area of structure from AMg5 alloy (δ = = 3–5 mm), being equal 0.9 m^2, that is close to geometry characteristics of studied samples.

Analysis of the Table data allows concluding that ΣE_k at EDT is significantly lower than ΣE_k corresponding to traditional types of straightening (see items 6 and 7) at equal area of surface to be treated. It indicates satisfactory energy efficiency of EDT process. At that, even the least efficient spot scheme of EDT of AMg6 alloy (δ = = 4 mm) with minimum energy input ΣE_k (item 1) allows providing for f_0 reduction to that corresponding to requirements of reference documents, for example OST 5.9079–72. At the same time, the values of energy consumption per 1 mm of deflection $\Sigma E_k/\Delta f$ for AMg6 alloy (δ = 2 mm) using spiral scheme (item 4) are close to $\Sigma E_k/\Delta f$ at spot scheme for δ = 4 mm (item 1). Comparison of $\Sigma E_k/\Delta f$ of circular (item 2) and spiral (item 3) EDT for AMg6 alloy (δ = 4 mm) shows that the latter has 2 times less consumption at approximately equal process efficiency.

EDT of St3 steel at δ = 2 mm (item 5) is the most energy-consuming at the level of accumulated energy. In it ΣE_k and $\Sigma E_k/\Delta f$ indices are 4 times higher than similar ones for AMg6 alloy at equal thickness (item 4) and $\Sigma E_k/\Delta f$ values are comparable with circular scheme for AMg6 alloy at δ = 4 mm.

It can be concluded, based on [6], that electric-pulse impacts have in whole positive effect on structure of structural materials. At the same time, formation of semi-spherical indentations of up to 0.3 mm depth is observed in localized sec-

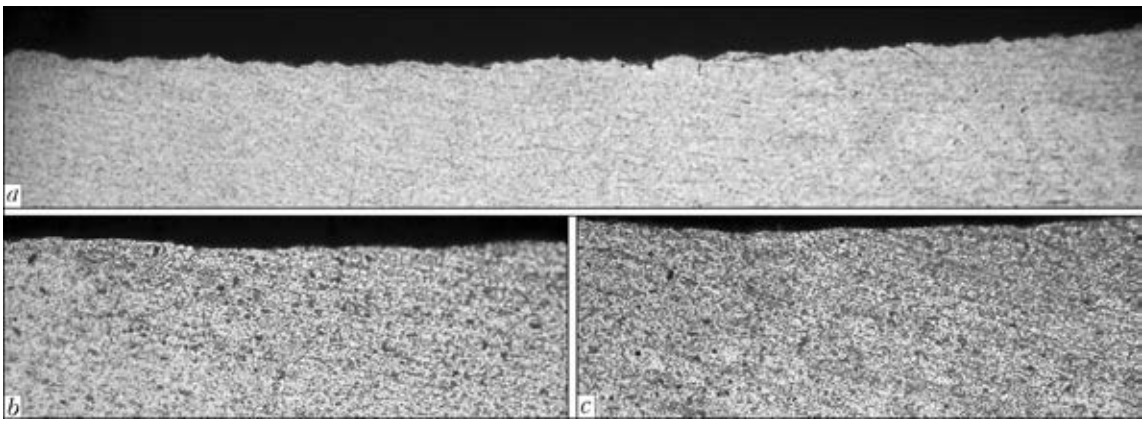

Figure 7. Microstructure of AMg6 alloy after EDT with M1 copper insert 0.5 mm thick: *a* — general appearance of indentation (×25); *b* — structure in indentation zone (×500); *c* — alloy AMg6 in initial condition (×500)

tions of zone of electrodynamic impact. They, in some cases, can influence the service characteristics of hulls. Optimizing of EDT technology based on mentioned above is directed to reduction of surface depth in zone of contact interaction.

Investigation was carried out on a method for minimizing of indentation depth. It is based on application of technological inserts from M1 grade copper, being set between electrode and metal to be treated.

Figure 6 shows the fragments of structure of St3 steel, treated through copper insert 0.5 mm thick at pulse energy E_k = 800 J. 0.1 mm depth indentation (see Figure 6, *a*) was formed in EDT zone. No metal changes were found on its surface. Examination of metal structure in EDT zone in the middle of indentation (see Figure 6, *b*) shows its identity to ferrite-pearlite structure of initial metal (see Figure 6, *c*).

Indentation of up to 0.3 mm depth (Figure 7, *a*) was formed on AMg6 surface after EDT using 0.5 mm thick inserts. No change of structure was found on surface of indentation. Microstructure of metal after EDT (Figure 7, *b*) and in the initial condition (Figure 7, *c*) consists of solid α-solution, in which β-phase (Mg_5Al_8) and Mg_2Si phase inclusions were observed.

Thus, application of copper inserts, providing virtually complete removal of EDT impact on surface structure of materials to be treated and minimizing indentation depth (see Figures 6 and 7), can be recommended for EDT technologies, using which minimum damageability of treated surface of welded hulls is allowed.

Conclusions

1. Effect of different EDT schemes on reduction of local deformations of buckling type in samples from AMg6 alloy and St3 steel, in particular, spot, circular and spiral ones in direction from center to edges, was investigated. It is determined that spot scheme is the least effective and energy-consuming, and circular and spiral ones can be compared by efficiency, but the latter requires lower energy-consumption for its realizing. Spiral EDT scheme is supposed to be the most relevant for straightening of local buckling deformations.

2. It was determined, based on data of comparative analysis, that energy consumption at EDT is significantly lower than in traditional straightening, such as heat and impact with preheating.

3. Using of metallographic analysis of microsections of AMg6 alloy and St3 steel allowed determining that application of technological inserts from M1 grade copper at EDT provides for virtually complete elimination of electrodynamic impacts on structure of metal to be treated.

1. Mikhajlov, V.S. (1972) *Straightening of hull welded structures*. Moscow: Sudostroenie.
2. Makhnenko, O.V., Muzhichenko, A.F., Seyffarth, P. (2009) Application of mathematical modeling in thermal straightening of shipbuilding panels. *The Paton Welding J.*, **1**, 6–11.
3. Tang, F., Lu, A.L., Mei, J.F. et al. (1998) Research on residual stress reduction by a low frequency alternating magnetic field. *J. Mat. Proc. Technol.*, **74**, 255–258.
4. Antonov, Yu.A., Rogozin, Yu.I. (2001) Pulse method of residual stress removal. *Fizika i Khimiya Obrab. Materialov*, **3**, 91–95.
5. Stepanov, G.V., Babutsky, A.I., Mameev, I.A. (2004) Non-stationary stress-strain state in long bar caused by electric current pulses of high density. *Problemy Prochnosti*, **4**, 60–67.
6. Strizhalo, V.A., Novogrudsky, L.S., Vorobiov, E.V. (2008) *Strength of materials at cryogenic temperatures considering the impact of electromagnetic fields*. Kiev: IPP.
7. Lobanov, L.M., Pashchin, N.A., Mikhoduj, O.L. (2013) Electrodynamic straightening of elements of sheet welded structures. *The Paton Welding J.*, **9**, 18–23.
8. Lobanov, L.M., Pashchin, N.A., Cherkashin, A.V. et al. (2012) Efficiency of electrodynamic treatment of aluminium alloy AMg6 and its welded joints. *Ibid.*, **1**, 2–6.
9. Johnson, K.L. (1989) *Contact mechanics*. Moscow: Mir.
10. Lobanov, L.M., Pashchin, N.A., Mikhoduj, O.L. (2012) Influence of loading conditions on deformation resistance of alloy AMg6 in electrodynamic treatment. *Problemy Prochnosti*, **5**, 15–26.

Received 20.06.2014

REDISTRIBUTION OF RESIDUAL WELDING STRESSES IN IN-VESSEL CORE BARREL OF WWER-1000 REACTOR DURING OPERATION

O.V. MAKHNENKO, E.A. VELIKOIVANENKO and **I.V. MIRZOV**
E.O. Paton Electric Welding Institute, NASU
11 Bozhenko Str., 03680, Kiev, Ukraine. E-mail: office@paton.kiev.ua

Reactor baffle is subjected to high radiation doses that results in its swelling and change of form in operation. Inside pressure of baffle on core barrel creates additional stresses in zone of contact. Residual welding stresses can also significantly effect a level of stressed state of core barrel wall, that should be considered in estimation of working capacity of vessel internals for extension of WWER-1000 reactor service life. Thus, a relevant task is an estimation of stressed state of in-vessel core barrel in area of its contact with baffle, in particular, when place of contact coincides with welded joint zone. Aim of present work is an investigation of stressed state in zone of welds of in-vessel core barrel of WWER-1000 reactor during operation considering radiation swelling and contact interaction of baffle and core barrel. A problem was solved by 2D finite element method using current mathematical models of radiation swelling and change of mechanical properties of 08Kh18N10T steel. Calculations show that effect of only temperature deformation does not promote high stresses in the core barrel wall, but degree of stress redistribution in it due to radiation swelling depends on residual welding stresses. Circumferential and axial stresses, caused by contact interaction of core barrel with baffle, have the largest impact on stressed state of the in-vessel core barrel wall in course of 60 years of operation. Stresses in the in-vessel core barrel welds at the end of extended operation period (60 years) are close to the values of yield strength of irradiated material. Residual welding stresses can significantly effect the level of stressed state of the core barrel wall, that should be considered in estimation of working capacity of vessel internals at extension of service life of WWER-1000 reactor. 4 Ref., 2 Tables, 11 Figures.

Keywords: *in-vessel core barrel, WWER-1000 reactor, vessel internals, residual welding stresses, irradiation, 08Kh18N10T steel, life extension*

In-vessel core barrel of WWER-1000 reactor is a welded cylinder structure manufactured from austenite steel 08Kh18N10T. Location of the core barrel in reactor vessel and its drawing are given in Figure 1. In-vessel core barrel has external radius 1805 mm and wall thickness 60 mm at the level of setting of core baffle.

Reactor baffle is subjected to high radiation doses, that results in its swelling and change of form in operation. Gap between baffle rings and core barrel makes 2.5 mm under initial condition. Contact of baffle and in-vessel core barrel during operation should be taken into account based on calculation results [1]. Inside pressure of baffle on core barrel creates additional stresses in zone of contact. Residual welding stresses can also significantly effect a level of stressed state of a core barrel wall, that should be considered in estimation of working capacity of vessel internals (VI) for extension of WWER-1000 reactor service life. Thus, estimation of stressed state of the in-vessel core barrel in area of its contact with baffle, in particular, when place of contact coincides with welded joint zone, is a relevant task. It is necessary to note that the core barrel wall is also subjected to radiation swelling, however, damaging dose is an order of magnitude less than that in the baffle.

Aim of present work is investigation of stressed state in zone of the welds of in-vessel core barrel of WWER-1000 reactor during operation considering radiation swelling and contact interaction of baffle and core barrel.

Initially, this problem was studied in work [2]. Present study improves mathematical models of radiation swelling and mechanical properties of VI material, specifies values of volumetric heat generation and damaging dose in the core barrel, develops numerical model for calculation of stress-strain state in contact of baffle and core barrel as well as simulates residual welding stresses in the welds of in-vessel core barrel.

Procedure of investigations. Series of problems was solved for achievement of stated aim. Initially, the core barrel was considered in a free state without consideration of its contact with baffle. It was done in order to understand in what way operating temperature fields and ra-

diation swelling effect its stressed state. Contact with baffle is taken into account in the second problem. The two following problems are similar to the first ones, but they study the core barrel with residual welding stresses, which have simplified distribution.

Solving of these problems provides for understanding of redistribution of residual welding stresses in the core barrel and the way they are summarized with stresses from contact interaction of baffle and core barrel. The latter problem includes the whole experience of pervious problems, but it considers the real residual welding stress fields, obtained in course of separate numerical calculation, in the core barrel.

All problems were solved using 2D finite element method under condition of generalized plane deformation. VI material is 08Kh18N10T steel. Perfect plasticity model was used. Problem of estimation of stress-strain state under condition of radiation creep with swelling is solved at recalculation of stresses and deformations in each step of tracing. Heat exchange between baffle and core barrel is not considered during contact. Their contact interaction influences the stressed state of core barrel as well as baffle, both VI are simultaneously simulated with initial 2.5 mm gap. Internal pressure in reactor vessel is 16 MPa.

Stopping of heavy particles in VI metal promotes material heating-up. Capacity of volumetric heat generation in the core barrel is linearly changed from 5.0 (on inner surface) to 0.5 W/cm^3 (on outer one). Rate of accumulation of damaging dose in the core barrel is also linearly changed from 0.2 (on inner surface) to 0.02 dpa/year (on outer one). Thermophysical properties of 08Kh18N10T steel are given in Table 1, and can be applied to base metal as well as weld metal. Poisson's ratio $\nu = 0.3$.

Mechanical properties of 08Kh18N10T base metal and welds depend on temperature and radiation dose and are described in [3]. A model, given below, describes change of mechanical

Table 1. Thermal-physical properties of 08Kh18N10T steel [1]

T, °C	E, GPa	$\alpha^t \cdot 10^{-6}$, K^{-1}	λ, W·m^{-1}·K^{-1}	c_p, J·kg^{-1}·K^{-1}	ρ, kg/m^3
20	205	16.2	16.6	478	7900
100	200	16.6	17.2	495	7862
200	190	17.0	18.0	516	7821
300	180	17.4	18.7	537	7778
400	170	17.8	19.4	558	7732
500	165	18.2	20.1	579	7684
600	160	18.5	20.8	600	7634

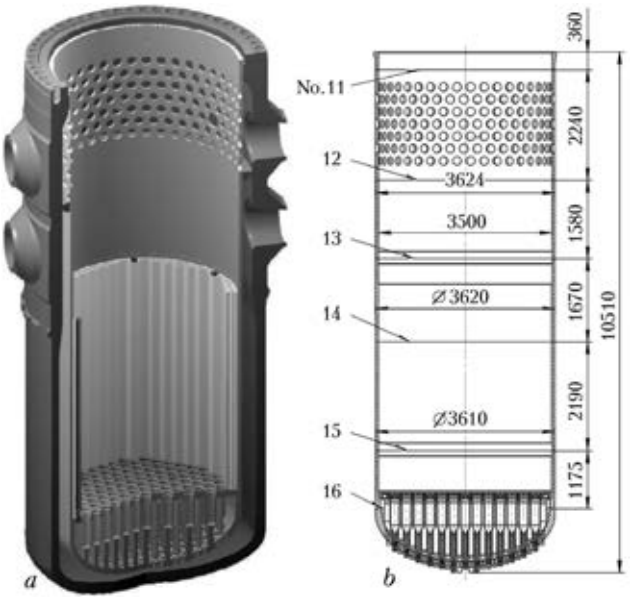

Figure 1. Location of in-vessel core barrel in structure of WWER-1000 reactor (*a*) and its drawing (*b*)

properties of 08Kh18N10T steel depending on temperature and damaging dose.

Base metal yield strength

$$\sigma_{0.2}(T, D) = \begin{cases} \sigma^0_{0.2}(T) + \Delta\sigma^{\text{y}}_{0.2}(T, D), & D < D^*, \\ \sigma^*_{0.2}(T) + \Delta\sigma^*_{0.2}(T, D), & D \geq D^*, \end{cases}$$

$$\sigma^0_{0.2}(T) = 155 + 239 \exp\left(-2.22 \cdot 10^{-3}(T + 273)\right) \text{ (MPa)},$$

$$\Delta\sigma^{\text{y}}_{0.2}(T, D) = (\sigma^*_{0.2}(T) - \sigma^0_{0.2}(T)) \times$$

$$\times \frac{\sqrt{1 - \exp\left(-C_{\sigma_{0.2}} D\right)}}{\sqrt{1 - \exp\left(-C_{\sigma_{0.2}} D^*\right)}},$$

$$\sigma^*_{0.2}(T) = 650 + 1405 \exp\left(-5.9 \cdot 10^{-3}(T + 273)\right) \text{ (MPa)},$$

$$\Delta\sigma^*_{0.2}(D) = A_{\sigma_{0.2}} \times$$

$$\times \left(\sqrt{1 - \exp\left(-C_{\sigma_{0.2}} D\right)} - \sqrt{1 - \exp\left(-C_{\sigma_{0.2}} D^*\right)}\right),$$

$$D^* = 7 \text{ dpa}, \quad C_{\sigma_{0.2}} = 0.126 \text{ dpa}^{-1}, \quad A_{\sigma_{0.2}} = 621 \text{ MPa}.$$

Weld metal yield strength

$$\sigma_{0.2}(T, D) = \sigma^0_{0.2}(T) + \Delta\sigma_{YG}(D) \text{ (MPa)},$$

$$\sigma^0_{0.2}(T) = 255 + 420 \exp\left(-2.22 \cdot 10^{-3}(T + 273)\right) \text{ (MPa)},$$

$$\Delta\sigma_{YG}(D) = 498\sqrt{1 - \exp\left(-0.3D\right)} \text{ (MPa)}.$$

Base metal tensile strength

Table 2. Temperature of heat carrier and coefficient of heat transfer for different surfaces of core barrel [1]

Core barrel surface	Temperature on surface, °C	Coefficient of heat transfer, W/(m^2·K)
Outer	291.7	15,900
Inner	320.0	39,017

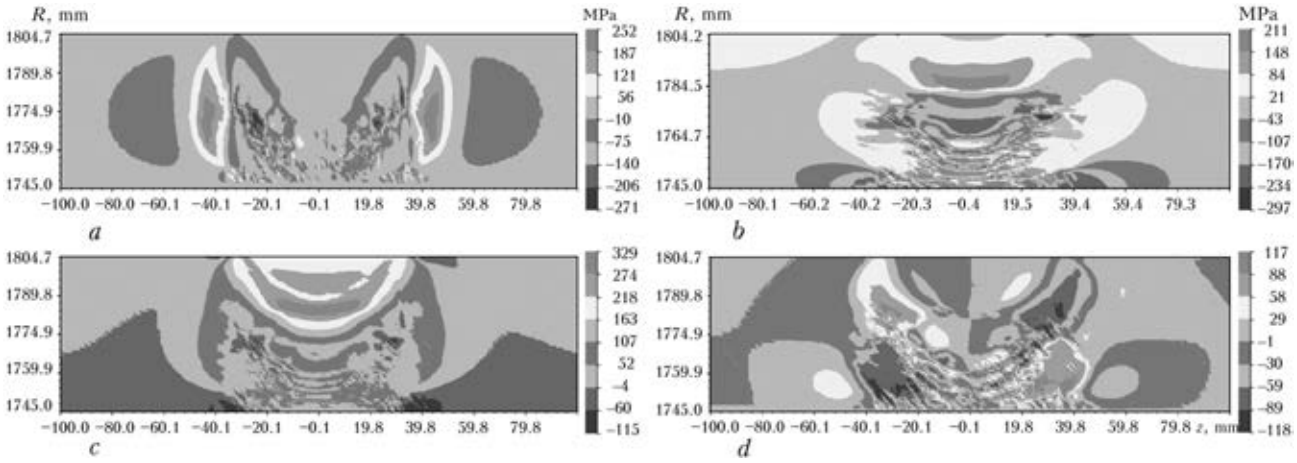

Figure 2. Residual welding stresses in core barrel of WWER-1000 reactor in cylindrical coordinates a — σ_{rr}; b — $\sigma_{\beta\beta}$; c — σ_{zz}; d — $\sigma_{r\beta}$

$$\sigma_t(T,D) = \sigma_t^0(T) + \Delta\sigma_t(D)\ \text{(MPa)},$$
$$\sigma_t^0(T) = 350 + 247\ \exp\ (-6.6\cdot10^{-3}T)\ \text{(MPa)},$$
$$\Delta\sigma_t(D) = 483\sqrt{1 - \exp\ (-0.11D)}\ \text{(MPa)}.$$

Weld metal tensile strength

$$\sigma_t(T,\ D) = \sigma_t^0(T) + \Delta\sigma_t(D)\ \text{(MPa)},$$
$$\sigma_t^0(T) = 439 + 222\ \exp\ (-9.74\cdot10^{-3}T)\ \text{(MPa)},$$
$$\Delta\sigma_t(D) = 440\ \sqrt{1 - \exp\ (-0.25D)}\ \text{(MPa)}.$$

Temperature problem with boundary conditions of the third kind was solved for estimation of stationary temperature in the wall of in-vessel core barrel. Table 2 gives heat carrier temperature and values of coefficients of heat transfer for different surfaces of the core barrel.

Numerical calculation of volumetric deformations of swelling was carried out in accordance with [4]. This mathematical model considers dependence of swelling on radiation dose, temperature, type of stressed state, values of stresses and radiation creep. The main relationships and parameters of this model are given below:

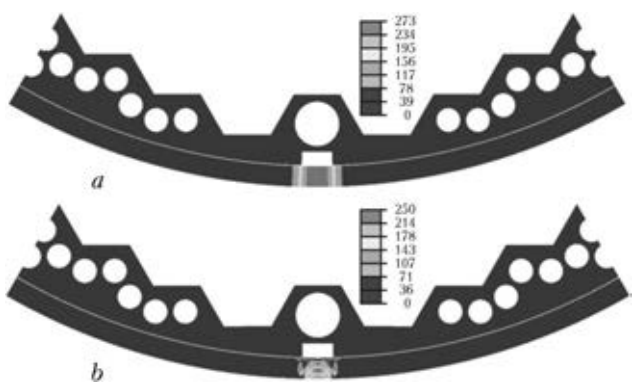

Figure 3. Intensity of stresses (MPa) in longitudinal weld of core barrel under initial condition: a — simplified task; b — simulated residual welding stresses

$$\frac{d\varepsilon_{eq}^c}{dt} = \left(B_0\ \frac{dD}{dt} + \omega\ \frac{dS}{dt}\right)\sigma_{eq},\ d\varepsilon_{eq}^c > 0,\ \varepsilon_{eq}^c|_{t=0} = 0,$$
$$\frac{dS}{dt} = C_D n D_i^{n-1} f_0(T) f_1(\sigma_m) f_3(\kappa) dD,\ dS > 0,\ S|_{t=0} = 0;$$
$$f_0(T) = \exp\ (-r(T - T_{\max})^2),$$
$$f_1(\sigma) = 1 + 8\cdot10^{-3}(0.85\sigma_m + 0.15\sigma_{eq}),\ f_3(\kappa) = \exp\ (-\eta\kappa);$$
$$B_0 = 10^{-6}\ \text{dpa}^{-1},\quad \omega = 2.95\cdot10^{-3}\ \text{MPa}^{-1},$$
$$C_D = 1.035\cdot10^{-4}\ \text{dpa}^{-n},\ n = 1.88,\ r = 1.825\cdot10^{-4}\ ^\circ\text{C}^{-2},$$
$$T_{\max} = 470\ ^\circ\text{C},\ P = 4\cdot10^{-1}\ \text{MPa},\ \eta = 8.75,$$

where S is the swelling; D is the damaging dose; σ_m is the medium stress; κ is the Odqvist parameter.

Fields of residual welding stresses in the core barrel were received by calculation method using WeldPredictions software, developed the PWI staff. Simulation of longitudinal multi-pass welded joint (six passes) of cylindrical shell with inside diameter D_{in} = 3490 mm, δ = 60 mm thickness and 30° grooving for the following mode: I = 200 A, U = 17 V, v_w = 3 mm/s (heat input Q_h = 850 J/mm, efficiency rate 0.75), was carried out. Boundary problem of determination of kinetics of stress-strain state was solved in cylindrical coordinates using FEM (size of element 1 × 1 mm) by means of sequential tracing of elasto-plastic deformations from beginning of welding of the first pass to cooling after the sixth pass considering Mises yield criterion. Figure 2 shows the results of calculation of residual stress fields.

Vertical weld, located based on conservative assumptions in the contact area of baffle to core barrel (Figure 3), was investigated in this case.

Residual welding stresses for simplified problems contain only axial component. Stress in the core barrel reduces from 270 to 0 MPa moving

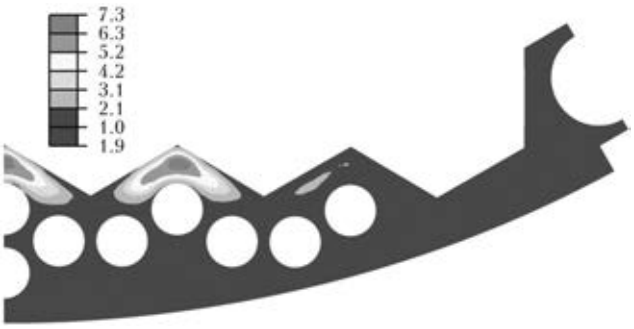

Figure 4. Field of volumetric deformations of baffle swelling after 60 years of reactor operation (calculation was carried out considering radiation creep [4])

away from center of baffle large channel in circumferential coordinate (Figure 3, *a*).

Results and discussion. Figure 4 shows a field of volumetric deformations of baffle swelling after 60 years of reactor operation. The baffle is deformed in radial direction due to non-uniform swelling. Radial movements are maximum in area of large channel. The same area influences the in-vessel core barrel at it contact with baffle.

Temperature distribution over thickness of the core barrel wall in mode of reactor normal operation (NO) for problems 1–5 is shown in Figure 5. The core barrel is heated due to stopping in metal of heavy particles, and inner and outer surfaces of the core barrel are water-cooled, therefore, temperature maximum is found inside the wall and makes 306 °C. Temperature on internal and external surfaces is virtually the same and makes 290 °C. Yield strength of weld metal in the core barrel under the effect of irradiation in a course of 60 years of operation was set at the level of 850 (on inner surface) and 500 MPa (on outer one) and being linearly changed over thickness. In-vessel core barrel has cylindrical form, therefore, stress-strain state of VI will be considered in cylindrical coordinates, axis of which is co-directional with core barrel axis.

1. *Core barrel in free state: heating, irradiation and cooling*. Non-uniform heating promotes appearance of stresses in the core barrel wall. Quality redistributions of circumferential and axial stresses are close, therefore, only axial stresses S_z appearing during operation will be given (Figure 6). Radial stresses are virtually constant over wall thickness and make 16 MPa, which is caused by internal pressure in the reactor.

Since temperature on inner and outer surfaces of the core barrel wall is lower than in internal area, stresses on the surfaces are tensile ones (Figure 6, curve *2*) and compression is observed inside the wall. Irradiation during reactor operation promotes swelling of material on inner surface of core barrel wall (~0.01 %), that reduces

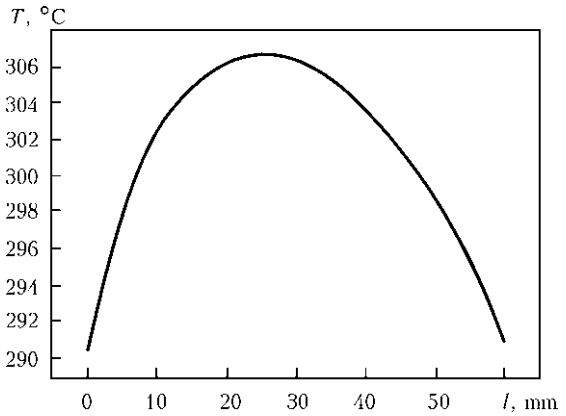

Figure 5. Distribution of temperature over thickness of core barrel wall in mode of reactor NO (hereinafter l — distance from inner surface of core barrel wall)

tensile stresses in this area (Figure 6, curves *3* and *4*). Based on equilibrium condition, tensile stresses on outer surface show insignificant increase. Shutdown of reactor at the end of operation period removes temperature deformations, however, redistribution of stresses, promoted by radiation swelling of material, is preserved (Figure 6, curve *5*).

Thus, radiation swelling of material of the core barrel wall promotes 10 MPa reduction of stresses on inner surface, that based on equilibrium condition is accompanied by their insignificant growth on outer surface of the core barrel wall. Temperature deformations in the core barrel wall provoke stresses at the level of ±30 MPa.

2. *Contact of core barrel with baffle: heating, irradiation and cooling*. Effect of radiation on the baffle promotes its swelling, that results in change of its form and contact with the core barrel after 25th year of operation (in «hot» state). Figure 7 shows redistribution of circumferential and axial stresses in the reactor core barrel during operation considering contact with the baffle. Values of stresses were taken along

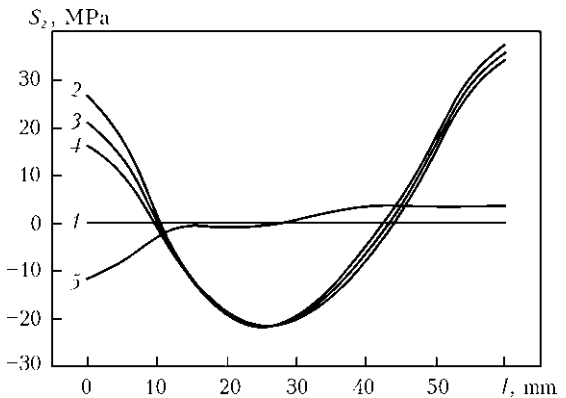

Figure 6. Redistribution of axial stresses over thickness of reactor core barrel wall during operation: hereinafter *1* — initial condition; *2* — reaching of NO mode; *3*, *4* — after 30 and 60 years of irradiation, respectively; *5* — shutdown of reactor after 60 years

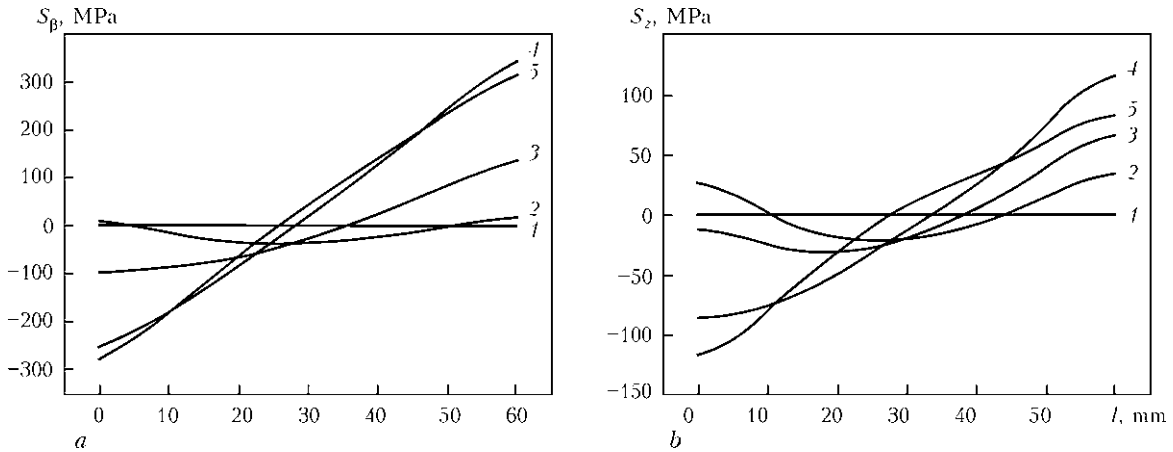

Figure 7. Redistribution of circumferential (*a*) and axial (*b*) stresses over thickness of reactor core barrel wall during operation considering contact with baffle

core barrel thickness in area of contact with the baffle. Curves *3–5* represent that internal pressure of baffle on core barrel wall promotes appearance of compressive circumferential and axial stresses on inner surface, as well as growth of tensile circumferential and axial stresses on outer surface of the core barrel.

Pressure of baffle on core barrel does not provoke significant rise of radial stresses. Compressive and tensile circumferential stresses are significantly larger than corresponding axial ones, and after 60 years of reactor operation they achieve −280 MPa (compression) on inner surface of the core barrel and +340 MPa (tension) on outer one. At the same time, axial stresses on inner surface of the core barrel wall make −110 and on outer one +100 MPa.

3. *Simplified welded joint. Core barrel in free state: heating, irradiation and cooling*. Understanding of redistribution of compressive and tensile residual welding stresses in the core barrel during reactor operation was received by means of solving of two problems, in which the residual welding stresses in simplified welds had different signs. Redistribution of simplified residual welding stresses in the reactor core barrel during operation is shown in Figure 8. Reduction (relaxation) of tensile axial residual welding stresses in Figure 8, *a* during reactor operation is explained by swelling of material close to inner surface of the core barrel wall. This is also the reason why compressive axial residual welding stresses rise on absolute value (Figure 8, *b*). In this problem the level of effect of swelling deformations on stresses is significantly higher than in the case of absence of welded joint in the core barrel wall (problem 1). This is explained by dependence of swelling on stressed state. Tensile axial stresses in the core barrel wall reduced by 125 MPa on inner surface and by 60 MPa on outer one during 60 years of operation. At the same time, compressive axial stresses grew by 85 MPa on inner surface and reduced by 20 MPa on outer surface of the core barrel.

4. *Simplified welded joint. Contact of core barrel with baffle*: *heating, irradiation and cooling*. Consideration, the same as in problem 3, is given to redistribution of tensile (Figure 9, *a*) and compressive (Figure 9, *b*) simplified residual welding stresses in the core barrel during reactor

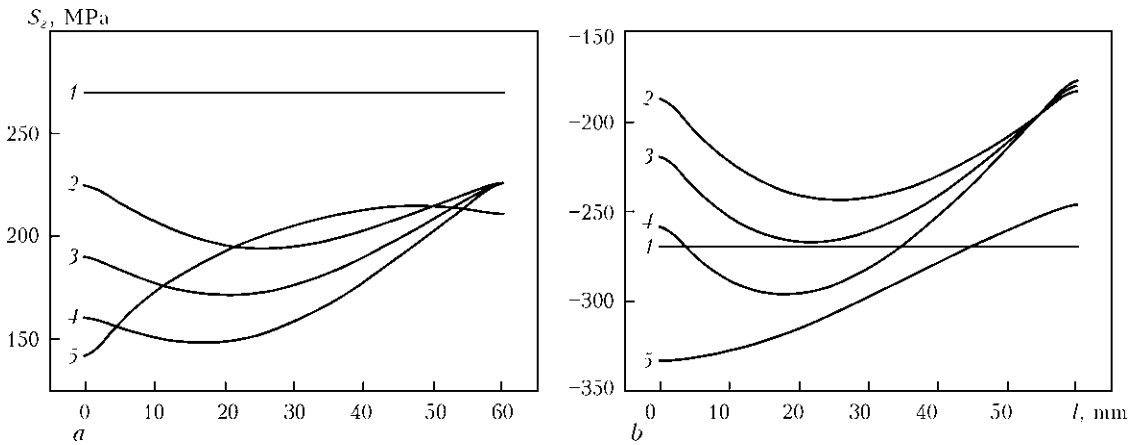

Figure 8. Redistribution of simplified residual welding stresses over thickness of reactor core barrel wall during operation: *a* — tensile; *b* — compressive axial stresses

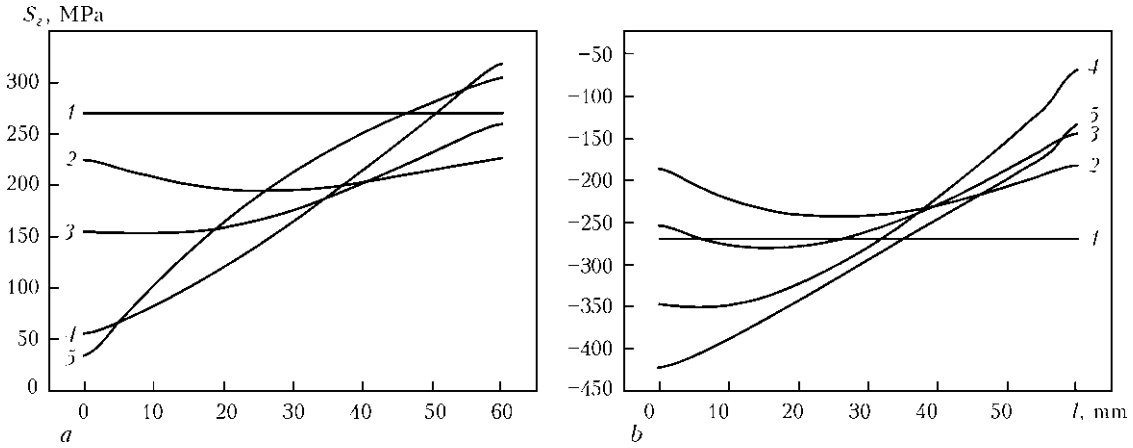

Figure 9. Redistribution of simplified residual welding stresses over thickness of reactor core barrel wall during operation considering baffle pressure: *a* — tensile; *b* — compressive axial stresses

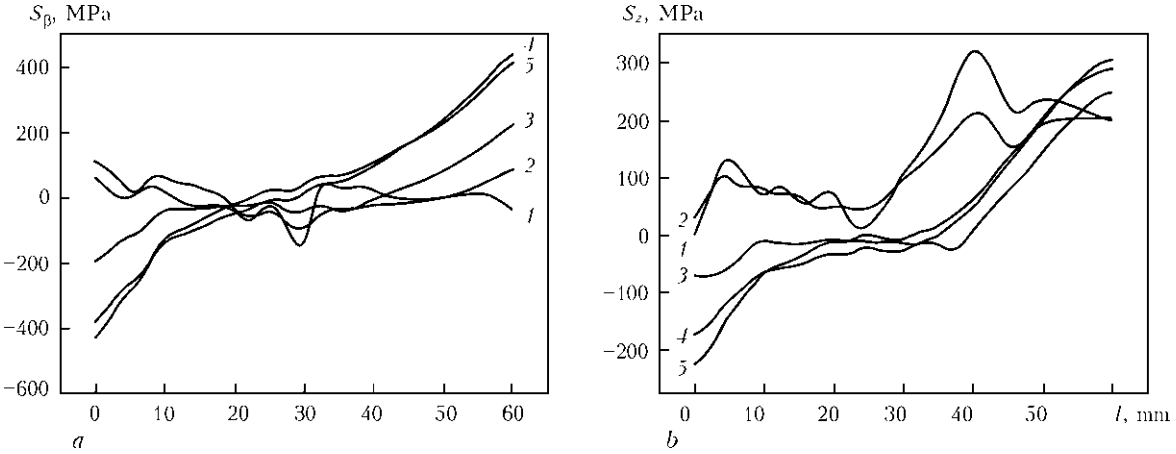

Figure 10. Redistribution of circumferential (*a*) and axial (*b*) stresses in zone of simplified weld of in-vessel core barrel of reactor during operation considering contact with baffle

operation. Contact interaction of in-vessel core barrel with baffle is considered in this problem. This problem is virtually a superposition of problems 2 and 3 and change of stressed state can be estimated based on their solving. Tensile axial stresses (see Figure 9, *a*) on inner surface reduce by 125 + 110 = 235 MPa as a result of radiation swelling and pressure of baffle, and on outer surface they increase by −60 + 100 = 40 MPa. Compressive axial stresses on inner surface (see Figure 9, *b*) rise by 85 + 110 = 195 MPa due to radiation swelling and pressure of baffle, and they decrease by 20 + 100 = 120 MPa on outer surface of the core barrel.

5. *Contact with baffle: heating, irradiation and cooling. Stress behavior in weld*. Redistribution of simulated residual welding axial and circumferential stresses in the reactor core barrel during operation is shown in Figure 10. Contact with baffle is considered. Axial and circumferential stresses are the maximum ones for the in-vessel core barrel weld after 60 years of reactor operation, that are caused by baffle pressure. Figure 11 shows their redistribution.

Pressure of baffle on core barrel, similar as in problems 2 and 4, promotes growth of compressive circumferential and axial stresses on inner surface of the core barrel and tensile circumferential and axial stresses on outer surface (see Figure 10).

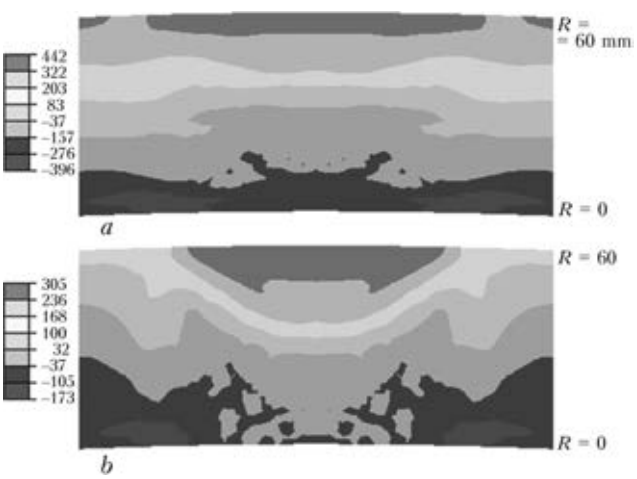

Figure 11. Distribution of circumferential (*a*) and axial (*b*) stresses (MPa) in zone of weld on in-vessel core barrel of reactor at the end of extended service life (60 years) considering contact with baffle

Circumferential stresses in weld zone achieve the values (440 MPa) close to yield strength of irradiated material of the core barrel wall (Figure 11, *a*).

Conclusions

1. Stresses of ±30 MPa level appear in the core barrel wall as a result of temperature deformations in reaching of NO mode of reactor.

2. Radiation swelling without consideration of residual welding stresses for 60 years of operation promotes change of stresses in ±10 MPa limits.

3. Redistribution of stresses due to radiation swelling in zone of the welded joints on core barrel wall depends on level of residual welding stresses. Reduction of residual tensile stresses can achieve 125 MPa.

4. Contact interaction of core barrel with baffle can make the largest (up to 340 MPa) impact in stressed state of the in-vessel core barrel in course of 60 years of operation.

5. Circumferential stresses in zone of welds of the in-vessel core barrel at the end of extended operation period (60 years) considering residual welding stresses and contact with baffle can reach high values (440 MPa) close to yield strength of irradiated material.

6. Residual welding stresses can significantly effect the level of stressed state of the core barrel wall, that is necessary to be considered in estimation of VI working capacity in extension of service life of WWER-1000 reactor.

1. Makhnenko, O.V., Mirzov, I.V. (2013) Investigation of stress-strain state of welded structures from austenitic steel at radioactive irradiation. *The Paton Welding J.*, **1**, 5–10.
2. Makhnenko, V.I., Makhnenko, O.V., Kozlitina, S.S. et al. (2012) Welded structures from austenitic steel of 10Kh18N10T type under conditions of radiation-induced swelling. *Ibid.*, **2**, 6–10.
3. Sorokin, A.A., Margolin, B.Z., Kursevich, I.P. et al. (2011) Influence of neutron irradiation on mechanical properties of materials of in-vessel internals of WWER type reactors. *Voprosy Materialovedeniya*, **2**, 131–151.
4. Margolin, B.Z., Murashova, A.I., Neustroev, V.S. (2012) Analysis of influence of strained state type on radiation swelling and radiation creep of austenitic steels. *Problemy Prochnosti*, **3**, 5–24.

Received 13.02.2014

CRACKING SUSCEPTIBILITY OF WELDED JOINTS IN REPAIR STRUCTURES ON MAIN GAS PIPELINES

V.S. BUT, S.Yu. MAKSIMOV and **O.I. OLEJNIK**
E.O. Paton Electric Welding Institute, NASU
11 Bozhenko Str., 03680, Kiev, Ukraine. E-mail: office@paton.kiev.ua

Repair of main pipelines under pressure involves application of various reinforcing welded structures. Operation periods of trunk lines in many cases are longer than 30 years, and pipe material can have an unfavourable structure, hence the need to broaden the concepts of ensuring the technological strength of welded joints under repair conditions. The work gives the results of studying the susceptibility of low-alloyed steel welded joints to cold and lamellar cracking. For this purpose, experiments were conducted on technological samples, simulating the real welded joints of repair structures. Positive impact of preheating, postweld heating and thermal annealing effect on cold cracking resistance is shown, as well as significant influence of sulphur on lamellar cracking susceptibility of steels. Possibility of prediction of lamellar cracking probability by the indices of reduction in area, impact toughness and critical crack opening displacement, as well as by delayed fracture critical stresses and fractographs of base metal fracture surface, is shown. 18 Ref., 2 Tables, 12 Figures.

Keywords: *repair welded structures, main pipelines, cold cracks, lamellar cracking, thermal annealing effect, technological samples*

Ukraine has a powerful oil-and-gas complex that enables the country playing an important role in transportation of energy resources from supplier to consumer. Analysis of structural distribution of Ukraine's main gas pipelines (MGP) by their length shows that 23 % of them have been in operation for more than 40 years, 32 % — from 30 to 40 and 45 % — up to 30 years [1]. It is understandable that ensuring the appropriate technical condition and continuous operation of pipelines in the near future will require a large scope of repair-reconditioning work.

Readiness for emergency situations and ability of taking action in these cases is an overimportant problem, from the moment of creating pressure in the pipeline and during its entire operation life. In this connection, each emergency or case of detection of inadmissible defects in pipeline linear part requires availability of a repair strategy, based on the following criteria: selection of repair method, safety of reconditioning operations performance, repair structure reliability (absence of cracks), environmental impact, uninterrupted product transportation, repair duration and cost-effectiveness. Preference should be given to procedures of repair without interruption of pipeline operation so as avoid reduction of pumped product volume or only slightly reduce it for a short time interval, and not cause considerable material-financial and environmental damage.

For Ukraine such methods are particularly important, in view of a high population density in MGP zone, high gas prices and need for unconditional fulfillment of contractual obligations on gas supply both to local and foreign users.

Performed diagnostics of technical condition of Company «Ukrtransgaz» MGP revealed extensive corrosion damage in the linear part, which is equal to about 50 % of the total number of detected defects, individual areas of metal delamination, as well as defects in circumferential welded joints inadmissible by the currently valid normative-technical documents [2], which usually form in the closing butt joints («overlaps») in pipeline construction.

Proceeding from analysis of the nature and geometrical parameters of the detected defects, PWI proposed a structural approach to development of technologies for restoration of load-carrying capacity of MGP linear part under pressure with arc welding application [3]. Repair methods were grouped by defect kinds and purpose [4]. For each group safe conditions of welding performance were determined, allowing for working parameters of gas transportation, trunk line geometry, pipe metal mechanical properties and welded joint type.

The majority of the proposed methods for repair of MGP linear part in service [4] envisage application of reinforcing structural elements with typical welded joints (Figure 1). Before recommending the developed engineering solutions for practical application, it was necessary to determine the conditions of provision of welded joint technological strength, i.e. elimi-

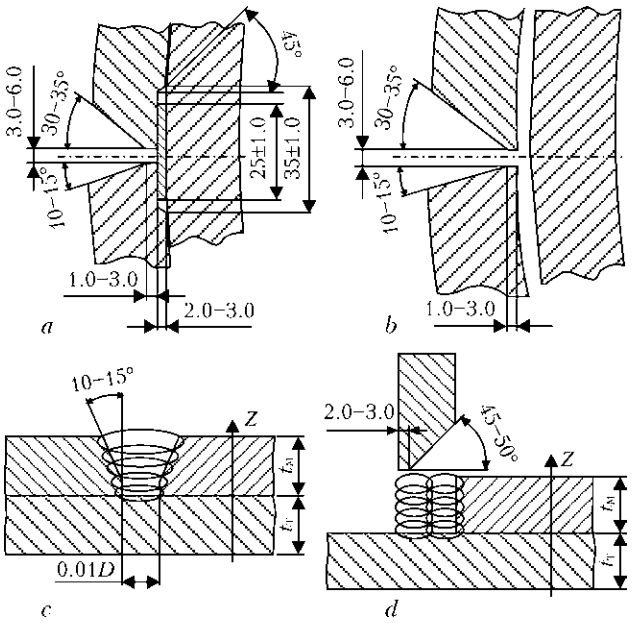

Figure 1. Typical welded joints in repair structures mounted on MGP in operation: *a*, *b* — longitudinal butt weld of sleeve; *c* — overlap-butt joint; *d* — branchpipe–sleeve joint

nate cracking. Results of studies in this direction are presented in part in [5] which focused on evaluation of structural strength of welded joints of reinforcing elements to pipeline. This paper is devoted to technological aspects of pipe steel weldability.

Cold cracking resistance of welded joints. Ability of welded joints to stand thermomechanical impact without fracture (cold cracking) during stick electrode arc welding was evaluated on samples of pipe steels of typical grades 17G1S and X60, which were extensively applied in MGP construction in the 1980s of the previous century. This enabled a closer simulation of real welded joints of repair structures [4]. So, for longitudinal butt joints of sleeves (Figure 1, *a*, *b*) this was Tekken test sample; for overlap-butt joints of structural elements to pipeline (Figure 1, *c*) — Implant sample; for branchpipe–sleeve joints (Figure 1, *d*) — «window» sample; for «patch-sleeve» repair structure it was the circumferential sample. Table 1 gives the composition of the studied steels.

For comparative analysis of steels, allowing for preheating conditions ensuring the required cracking resistance, experiments were conducted on Tekken samples [6] from 16 mm thick plates, as thicker rolled stock is not yet applied for fabrication of reinforcing structural elements [7]. Thermocouples were welded to plate surface near the edge chamfers to determine the preheating temperature. Welding of control section of the joint was performed with 3 mm electrodes UONI-13/55 with basic coating type and 3.2 mm Lincoln Electric Shield-Arc 65 electrodes with cellulose coating at base metal initial temperature of 20, 50, 100, 150 and 200 °C. After welding macrosections were cut out of the control section for evaluation of crack presence/absence. Relative extent of cracks was determined in MBS-2 microscope as a ratio of crack length in the weld to total weld length.

Proceeding from the conducted studies graphic dependencies of relative extent of cracks L_{cr} on preheating temperature T_{pr} were plotted (Figure 2). They showed that welded joints of X60 steel are more prone to cold cracking than those made on steel 17G1S. Application of cellulose coating electrodes significantly lowers crack resistance of both welded joints, because of high content of diffusible hydrogen, which can reach 40 $cm^3/100$ g in deposited metal [8]. According to Tekken procedure, the optimum preheating temperature for prevention of cold cracking in real welded joints is selected by the criterion of total crack length of 50 % in the control weld. Thus, in welding with electrodes with basic coating type T_{pr} = 20–50 and 70–100 °C for steel 17G1S and X60, respectively, and at application of electrodes with cellulose coating preheating temperature will be higher by 60–80 °C (see Figure 2).

In order to determine cracking conditions in welded joints of «patch-sleeve» repair structure [4] investigations were performed on a circular sample (Marine sample of US Department of the Marine) by the procedure of [6]. Minimum sample diameter was 100 mm, sleeve width was 500 mm. Results of investigation of the influence of gap *a* between abutted elements of the structure and welding heat input *q* on cold cracking susceptibility are shown in Figure 3, *a*. Presence/absence of cracks was determined on trans-

Table 1. Composition of studied pipe steels

Steel	Composition, wt.%									C_{eq}, %
	C	Si	Mn	Cr	Ni	S	P	V	Nb	
17G1S	0.170	0.467	1.60	0.06	0.05	0.025	0.036	0.02	0.005	0.46
X60	0.121	0.219	1.54	0.10	0.05	0.011	0.027	0.04	0.051	0.41
Melt #47	0.160	0.292	1.50	0.12	0.16	0.045	0.008	0.02	0.005	0.45
Melt #65	0.148	0.179	1.49	0.11	0.07	0.030	0.007	0.02	0.005	0.33

*Carbon equivalent was calculated by formula $C_{eq} = C + Mn/6 + (Cr + Mo + V)/5 + (Ni + Cu)/15$.

verse macrosections cut out of the closing quarter of the circular weld, where the highest tensile stresses are induced at weld metal shrinkage. It was obvious that the crack initiates at the stress raiser — in the point of deposited metal to base metal transition (Figure 3, *b*) and it is exactly in the zones of tensile stress concentration that diffusible hydrogen content increases markedly, promoting cold crack initiation [9].

From Figure 3 it is seen that with increase of the gap in the groove and respective increase of heat input, when making the root pass, cracks becomes shorter. At $a > 8$ mm practically no cracks form in welded joints of X60 steel. To eliminate the probability of cold cracking in weld metal of 17G1S steel circular sample, $a > 6$ mm is sufficient. Weld form factor K_w at maximum cracking is close to a unity, and in the absence of cracks $K_w \sim 4$. As it is known, cold cracking resistance of welds also depends on their metal structure, which is related in a certain way to weld form factor [10].

Note that during testing of Marine samples the effect of additional cooling of welded joints during welding due to transported product was not taken into account. Therefore, when mounting such repair structures on MGP near compressor stations, under the conditions of intensive heat removal by gas flowing at a high speed, preheating up to 100–150 °C will be obviously required.

In our opinion, Implant test is the most effective method for evaluation of cold cracking resistance of low-alloyed steel welded joints [11]. This procedure allows for practically all the factors causing cold cracking, namely low-ductility structure of HAZ metal, high level of tensile stresses, presence of stress raiser and significant

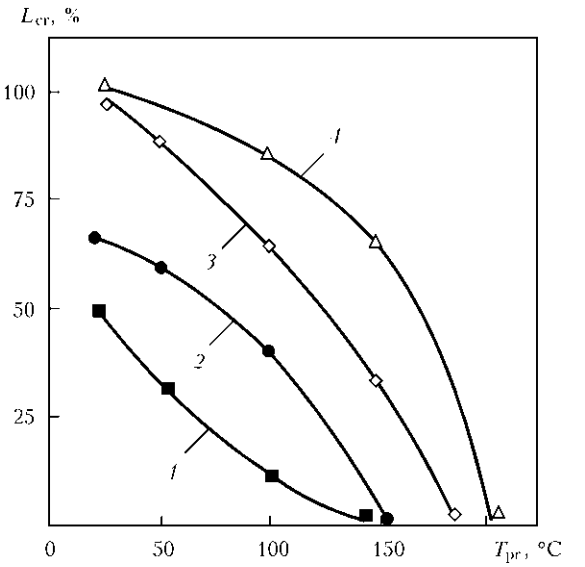

Figure 2. Dependence of crack length on preheating temperature, electrode coating type and steel grade for Tekken test weld: *1*, *3* — 17G1S steel; *2*, *4* — X60; *1*, *2* — UONI 13/45 electrodes; *3*, *4* — Shield-Arc 65

content of diffusible hydrogen. High tensile stresses, which are induced at raisers of geometrical origin (this, for instance, is the interlayer gap in overlap-butt joints of reinforcing elements to the pipeline), even at low hydrogen level, may lead to cold crack initiation and furtheron to welded joint fracture at long-term loading.

Experiments were conducted in keeping with IIW recommendations [11] for two variants. In the first case, samples were cut out of plates of 17G1S and X60 steels along the rolling direction, in order to study the influence of structural factor, diffusible hydrogen and welding technique on critical stresses at delayed fracture of welded samples in AIMI-5 testing machine. In the second case Im-

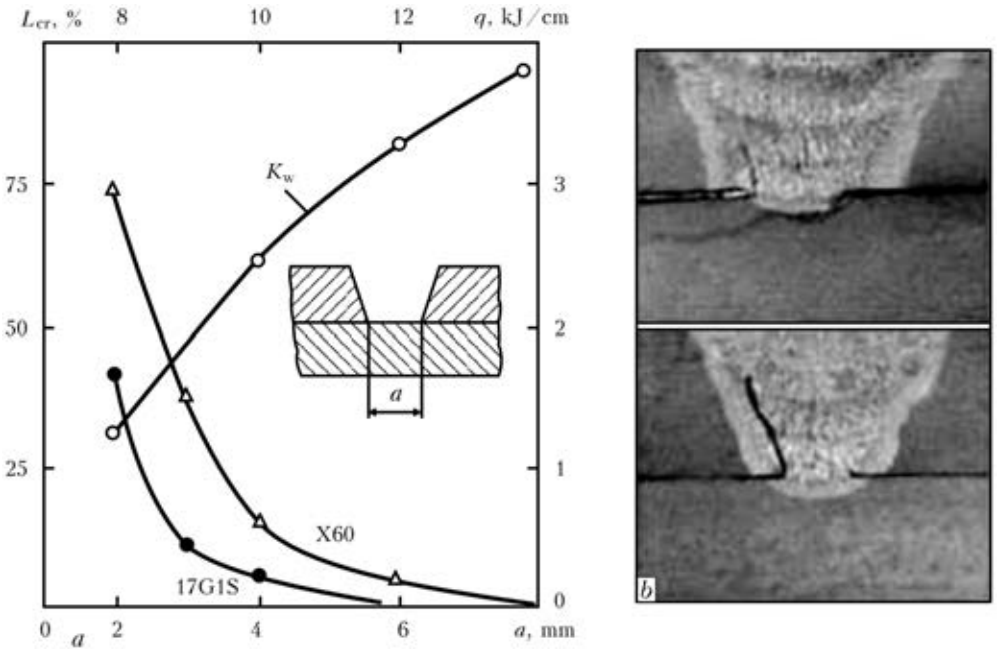

Figure 3. Conditions of crack initiation in circular sample (*a*), and crack initiation region (*b*)

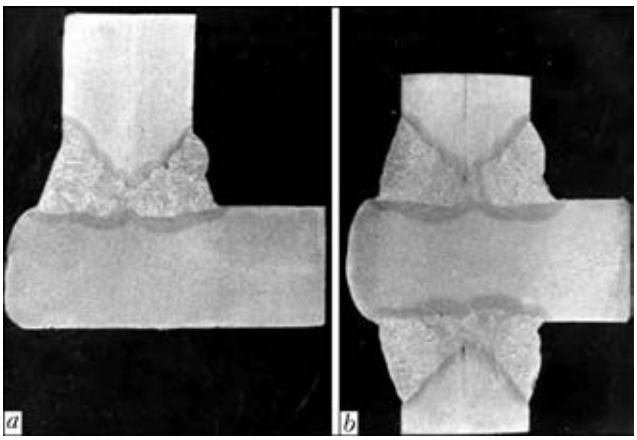

Figure 4. Macrosections of welded joints for preparing composite Implant samples with notch parallel to rolling direction for testing by tension along *Z* axis (*a*); for impact toughness and crack opening displacement (*b*)

plant samples were cut out of tee-joints (Figure 4) of all the examined steels to study the influence of diffusible hydrogen and impurities (sulphur) on cold cracking susceptibility under the impact of stresses in the direction normal to metal texture.

Welding of samples simulating real welded joints of repair structures (Figure 5) was performed with stick electrodes of 3.0 and 3.2 mm diameter with basic and cellulose coating in the following mode: I_w = 110–120 A, U_a = 24–26 V, v_w = 1.9–2.5 mm/s, ensuring heat input q = = 0.8–1.2 kJ/mm. In two-pass welding the thermally annealing layer was deposited with the heat input 1.4–1.7 times higher than that in single-pass welding. After weld metal cooling to 100 °C, the samples were tested by constant loading in a standard machine.

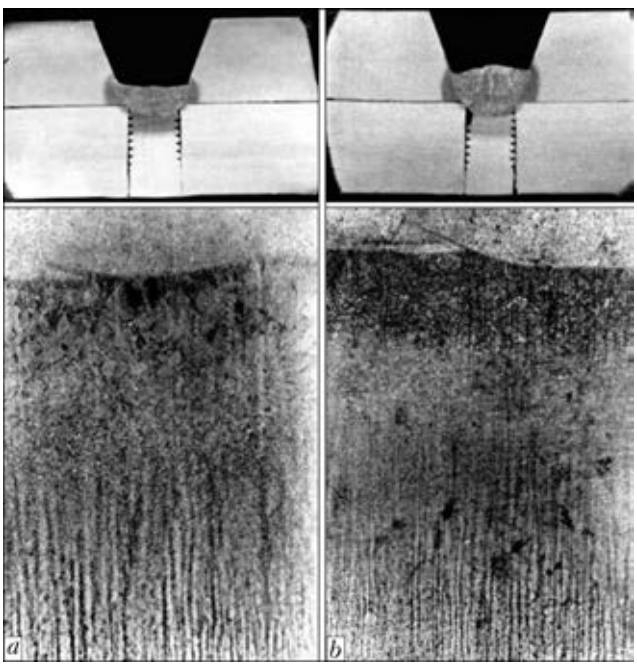

Figure 5. Single- (*a*) and two-pass (*b*) welding of Implant samples to produce joints simulating the real ones

Critical stresses not leading to sample cracking for 16 h were taken as the criterion of evaluation of welded joint cold cracking resistance. Diffusible hydrogen content in weld metal was determined by chromatographic method [12] on samples made under identical conditions.

It is established that in joints welded with Shield-Arc 65 electrodes diffusible hydrogen content $[H]_{diff}$ = 19–24 $cm^3/100$ g. In their turn, UONI 13/55 electrodes after baking at 380–400 °C ensure the level of 5.0–7.4 $cm^3/100$ g, and without baking (after soaking in air with relative humidity of 90 % for more than 3 days) a significant increase of hydrogen content in the deposited metal was noted — up to $[H]_{diff}$ = = 12–16 $cm^3/100$ g.

By the results of testing welded Implant samples, cut out of the studied steels along the rolling direction, graphic dependencies of variation of delayed fracture stresses in time were plotted for different content of diffusible hydrogen in the deposited metal, as well as for the case of application of thermally annealing layer (Figure 6, *a*). These graphs confirmed running of delayed fracture in samples, welded in one pass, and leading role of hydrogen in this process. With increase of diffusible hydrogen content critical fracture stress decreases, and duration of incubation period of crack initiation is also reduced. This is readily illustrated by fracture surface of Implant samples (Figure 7). Application of electrodes with basic coating type without baking (see Figure 6, *a*; curve *6*) leads to lowering of joint crack resistance almost to the level of values derived at application of cellulose coating electrodes (curve *2*). Use of thermal annealing effect at deposition of the weld second layer (curve *3*) allows lowering the probability of delayed fracture, owing to improvement of HAZ microstructure (see Figure 5, *b*) and, obviously, lowering diffusible hydrogen content in deposited metal.

When testing samples with a mechanical notch, made along the rolling direction (Figure 8, *a*), combined influence of hydrogen and nonmetallic inclusions (by sulphur content) on cracking resistance was studied. For this purpose, test PWI melts of low-alloyed steels (see Table 1) were used in addition to batch-produced pipe steels. The composition of these melts was changed by variation of the content of main alloying elements (carbon, silicon, manganese), as well as sulphur.

Results of testing composite Implant samples showed (see Figure 6, *b*) that the nature of delayed fracture resistance of pipe steels changed essentially, compared to the case of load appli-

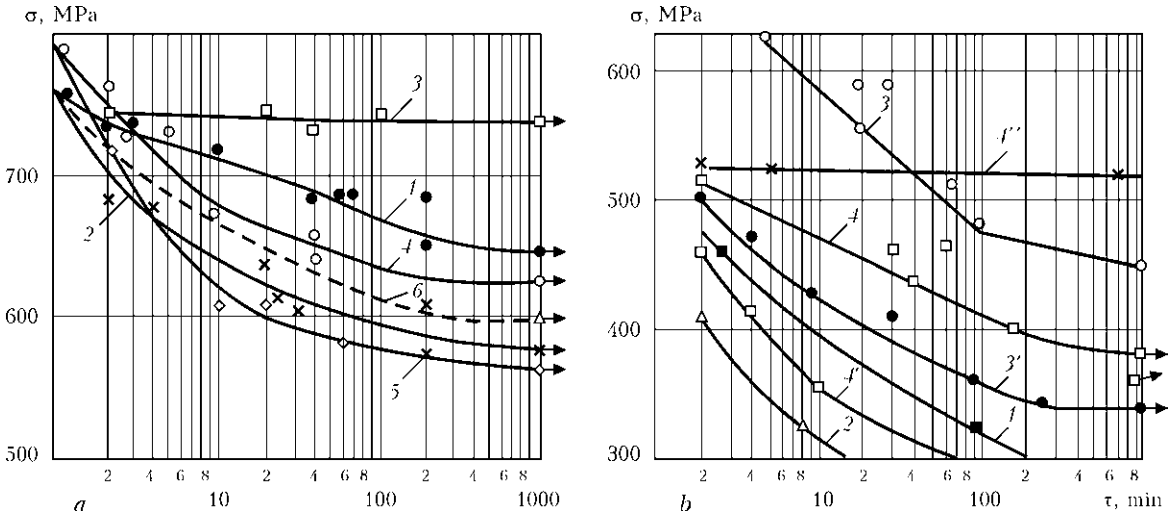

Figure 6. Results of testing Implant samples for long-term strength at loading along rolling direction (*a*: *1*, *4* — UONI 13/55 electrodes after baking, $[H]_{diff}$ = 4.0–7.4 cm^3/100 g; *2*, *5* — Shield-Arc 65, $[H]_{diff}$ = 19–24 cm^3/100 g; *3* — thermal annealing pass; *4*, *6* — UONI 13/55 without baking, $[H]_{diff}$ = 12–16 cm^3/100 g; *1–3*, *6* — 17G1S steel; *4*, *5* — X60) and along *Z* axis (*b*: *1* — melt #65; *2* — #47; *3* — X60 steel; *4* — 17G1S; *1–4*, *4″* — UONI 13/55 electrodes; *3′*, *4′* — Shield-Arc 65; *4″* — postweld heating)

cation along the rolling direction (Figure 6, *a*). Welded joints of X60 steel (Figure 6, *b*; curves *3*, *3′*) demonstrate higher cracking resistance than 17G1S steel joints (curves *4*, *4′*). This, in our opinion, is related to lower content of sulphur and absence of stringer structure in base metal, although absolute values of delayed fracture critical stresses were much lower than for Implant samples with a notch across metal rolling direction. Fracture mode of 17G1S steel samples with a high content of diffusible hydrogen in the deposited metal after the applied heating and soaking at 150 °C for 16 h is illustrated by Figure 8, *b*, *c*. Note that after removal of hydrogen from the HAZ, samples failed in the base metal in sections weakened by nonmetallic inclusions (Figure 8, *c*), critical fracture stresses were at a high enough level (see Figure 6, *b*, curve *4″*), sample fracture at initial content of diffusible hydrogen ran through the HAZ (Figure 8, *b*).

Under the effect stresses applied across metal thickness (notch parallel to rolling direction), the simultaneous negative influence of diffusible hydrogen and nonmetallic inclusions (sulphides) on delayed cracking resistance of welded joints is manifested. Hydrogen accumulates in voids containing inclusions, transforming from atomic into molecular form, and creates high pressure in them, thus facilitating metal matrix destruction at small radii of curvature of inclusion edges (considerable stress concentration on matrix–inclusion boundary). This is confirmed by the results of testing other experimental steels with different sulphur content (see Figure 6, *b*; curves *1*, *2*) and of fractographic analysis of fracture surface of Implant samples (Figure 9) in scanning electron microscope JEOL JSM-35CF. Studies showed that 17G1S steel samples are characterized by coarse-cellular structure, containing sulphide and sulphosilicate nonmetallic inclusions of ellipsoidal, globular and plate-like shape (Figure 9, *a*). Structure of X60 steel is fine-grained with a small quantity of globular-shaped nonmetallic inclusions of less than 2 μm size (Fi-

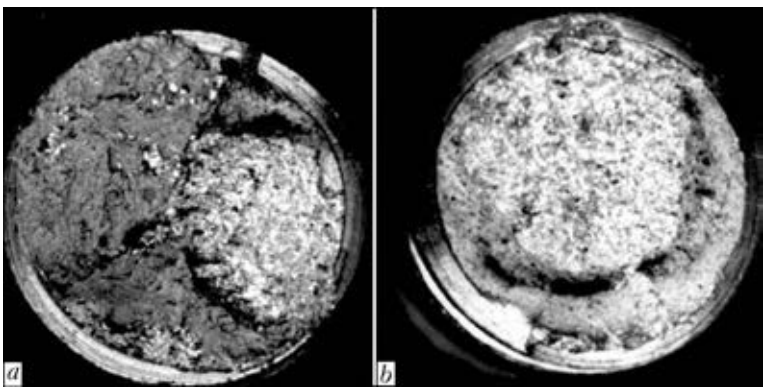

Figure 7. Fracture surface (×10) of Implant samples from X60 steel, welded with Shield-Arc 65 electrodes: *a* — σ = = 615 MPa, τ = 40 min; *b* — σ = 565 MPa, τ = 100 min

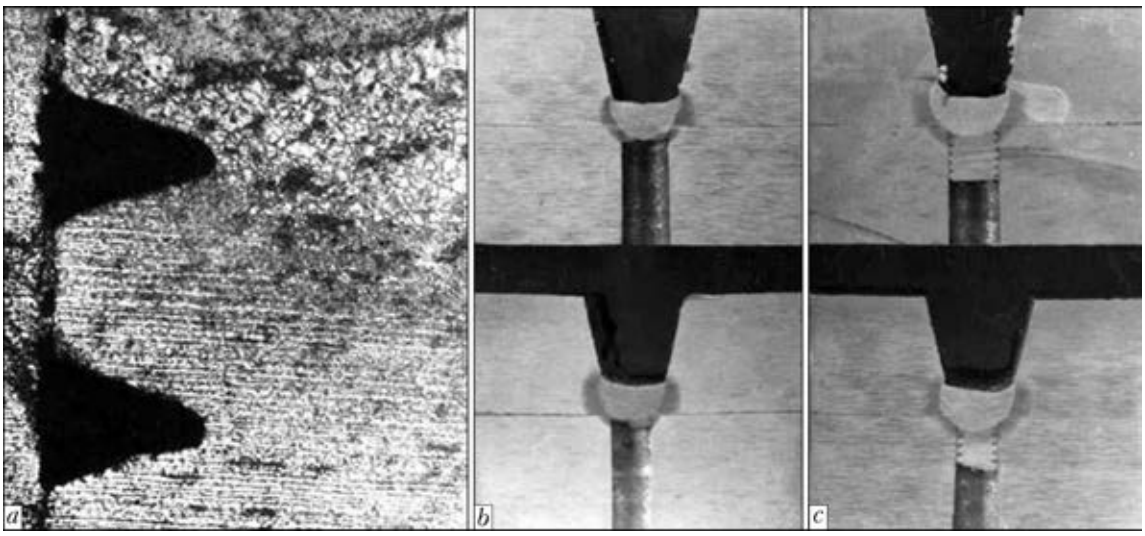

Figure 8. Notch location in HAZ of Implant sample (*a* — ×63), fracture through the HAZ (*b*) and base metal (*c*)

gure 9, *b*). A considerable quantity of plate-like nonmetallic inclusions is observed on fracture surface of steel from melt #47 (Figure 9, *c*) with the highest sulphur content (see Table 1).

Thus, summing up the results of testing welded joints for cold cracking resistance leads to the following conclusions. First, repair operations in operating MGP should be performed with application of electrodes with a basic coating, ensuring a low content of diffusible hydrogen in the deposited metal. Secondly, thermal annealing effect of multilayer weld second pass, which improves HAZ microstructure and ensures partial evacuation of hydrogen from problem zone, should be used. Thirdly, postweld heating should be performed for joints, in which loads can be applied later on in the direction normal to pipe metal texture. And, finally, traditional preheating up to 100–150 °C is required under the conditions of intensive heat removal in the repaired MGP section.

Evaluation of welded joint susceptibility to lamellar cracking. Lamellar cracking is one of the most common kinds of cracks in welded structures. Determination of material susceptibility to lamellar cracking is an important aspect of evaluation of low-alloyed steel weldability. Steplike form of cracks and their location, mainly, outside the HAZ, allows distinguishing these cracks from cold cracks. It is characteristic that such precautions as preheating and application of low hydrogen electrodes, that are effective for cold crack prevention, have an only slight influence on the probability of lamellar crack initiation.

As shown by world experience, overlap-butt and tee welded joints of low-alloyed steels can develop lamellar cracking at application of tensile stresses across the rolling stock direction. This problem is urgent also for welded joints of

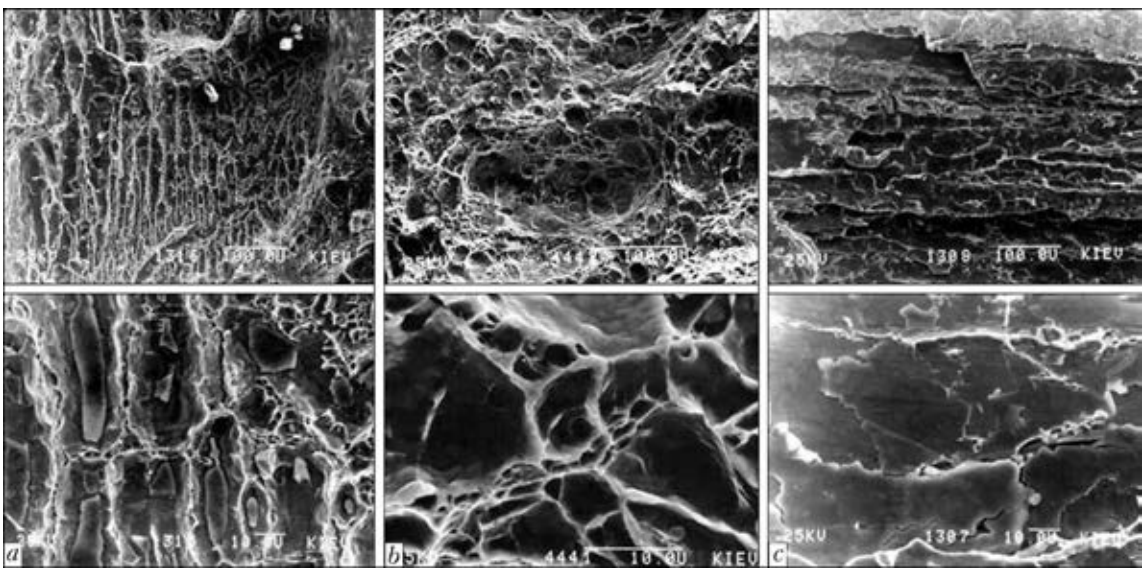

Figure 9. Fractographs of fracture surface of samples failing along *Z* axis: *a* — 17G1S steel; *b* — X60; *c* — melt #47 (upper row — ×300, lower row — ×3000)

structures (reinforcing sleeves, tee-pieces), mounted on MGP in service, as lowering of inner pressure in the pipeline in circumferential overlap-butt joints induces considerable radial stresses that is related to different deformability of welded shells.

It is also known [13] that lamellar cracking susceptibility of welded joints is influenced by the following factors:

- high content of nonmetallic inclusions of the type of manganese and iron sulphides and oxysulphides;
- unfavourable morphology of nonmetallic inclusions;
- weakening of metal matrix because of the high content of nonmetallic inclusions in one rolled stock plane;
- considerable extent of fusion boundaries along the rolling direction (parallel to metal texture);
- stress application across the rolled stock thickness (Z axis).

Steels of different strength classes (20, 09G2S, X70) were additionally used for evaluation of lamellar cracking susceptibility of base metal. Experiments were performed on cylindrical composite samples with gauge diameter of 6 mm, which were made from cruciform welded joints (see Figure 4, *b*). Six samples of each steel grade were prepared and tested at uniaxial tension, when in the studied metal section stresses are applied along Z axis. After breaking of cylindrical samples reduction in area ψ in the fracture butt was measured in keeping with the procedure of [13]. Derived results are given in Table 2.

For illustration purposes a histogram of steel distribution by reduction in area was plotted by average values of this characteristic (Figure 10). Steels 20, X60, X70 have the highest ductility at application of stresses across sheet thickness, and, hence lower lamellar cracking susceptibility, and 17G1S and test melts #65 and 47 are the least susceptible.

Fractographs of fractures of Implant samples failing through base metal also characterize steel ductility in the direction of axis Z. Using criteria proposed in [13], derived results can be assessed as follows (Table 2): formation of lamellar cracks in welded joints of steels 20 and X70 is improbable ($\psi \geq 25$ %); for 17G1S, 09G2S and X60 steels testing of reference «window» type restrained joints ($15 \leq \psi < 25$ %) is required; steels of melts #47 and 65 are prone to lamellar cracking and are not recommended for fabrication of critical welded structures ($\psi < 15$ %).

Influence of sulphur content on physico-mechanical properties of metal was studied with the notch made parallel to rolling direction that also characterizes steel susceptibility to lamellar cracking [14]. Toughness evaluation was performed on Mesnager samples at shock loading,

Table 2. Results of testing composite samples for lamellar cracking susceptibility

Steel	σ_t, MPa	ψ, %
17G1S	504–546 / 516	11.0–17.6 / 14.7
X60	572–580 / 574	20.2–26.0 / 23.2
Melt #47	420–480 / 452	6.1–11.3 / 7.4
Melt # 65	464–510 / 485	10.0–14.2 / 13.0
20	466–480 / 469	22.1–30.6 / 25.7
09G2S	470–492 / 481	19.0–27.2 / 20.3
X70	642–660 / 648	21.6–28.2 / 26.1

and brittle fracture susceptibility was determined on samples which allowed recording crack opening displacement (COD) at three-point bending. All the samples were cut out of cruciform welded joints (see Figure 4, *b*). Results of testing composite samples are given in Figure 11. One can see that impact toughness of metal decreases with increase of its sulphur content, particularly at negative temperatures (Figure 11, *a*). As regards pipe steels, X60 has higher characteristics than 17G1S, which has more sulphur (see Table 1). This is another confirmation of conclusions of [14] that sulphur content in steel above 0.012 % lowers welded structure reliability.

Preparation and testing of samples for COD determination was performed in keeping with procedure of [15]. Similar temperature dependencies were derived from COD which characterizes brittle fracture resistance of metal under static three-point loading of samples with a notch parallel to rolling direction (Figure 11, *b*). Graphs demonstrate that steel of melt #47

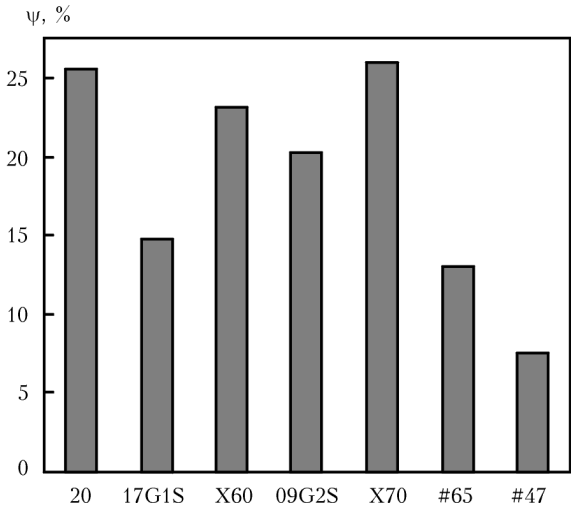

Figure 10. Steel distribution by the characteristic of lamellar cracking susceptibility depending on relative reduction along Z axis

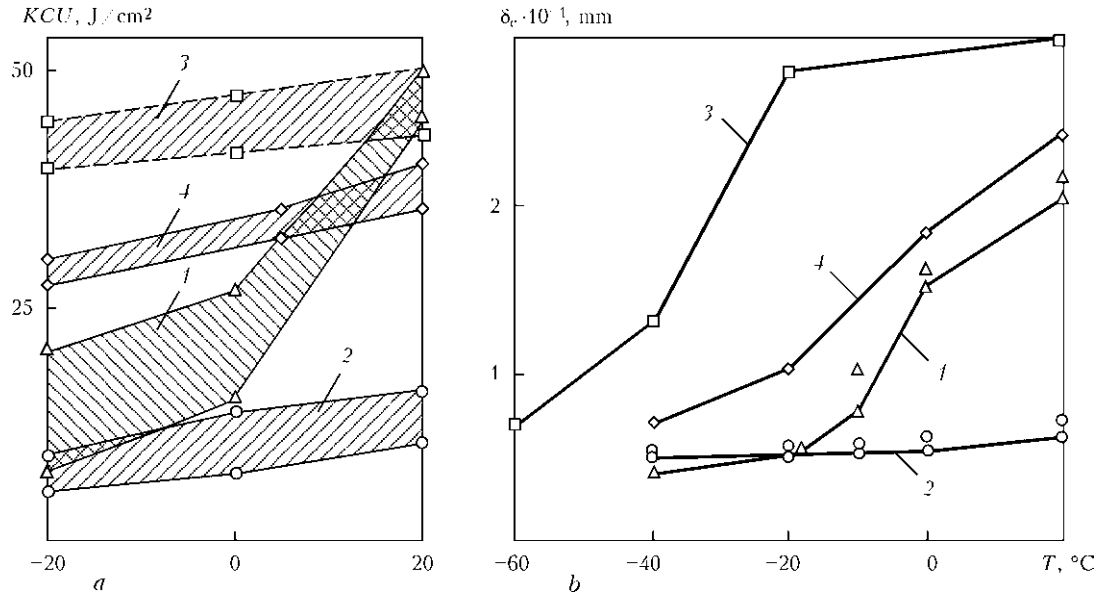

Figure 11. Toughness of samples with notch along rolling direction at shock loading (*a*) and three-point bending (*b*): *1* — melt #65; *2* — #47; *3* — steel X60; *4* — 17G1S

(curve *2*) with high sulphur content has very low COD values at three-point bending in the entire testing range and by the criterion of brittle fracture resistance of metal ($\delta_c > 0.12$ mm) it cannot be applied for fabrication of critical welded structures. Steel of melt #65 (curve *1*) under the conditions of application of tensile stresses across sheet thickness can be in service only at above zero temperatures, 17G1S steel (curve *4*) — at temperatures down to −15 °C, X60 (curve *3*) — down to −40 °C.

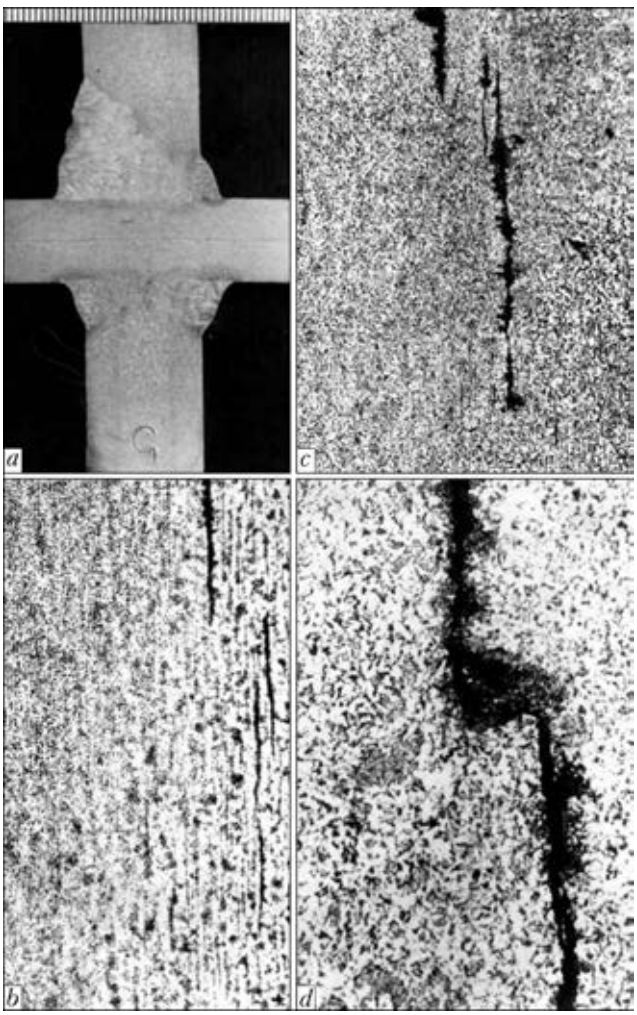

Figure 12. Macrosection of «window» sample (*a*), lamellar cracking in base metal (*b* — ×100) and HAZ (*c* — ×100; *d* — ×500)

17G1S steel, having intermediate values of toughness and ductility from those obtained on all the composite samples, was selected to verify welded joint susceptibility to lamellar cracking. It was used to make a sample, welded into a slot on a rigidly restrained 25 mm thick plate of 300 × × 300 mm size from 09G2S steel. This sample, according to [16], is called «window» sample and allows inducing in studied metal a high level of tensile stresses across the rolling direction at shrinkage of closing multilayer weld in V-shaped groove. Macrosection of this welded joint and formation of lamellar cracking in it are shown in Figure 12. Cracks are located in base metal, HAZ and at a certain distance from it. It is seen that crack opening occurred in points of location of nonmetallic inclusions of unfavourable plate-like shape with sharp edges.

Thus, for pipelines, manufactured from steels of such composition, after repair structures have been welded-on without interrupting pipeline operation, considerable internal pressure gradients are inadmissible, and in case of mounting reinforcing elements design-technological measures should be envisaged which lower lamellar cracking probability. The most effective method to reduce lamellar cracking susceptibility is regulation of sulphur content in steel in melting by addition of rare-earth elements, which not only are active deoxidizers, but also bind sulphur into finely-dispersed globular particles of oxysul-

phides and sulphides, uniformly distributed in steel. As was mentioned above, residual sulphur content in steel should not be higher than 0.012 % and REM:S ratio should be ≥ 4:1 [14].

Repair operations are performed on MGP built a long time ago, and pipe steel used in them is not quite favourable by its composition in terms of weldability, so that welders have to apply design-technological measures for prevention of lamellar cracking of repair structures. One of such approaches, tried out in practice, is pre-deposition of a buffer layer of less strong metal than that of the weld that was the basis for engineering solution of connecting branchpipes to MGP in operation [17]. Preliminary cutting out of pipe wall surface layer with subsequent filling of the groove by welding consumable, ensuring weld strength equivalent to that of base metal, can be regarded as another effective solution at repair [18].

In this connection, performance of research to evaluate the effectiveness of local remelting of surface layer of pipe wall under pressure by argon-arc or plasma method to reduce nonmetallic inclusion content in the produced welded joints and, therefore, lowering the lamellar cracking probability, is promising.

Conclusions

1. Comparative testing with application of Tekken sample showed higher crack resistance of welded joints of 17G1S steel than that of X60 steel. It is found that in welding with basic coating electrodes, preheating temperature should be 20–50 °C for 17G1S steel and 70–100 °C for X60 steel in order to prevent cold cracking. At application of electrodes with cellulose coating the temperature should be increased by 60–80 °C.

2. Testing of Implant samples with a notch along and across the rolling direction showed differences in delayed cracking resistance of steel. In the first case, because of simultaneous negative influence of diffusible hydrogen and sulphide inclusions cold cracking resistance of X60 steel is higher than that of 17G1S steel. In the second case 171GS steel had higher values of critical breaking stresses.

3. By the results of testing samples for tension along Z axis the studied steels were ranged by their lamellar cracking susceptibility in the joint zone, depending on sulphur content.

4. Possibility of prediction of lamellar cracking probability by the following parameters was established: reduction along Z axis, impact toughness and crack opening displacement on samples with a notch along the rolling direction; delayed fracture critical stress; base metal fracture surface fractographs.

5. To lower the risk of cold cracking during repair performance in operating MGP, it is necessary to apply electrode materials, ensuring a low content of diffusible hydrogen in the deposited metal, use thermal annealing effect from the previous pass of multilayer weld, perform welded joint postweld heating in the case of load application in the direction normal to pipe surface.

6. To prevent lamellar cracking in repair structures on main pipelines it is rational to first perform deposition of a buffer layer of less strong metal or cutting out the pipe wall surface layer with its subsequent filling by welding consumable ensuring equivalent strength of welded joint.

1. But, V.S., Gretsky, Yu.Ya., Rozgonyuk, V.V. (2001) Substantiation of new approach to realize welding operations on pipelines under pressure. *Naft. i Gaz. Promyslovist*, **4**, 33–39.
2. Drogomiretsky, M.M. (2006) In-pipe diagnostics of main gas pipelines and repair of detected defects. In: *Proc. of Sci. Seminar on Reliability Assurance of Pipeline Transport Systems* (Kiev, 11 April 2006). Kiev: Ekotekhnologiya.
3. But, V.S., Olejnik, O.I. (2007) Main trends in technology for repair of active pressurized main pipelines. *The Paton Welding J.*, **5**, 30–35.
4. *GBN V.3.1-00013741-12:2011*: Main gas pipelines. Repair arc welding in service conditions. Introd. 06.09.2011. Kiev: Ministry of Energy and Coal Industry of Ukraine.
5. But, V.S., Olejnik, O.I. (2011) Evaluation of technological and structural strength of welded joints of structures to be repaired on main pipelines. In: *Proc. of Sci.-Pract. Conf. on Residual Resource and Problems of Modernization of Systems of Main and Commercial Pipelines* (Kiev, 12–13 April 2011). Kiev: PWI.
6. Shorshorov, M.Kh., Chernyshova, T.A., Krasovsky, A.I. (1972) *Weldability testing of metals*. Moscow: Metallurgiya.
7. *TU U 27.2-19305558-001:2007*: Structural reinforcing elements of pipelines. Valid from 03.07.2007.
8. (1998) *Kobelko Welding Today*, **2**, 2.
9. Makarov, E.L. (1981) *Cold cracks in welding of alloy steels*. Moscow: Mashinostroenie.
10. (1974) *Technology of electric fusion welding of metals and alloys*. Ed. by B.E. Paton. Moscow: Mashinostroenie.
11. Granjon, H.J. Recommendation for the use of Implant test as a complementary information test on the cold cracking susceptibility during the welding of steels. *IIW Doc. IX 830–73*.
12. *GOST 23338–91*: Welding of metals. Methods for determination of diffusion hydrogen content in deposited and weld metal. Introd. 01.07.92. Moscow: Gosstandart SSSR.
13. Suzuki, H. (1983) Weldability of modern structural steels in Japan. *Transact. Iron and Steel Inst. of Japan*, 23(**3**), 189–204.
14. Vikhlevshchuk, V.A., Chernogritsky, V.M., Fedorova, I.P. (1989) Improvement of reliability of welded structures by reduction of sulfur content in steel. *Avtomatich. Svarka*, **4**, 1–6.
15. Kirian, V.I. (1984) Method of evaluation of structural steel resistance to ductile fracture. *Ibid.*, **11**, 1–6.
16. Farrar, J.C.M., Dolby, R.E., Baker, R.G. (1969) Lamellar tearing in welded structural steels. *Welding J.*, **7**, 274–282.
17. But, V.S., Marchuk, Ya.S., Mandra, A.S. *Method of joining of branchpipe to gas pipeline in service*. Pat. 40033 Ukraine. Int. Cl. F16L 41/00. Publ. 25.03.2009.
18. But, V.S., Maksimov, S.Yu., Olejnik, O.I. et al. *Process of liquidation of technological openings in main pipelines*. Pat. 11796 Ukraine. Int. Cl. F16L 55/16, E21F5/00. Publ. 16.01.2006.

Received 05.06.2014

INTEGRATED EVALUATION OF EFFECT OF MAIN IMPURITIES ON WELDABILITY OF COPPER

V.A. ANOSHIN[1], **V.M. ILYUSHENKO**[1], **A.N. BONDARENKO**[1], **E.P. LUKIANCHENKO**[1] and **A.K. NIKOLAEV**[2]
[1]E.O. Paton Electric Welding Institute, NASU
11 Bozhenko Str., 03680, Kiev, Ukraine. E-mail: office@paton.kiev.ua
[2]OJSC «Institute Tsvetmetobrabotka»
5 Pyzhevsky Lane, 119017, Moscow, RF. E-mail: post@cmet.ru

The wide application of commercial grades of copper, containing different impurities, in many fields of industry requires profound analysis of their influence on weldability. At the present work the integrated evaluation of effect of main impurities on copper susceptibility to formation of cracks and pores was made using electron-fractographic and X-ray analysis and also new methods, developed by the authors, for evaluation of tendency of copper to formation of solidification cracks. It is shown that simultaneous presence of different impurities in copper unlike the binary system of copper–impurity reduces its tendency to solidification crack formation. Content of 0.2 % Ni increases the crack resistance of copper. It was established that level of influence of low-melting impurities on crack formation in weld metal and near-weld zone depends on their distribution coefficient. It was for the first time established that low-melting surface-active impurities with a low distribution coefficient ($K < 0.05$) increase the tendency of welds to pore formation. The obtained results of investigations allow developing new consumables for welding of copper and its alloys. 15 Ref.. 2 Tables, 3 Figures.

Keywords: *copper, impurities, solidification cracks, pores, electron-fractographic and X-ray spectral analysis, distribution coefficient*

The copper is widely applied in different fields of industry, including manufacture of welded assemblies and structures. The practical experience shows that copper in welding possesses an increased tendency to formation of cracks and pores [1–7]. Earlier, in collaboration with the Institute «Gidrotsvetmetobrabotka» (Moscow) the investigations of influence of harmful impurities on tendency to formation of cracks in weld metal on copper–impurity binary systems [7] were carried out. Some results of these investigations are presented in Figure 1.

In the present work the results of investigations of influence of different combinations of impurities (13 impurities within the limits of GOST 859–78 «Copper. Grades» for the copper M2) on tendency to formation of solidification cracks are given.

To carry out these investigations using method of mathematical planning of experiments the compositions of experimental melts of copper with different content of impurities were calculated. At the Institute «Gidrotsvetmetobrabotka» the ingots were melted, from which after

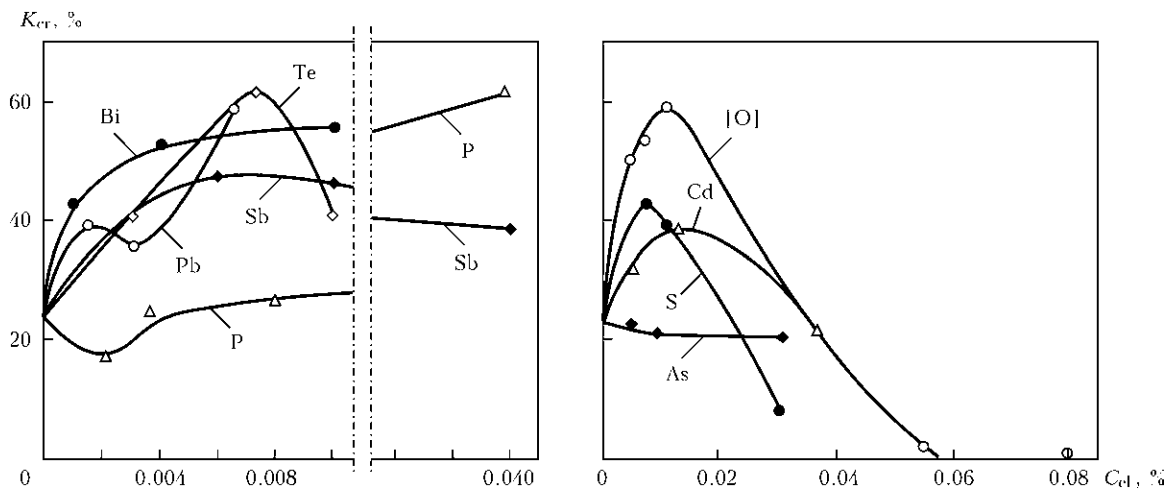

Figure 1. Influence of impurities on crack formation in copper [7]

Table 1. Calculation content of impurities and tendency of experimental melts of copper to crack formation

Number of alloy	Content, wt.%													K_{cr}, %, at v_w, m/h		
	Bi	S	Pb	[O]	P	Sb	As	Cd	Se	Te	Fe	Ni	Sn	14	8	6
201	0	0	0.005	0.01	0.01	0	0.01	0	0.005	0.005	0.05	0	0.05	27	14	6
202	0.002	0	0	0.01	0	0	0	0	0	0	0	0	0.05	21	9	5
203	0	0.005	0	0.01	0.01	0	0	0.01	0.005	0.005	0	0.2	0	23	8	0.5
204	0.002	0.005	0.005	0.01	0.01	0.005	0	0	0.005	0	0.05	0	0.05	41	20	11
205	0	0	0	0	0	0.005	0.01	0.01	0	0.005	0	0	0	26	12	8
206	0.002	0	0.005	0	0.01	0.005	0.01	0	0.005	0.005	0	0.2	0.05	42	22.5	0
207	0	0.005	0.005	0	0	0.005	0.01	0	0.005	0	0.05	0.2	0	31	0.5	0.5
208	0.002	0.005	0	0	0	0	0	0.01	0	0.005	0	0	0	42.5	3.5	2
209	0	0	0.005	0	0	0.005	0	0.01	0	0.005	0.05	0.2	0.05	31	6	6
210	0.002	0	0	0	0	0.005	0	0	0	0	0	0.2	0.05	29	7	6
211	0	0.005	0	0	0.01	0	0.01	0	0.005	0	0	0	0	41	14	6
212	0.002	0.005	0.005	0	0.01	0	0	0	0	0	0	0.2	0	23	5	0.5
213	0	0	0	0.01	0.01	0.005	0	0.01	0	0.005	0.05	0.2	0	27	0.5	0
214	0.002	0	0.005	0.01	0	0	0.01	0.01	0.005	0.005	0.05	0	0	44	4	5
215	0	0.005	0.005	0.01	0	0	0.01	0.01	0.005	0	0.05	0.2	0.05	51	9	0.5
216	0.002	0.005	0	0.01	0.01	0.005	0.01	0.01	0	0	0.05	0	0.05	44	16	13
41	Copper of grade M00 acc. to GOST 859–78													23	9	0.5

rolling into strips of 3 mm thickness the specimens of the type LTPM (60 × 25 × 3 mm) were cut out. According to the methods described in [7] the tendency of experimental melts of copper to formation of cracks in weld metal were evaluated. The chemical composition of experimental melts and results of tests are given in Table 1.

As is seen from the Table the mutual presence of different impurities in copper decreases its tendency to crack formation as compared to the copper–impurity binary systems [7]. It is especially noticeable on the example of melts 201, 202, 205, that, in our opinion, is connected with the formation of chemical compounds between the impurities (Bi_2O_3, Bi_2S_3, PbO, PbS, PbSe, PbTe, As_2Te_3, Cd_3As_2, CdSe, CdTe, Se_2Te_3, Sb_2Se_3) and, respectively, with decrease of their surface activity. The similar phenomenon is observed in welding of low-carbon steel, when introduction of oxygen into weld metal resulted in sulfur binding into low-melting oxysulfides, but here the surface activity of sulfur decreased and resistance to formation of solidification cracks increased. The presence of 0.2 % of nickel in copper (copper M2, M3 according to GOST 859–78) decreases considerably its tendency to crack formation (see Table 1, melts 203, 207, 212, 213) and its tendency to formation of solidification cracks is at the level of copper M00 (melt 41). In our opinion, this is also explained by the formation of chemical compounds of harmful impurities with nickel (NiO, NiSe, NiTe, NiSb, Ni_3P, NiBi).

To study the nature of crack formation, caused by harmful impurities, the electron fractographic and X-ray spectral analysis of structure and composition of crack surface was carried out. As is seen from Figure 2, *a*, cracks have an intercrystalline nature. At the surface of cracks in copper, containing harmful impurities (bismuth, sulfur, lead), the traces of liquid phase in the form of drop-like shaped branches, beads and dendrite crust are observed (Figure 2, *b–d*). In Figure 2, *e* the liquid interlayer, containing selenium is presented; in Figure 2, *f* the structure of crack surface on copper of grade M1 without introduction of any impurities is shown. The results of electron-fractographic analysis of crack surface evidences of crystallization nature of cracks forming in welding of copper.

X-ray spectral analysis of crack surface composition showed considerable (by one order and higher) enrichment of liquid interlayer with harmful impurities. It should be noted that the investigated low-melting impurities are the surface-active elements. This was shown by our calculations according to the criterion of Zhukovitsky ($\Delta\sigma = \sigma_{me} - \sigma_{im} >> 0$), and also experimental data [8–11] for some impurities (bismuth, lead, phosphorus, antimony). The mechanism of influence of harmful impurities on tendency to formation of solidification cracks, in our opinion, is connected with behavior of effect of adsorption decrease in ductility and strength (liquid-metal embrittlement) as a result of physical and chemical interaction of crystallizing liquid metal, enriched with harmful impurities with a solid phase. This is confirmed by an abrupt embrittlement action of molten bismuth in the contact with copper during tests at elevated temperatures. The same embrittlement effect is observed

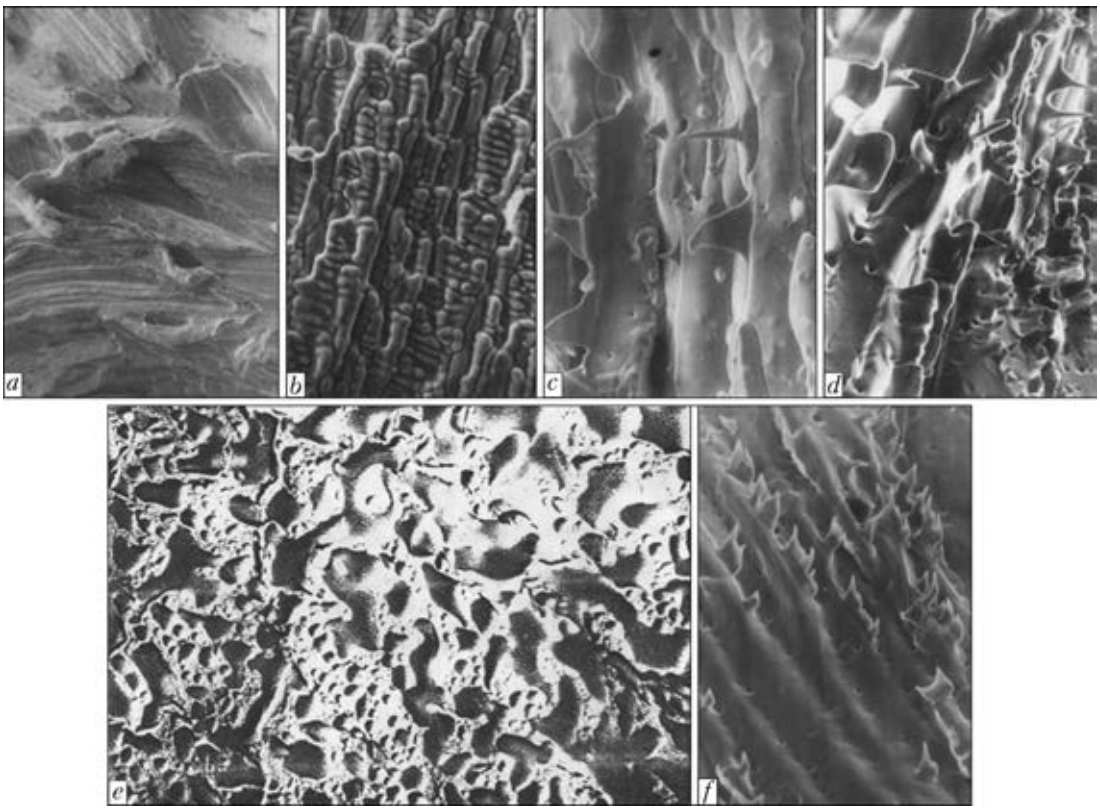

Figure 2. Typical intercrystalline character of cracks (*a* — ×100), structure of surface of cracks on copper, containing bismuth (*b* — ×1000), sulfur (*c* — ×600), lead (*d* — ×800), selenium (*e* — ×12000), and on copper M1 (*f* — ×800)

at interaction of sulfur and other surface-active elements with nickel, copper and also alloy of nickel with copper [12].

To study the influence of some harmful impurities (bismuth, lead, phosphorus) on tendency of crack formation in the near-weld zone, the ingots of copper–impurity binary alloy with different content of mentioned impurities were melted in vacuum induction furnace at the E.O. Paton Electric Welding Institute. The alloys were preliminary rolled for strips of 5 mm thickness. The evaluation of experimental alloys was carried out according to the special methods developed by us [13] on «fish skeleton» specimens of a variable rigidity. The specimens were welded using tungsten electrode with partial penetration in argon at different energy inputs.

It is seen fom the test results (Table 2) that the most negative influence have bismuth and lead (cracks in near-weld zones are formed on cross and longitudinal notches) and phosphorus in the least degree, the negative influence of which begins to be revealed only at higher concentrations (>0.005 %). The correlation between the coefficient of impurity distribution and tendency to formation of near-weld cracks is observed, i.e. the lower it is, the more enriched will be grain boundaries with harmful impurity and, correspondingly, the tendency to crack formation will be higher.

Table 2. Tendency of copper welded specimens to crack formation and equilibrium coefficient of impuritty distribution in them

Content of impurity, wt.%		Welding mode						*K*
		I_w = 160 A, v_w = 17 m/h		I_w = 200 A, v_w = 23 m/h		I_w = 200 A, v_w = 25 m/h		
		n_{long}	a_{trans}	n_{long}	a_{trans}	n_{long}	a_{trans}	
Bi	0.001	+ + –	– – –	+ – –	– – –	+ –	10 –	0.0001
	0.004	+	13, 15	– +	– – 15	+	– 13 –	
	0.1	+	10, 13, 15, 18	+	13, 15, 18	+	10, 13, 15, 18	
Pb	0.005	+	13	+	10, 13	+	10, 13, 15	0.01
	0.01	+	13	+	15	–	13	
	0.05	+	10, 13, 15, 18	+	10, 13, 15, 18	+	10, 13, 15	
P	0.005	–	–	–	–	–	–	0.2
	0.05	+	–	+	10	+	10	

Notes. 1. n_{long} — presence/absence of cracks in longitudinal notch. 2. a_{trans} — distance between transverse notches.

The influence of bismuth and lead on porosity of welds on copper, containing 0.04 % P, was also studied. The results of tests of experimental specimens, welded using tungsten electrode in argon, showed that in absence of bismuth and lead the porosity is not observed, at 0.003 % Bi 10 pores were observed, at 0.003 % Bi and 0.03 % Pb 20 pores were revealed. Thus, bismuth and its mutual action with lead increase the porosity of welds even at their low concentrations. In our opinion, this is explained by the fact that due to low distribution coefficient of these elements in copper they sufficiently (as was mentioned above, are by one order and higher) enrich liquid metal at the solidification front and at the final stage of solidification. Being surface-active elements, they decrease surface tension of liquid copper and, thereby, reduce critical radius of gas nucleus:

$$r_{cr} = \frac{2\sigma M}{\rho RT \ln (c/c_s)} \text{ [14]},$$

which, in its turn, decreases considerably the work of its formation:

$$\Delta\sigma_{cr} = \frac{4}{3}\pi r_{cr}^2 \sigma.$$

Besides, low-melting impurities with small distribution coefficient due to concentration overcooling facilitates the formation of toothed (cellular) solidification front, that also increases the feasibility of pores origination. To compare the influence of impurities on pores formation below the values of equilibrium coefficient of their distribution are given, calculated by us according to the constitution diagrams of copper–impurity: $K = 0.0001$ (Bi); 0.02 (Te); 0.004 (S); 0.008 (Se); 0.01 (Pb); 0.01 ([O]); 0.036 (Cd); 0.2 (P); 0.35 (Sb).

The electron fractographic analysis showed (Figure 3) the presence of micropores (nuclei) forming in a liquid interlayer along the boundaries of crystallites under the influence of impurities with small distribution coefficient ($K \le 0.05$). At the presence of antimony ($K = 0.35$) and phosphorus ($K = 0.2$) in copper the pores were not revealed. It is obvious that phosphorus facilitates the suppression of pore formation as deoxidizer neutralizing the harmful effect of oxygen [15].

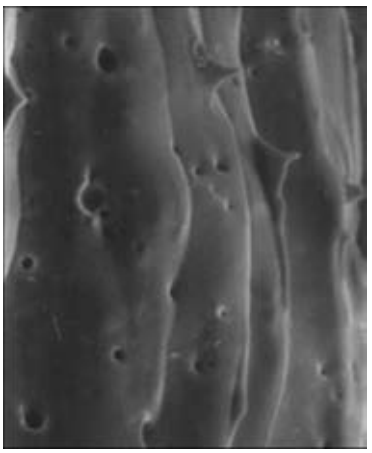

Figure 3. Pores in liquid interlayer along the boundaries of crystallites in the presence of impurities with $K < 0.05$ (×1250)

Conclusions

1. Study of influence of combined action of different impurities on tendency of copper to crack formation showed that simultaneous presence of different impurities in copper, including 0.2 % Ni, increases its resistance to crack formation that, in our opinion, is predetermined by formation of chemical compounds and decrease of surface activity of impurities.

2. The increased content of bismuth and lead in copper (within the limits of GOST 859–78) contributes to crack formation in the near-weld zone.

3. The level of influence of low-melting impurities on crack formation in weld metal and near-weld zone depends on their distribution coefficient.

4. It was for the first time established that low-melting surface-active impurities with small distribution coefficient ($K < 0.05$) increase tendency of welded joints to pore formation.

1. Nikolaev, A.K., Kostin, S.A. (2012) *Copper and heat-resistant alloys*: Fundament. Refer. Book. Moscow: DPK Press.
2. Korenyuk, Yu.M. (1967) Resistance to crack formation in welds containing Bi and Pb impurities in welding of copper. *Svarochn. Proizvodstvo*, **4**, 8–10.
3. Abramovich, V.R., Demyantsevich, V.P., Efimov, L.A. (1988) *Fusion welding of copper and alloys on copper base*. Leningrad: Mashinostroenie.
4. Kobayashi, T., Kuwana, T., Ando, M. et al. (1970) Gas metal-arc welding of copper. *Transact. of JWS*, **1**, 61–71.
5. Littleton, J., Lammas, J., Jordan, M.E. (1974) Nitrogen porosity in shielded gas arc welding of copper. *Welding J.*, 53(**2**), 561–566.
6. Ilyushenko, V.M. (1985) Weldability of commercial grades of copper. In: *Advanced methods of welding and surfacing of heavy non-ferrous metals and alloys*. Kiev: PWI.
7. (2013) *Welding and surfacing of copper and alloys on its base*. Kiev: IAW.
8. Yatsimirsky, V.K., Vyazmitinova, O.M. (1972) Surface activity of components in alloys and their catalytic properties. In: *Wettability and surface properties of melts and solids*, 134–136. Kiev: Naukova Dumka.
9. Grigoriev, A.G., Alshevsky, V.S., Zhukovitsky, A.A. et al. (1972) Effect of metal vapors on surface tension of solid copper. *Ibid.*, 171–174.
10. Nizhenko, V.I., Floka, L.I. (1981) *Surface tension of metals and alloys*: Refer. Book. Moscow: Metallurgiya.
11. Semenchenko, V.K. (1957) *Surface phenomena in metals and alloys*. Moscow: GITEL.
12. Anoshin, V.A., Gurevich, S.M., Ilyushenko, V.M. et al. (1981) Effect of surface-active elements on deformation capacity of nickel and monel. *Avtomatich. Svarka*, **7**, 46–48.
13. Anoshin, V.A., Ilyushenko, V.M., Bondarenko, A.N. et al. *Method for evaluation of metal susceptibility to cracking*. USSR author's cert. 747662. Int. Cl. B 23 K 28/00. Publ. 15.07.80.
14. Patskevich, I.R., Deev, G.F. (1974) *Surface phenomena in welding processes*. Moscow: Metallurgiya.
15. Ilyushenko, V.M., Anoshin, V.A., Bondarenko, A.N. et al. (1981) Weldability of copper deoxidized by phosphorus. *Avtomatich. Svarka*, **12**, 59–60.

Received 19.06.2014

INVESTIGATION OF WEAR RESISTANCE OF COMPOSITE ALLOYS UNDER THE CONDITIONS OF GAS-ABRASIVE WEAR AT ELEVATED TEMPERATURES

A.P. ZHUDRA
E.O. Paton Electric Welding Institute, NASU
11 Bozhenko Str., 03680, Kiev, Ukraine. E-mail: office@paton.kiev.ua

Given are the results of laboratory investigations of wear resistance of composite alloys, based on fused tungsten carbides WC + W_2C (relite), under conditions of gas-abrasive wear. Given is the technical characteristic of laboratory stand OB-876Ts for tests of deposited metal for gas-abrasive wear. The scheme of tests was developed, maximum corresponding to real conditions of service of parts during the effect of abrasive flow within the temperature range of 25–450 °C. It was established that wear of composite alloys bears a selective, cyclic character and does not essentially depend on properties and hardness of matrix at small attack angles. The application of tungsten carbide with spherical granules increases wear resistance of composite alloy, and the increase in temperature up to 400 °C considerably decreases it due to oxidation of carbide component of alloys. At room temperature the wear resistance of composite alloy 2.7 times exceeds the wear resistance of nickel carbide chromium alloy. 9 Ref., 3 Tables, 3 Figures.

Keywords: *gas-abrasive wear, composite alloys, fused tungsten carbide, spherical granules, matrix, microhardness, plasma-powder surfacing, relative wear resistance, test stand*

The present work is the continuation of the earlier investigations, performed at the E.O. Paton Electric Welding Institute, on gas-abrasive wear of different types of hardfacing alloys [1–4], among which the composite alloys on the base of fused tungsten carbides WC + W_2C (relite) are of a peculiar interest. These alloys are featured by a unique wear resistance and widely applied for deposition of drilling tool and a number of critical parts in metallurgy and machine building. In work [2] the investigations of wear resistance of such alloys under the conditions of gas-abrasive wear were conducted in machine OB-876 [5] at the temperature of 400 °C on cylindrical specimens of 60 mm diameter with different compositions of matrix alloys, reinforced with fused tungsten carbides by granulation from 0.18 to 2 mm. The specimens were manufactured using laboratory method in induction furnace by pouring the granules of crushed tungsten carbide through the layer of flux with the next cutting out of the most reinforced areas by the anode-mechanical method. The composite alloys produced on the specimens in such a way are considerably different from real ones deposited using the arc or gas method. Therefore, there was an interest to investigate the wear resistance of composite alloys produced using industrial conventional methods of hardfacing, among which the most characteristic method for producing of such alloys is the method of plasma-powder surfacing, which found over the recent years the wide development in the world practice. This method restricts the heat effect of the arc on the granules of carbides during their supply to weld pool that considerably decreases their dissolution in the matrix alloy. The concentration of reinforcing phase in the deposited layer can reach 50 %.

For the tests the specimens were prepared deposited using plasma-powder method by composite alloys in one layer. As the reinforcing phase the powders of fused tungsten carbides WC + W_2C (relite) with traditional crushed and also spherical granules were used. The spherical granules, produced according to the technology of thermal centrifugal spraying of ingots of fused tungsten carbides [6, 7] developed at the E.O. Paton Electric Welding Institute, are featured by high microhardness, homogeneous structure and as to the physical and chemical properties they are superior to the similar domestic and foreign materials produced according to other technologies [8, 9].

The granulation of powder of crushed and spherical tungsten carbides was within the limits of 50–250 μm. The averaged chemical composition and microhardness of both types of carbides are given in Table 1.

Table 1. Chemical composition and hardness of tungsten carbides with spherical and crushed particles (tungsten — base)

Type of granules of tungsten carbide	Chemical composition, wt.%				Microhardness *HV*100
	C_{total}	C_w	Fe	Impurities	
Spherical	3.98	0.05	0.10	0.95	2600–3100
Crushed	3.89	0.15	0.14	1.45	1900–2200

Table 2. Chemical composition and hardness of alloy of matrices (nickel — base)

Type of powder of matrix alloy	Chemical composition, wt.%					Hardness *HRC*
	C	Cr	Si	B	Cu	
PG-SP2	0.53	13.82	2.43	2.25	–	58.63
PG-ND42SR	0.15	–	1.05	1	42.5	38.46

For the matrix alloy the powders on nickel base PG-SR2 and nickel-copper base PR-ND42SR were used, the averaged chemical composition of which is given in Table 2.

After deposition the thickness of composite layer on the specimens was 5.0–5.5 mm. Here it should be noted that due to a great mass the reinforcing granules of tungsten carbide, as a rule, are located in the lower part of weld pool. Therefore, to obtain the optimal concentration of reinforcing phase on the surface of deposited layer, the specimens were subjected to grinding aflush for the depth of 1.0–1.5 mm. Finally the thickness of deposited layer amounted to about 4 mm, and concentration of carbide inclusions to the tested surfaces of specimens varied in the limits of 45–50 %.

As the reference, the specimens were accepted deposited by nickel carbide chromium alloy using flux-cored strip PL AN-111 in three layers with the thickness of deposition of 12 mm after grinding. The type of deposited metal is 500Kh40N40S2GRTs. The chemical composition of reference specimens is as follows, wt.%: 5.1 C; 34 Cr; 36 Ni; 2.1 Si; 1.2 Mn; 0.3 B; 0.3 Zr, the hardness of specimens was *HRC* 52–55.

Figure 1. General view of stand OB-876Ts

In all the cases the deposition was performed on the plates of steel of St3 grade 20 mm thick.

In Table 3 the types of specimens of deposited composite alloys for gas-abrasive wear tests at 25 and 400 °C are given. Each type of alloy for obtaining the maximum reliable data is represented by three specimens.

The tests on wear resistance of composite alloys, deposited using plasma-powder method, were carried out under the conditions of modeling the gas-abrasive wear on modified stand OB-876Ts. The stand allows performing wear of specimens using air-abrasive flow according to the certain scheme.

The acceleration of abrasive parts is performed by centrifugal accelerator in the form of a disc-rotor, in the centre of which the abrasive in the form of quartz sand of 0.05–0.50 mm granulation is gravity fed to the receiving hole.

Table 3. Types of specimens for tests on gas abrasive wear

Marking of specimens	Composition of matrix	Hardness of matrix *HRC*	Type of reinforcing phase	Hardness of reinforcing phase *HV*100
KN-1	Ni–Cr–Si–B	58–63	50 % crushed 50 % spherical	1800–2200 2800–2930
KN-2	Ni–Cr–Si–B	58–64	100 % spherical	2650–2880
KN-3	Ni–Cr–Si–B	54–59	Same	2730–3000
KM-4	Ni–Cu–Si–B	38–46	»	2750–3050
KM-5	Ni–Cu–Si–B	39–49	»	2800–2980
Reference specimen	C–Cr–Ni–Si–Mn	55–62	–	–

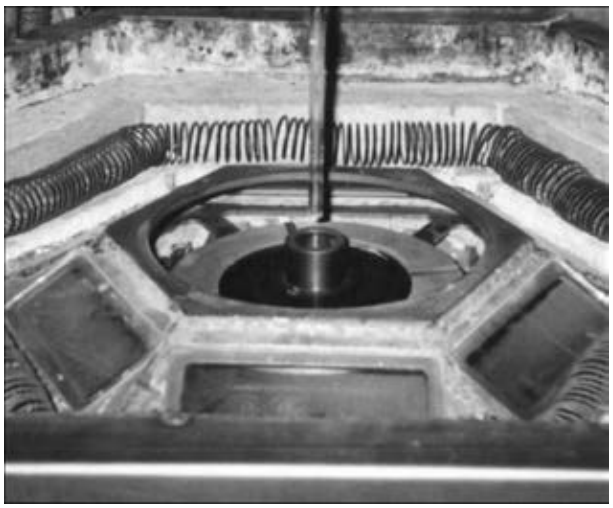

Figure 2. Cassette with specimens in heating chamber

The particles of sand are accelerated along four inner channels up to 200 m/s. Having achieved the outer diameter of rotor, the abrasive flow overcomes the air gap of 25 mm length and by the impacts of abrasive particles is wearing out the working surfaces of simultaneously six specimens of 170 × 70 × 19 mm. Here the angle of attack of abrasive with respect to the surface of specimens amounts to 15°. The cassette with specimens is located in the chamber, the temperature in which can be controlled in the limits of 25–450 °C. The general view of stand OB-876Ts and cassette with specimens are shown in Figures 1 and 2, and its main technical characteristics are represented below.

Technical characteristics of stand OB-876Ts

Rotor diameter, mm	220
Number of rotations of rotor, rpm	6000
Angle of attack of abrasive flow, deg	5–70
Temperature of heating of specimens, °C	up to 400
Duration of heating of specimens up to 400 °C, h	3.5
Consumption of abrasive, cm^3/s	0.5–0.3
Capacity of electric motor of rotor drive, kW	0.75
Number of test specimens, pcs	6

The wear of specimens was evaluated according to the decrease in volume in cm^3, which was determined by the method of hydrostatic weighing. Also the intensity of wear in cm^3 during consumption of each 100 kg of abrasive and relative wear resistance as to the reference, deposited by nickel carbide chromium alloy, were determined. The averaged data of investigations of three specimens of each type of composite alloy are given in Figure 3.

As it was expected, the general regularity of wear of composite alloys in gas-abrasive wear is its selectivity and cycling, i.e. change of wear resistance with time. Initially the matrix is worn out intensively, stripping the carbides, which protect matrix and sufficiently delay the wear of

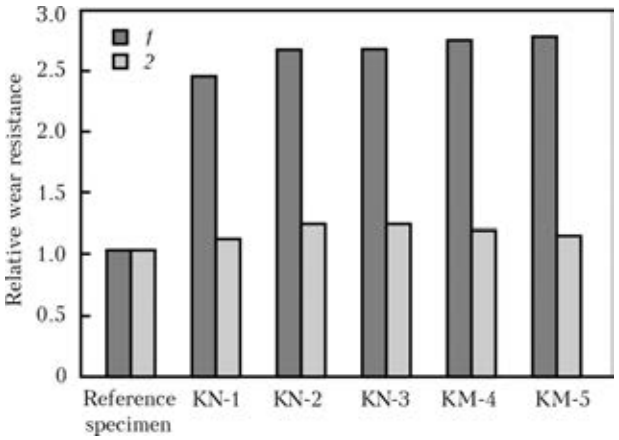

Figure 3. Relative wear resistance of specimens of composite alloys at 25 (*1*) and 400 (*2*) °C

alloy due to the shadow effect. After wear of matrix and washing out of carbides the cycle is repeated. The obtained results correlate well with the data of investigations described in [2].

At the angle of attack of abrasive of 15° the composition of matrix and its hardness practically does not influence the wear resistance of the composite alloy.

Under the conditions of room temperature the highest wear resistance belongs to composite alloys KN-2, KN-3 composed of spherical granules of tungsten carbide and matrices of the Ni–Cr–Si–B type. Their wear resistance approximately 2.7 times exceeds the wear resistance of reference specimen of nickel carbide chromium alloy. Alloy KN-1 with the similar matrix, but containing the mixture of spherical and crushed granules of tungsten carbides, possesses wear resistance of approximately lower by 10–12 %, that corresponds to the lower strength characteristics of crushed particles as compared to the spherical ones.

At 400 °C the wear resistance of composite alloys decreased considerably, though the tendency of increased resistance of compositions with spherical granules of carbides, as compared to the mixture, preserved. The increase in wear at elevated temperatures is, first of all, connected with oxidizing processes of the carbide component of alloys. The wear of tungsten carbides occurs not only due to the effect of abrasive flow, but also due to their oxidation. This factor should be considered during hardening of parts using composite alloys based on tungsten carbides operating at high temperatures in the oxidizing environment. In the restoration or inert environments the temperature almost does not influence the wear resistance of composite alloys. At the practice this is observed during operation of charging equipment of blast furnaces after hardfacing by composite alloys based on relite, which are operated in the restoration gas environment.

This equipment is labor-intensive in manufacture, however its resistance several times exceeds the equipment after hardfacing by carbide-chromium alloys.

Conclusions

1. The wear of composite alloys on the basis of fused tungsten carbides under the conditions of effect of gas abrasive flow bears selective, cyclic nature and negligibly depends on properties and hardness of matrix at the angle of attack of 15°.

2. Even partial use of spherical granules of tungsten carbide as the reinforcing phase instead of crushed increases the wear resistance of composite alloy by 10–12 %.

3. Wear resistance of composite alloys under the conditions of gas-abrasive wear at the room temperature approximately 2.7 times exceeds the wear resistance of nickel carbide chromium alloy, and at the temperature of 400 °C it decreases considerably due to oxidation of carbide component of the alloy.

1. Tereshchenko, N.F., Gavrish, V.A. (1971) Resistance of alloys in gas-and-abrasive wear. *Fiz.-Khimich. Mekhanika Materialov*, **4**, 18–21.
2. Yuzvenko, Yu.A., Zhudra, A.P., Frumin, E.I. et al. (1972) Peculiarities of gas-and-abrasive wear of composite alloys. *Avtomatich. Svarka*, **8**, 35–38.
3. Yuzvenko, Yu.A., Zhudra, A.P., Frumin, E.I. (1973) Abrasive wear of composite alloys. *Ibid*., **7**, 62–63.
4. Yuzvenko, Yu.A. (1978) *Investigation and development of materials and technologies of mechanized open-arc surfacing*: Syn. of Thesis for Dr. of Techn. Sci. Degree. Kiev: PWI.
5. Yuzvenko, Yu.A., Gavrish, V.A. (1972) Machine for assessment of wear resistance of deposited metal in gas-and-abrasive erosion. *Avtomatich. Svarka*, **6**, 73–74.
6. Litvinenko, A.I., Zhudra, A.P., Bely, A.I. (2013) Analysis and kinetics of centrifugal spraying of ingots from fused tungsten carbides. *Sovr. Elektrometallurgiay*, **2**, 29–36.
7. Dzykovich, V.I. (2009) Effect of the centrifugal thermal spraying process on properties of spherical tungsten carbide particles. *The Paton Welding J*., **4**, 43–45.
8. Dzykovich, V.I., Zhudra, A.P., Bely, A.I. (2010) Properties of tungsten carbide powders produced by different technologies. *Ibid*., **4**, 22–24.
9. Bely, A.I. (2010) Wear resistance and strength of tungsten carbides WC–W_2C produced by different methods. *Ibid*., **12**, 15–17.

Received 01.10.2014

SYSTEM FOR MEASUREMENT OF TEMPERATURE OF BIOLOGICAL TISSUES IN BIPOLAR HIGH-FREQUENCY WELDING

Yu.N. LANKIN, L.F. SUSHY and **E.N. BAJSHTRUK**
E.O. Paton Electric Welding Institute, NASU
11 Bozhenko Str., 03680, Kiev, Ukraine. E-mail: office@paton.kiev.ua

HF welding of soft biological tissues using bipolar electrosurgical instrument is basically similar to resistance spot welding of metals. Physical-biological processes, taking place in tissues during welding, mainly arise from their heating and applied pressure. Thus, information about temperature in contact of tissues during welding is very important. There are virtually no publications on equipment and measuring of temperature in welding of biological tissues. Standard thermocouples with wires of small diameter (70 μm), as the tiniest, were used as temperature probes. Heat generation of thermocouple due to welding current passing through it is virtually absent in comparison with heat generation in tissue. Distortion of electric and temperature fields in the vicinity of thermocouple can be neglected. Thermal time constant of chosen thermocouple makes around 8 ms based on reference data. Measurement system consists of chromel-alumel thermocouple with wire of 70 μm diameter, themoEMF amplifier, analog filer of lower frequencies, ADC and laptop. The experiments show that thermocouple can be represented by pure first-order time delay. Thermal time constant of thermocouple is 4.3 ms, time delay makes around 1 ms. Analog filter of lower frequencies completely suppresses welding current noises and determines general band of temperature measurement system of 25 Hz width. Developed system allows for measuring the temperature in contact of biological tissues during HF welding using bipolar electrosurgical instrument without dynamic errors and provides no distortions in tissue temperature field. 9 Ref., 6 Figures.

Keywords: *welding of biological tissues, measurement of temperature, thermocouple, thermal time constant, filtering of welding current noises*

Basically, bipolar HF welding of biological tissues is completely similar to resistance spot welding. Two parts of the tissue are compressed by two electrodes with some force and further heated by current passing through the tissue. Tissue significantly changes as a result of mutual effect of heat and applied pressure. It is denaturated, completely destructed and represents itself homogeneous mass of collagen, elastin and ground substances of tissues with significantly reduced boundaries between them, forming welded joint of two initially separated areas of tissue. Thus, heating of the tissues is a determining factor in HF welding of biological tissues. Therefore, it is important to know tissue temperature in welded joint being formed in study of all welding aspects. However, difficulties of measurement of temperature of joint during welding resulted in insufficient study of this problem.

We have found only one publication [1] providing experimental curves of change of temperature of albumin and wall of artery during heating by HF electric current using bipolar surgical instrument (Figure 1). Curves in this Figure are obviously significantly retouched and given only for illustration of dependencies of curve trend.

Several oscillograms of change of temperature of tissue in contact during welding (Figure 2) are also shown in the first PWI report on welding of biological tissues [2]. Unfortunately, the report does not provide for a procedure of temperature measurement. It was only indicted that the temperature was measured in «zone of welding».

Further the measurements of temperature were only carried out on the surface of tissue being welded in the electrode vicinity with the help of pyrometer. Experience of resistance spot welding of metals does not suppose sufficiently high correlation of this temperature with weld nugget parameters. Integral temperature of tissue surface in the electrode vicinity describes a width of HAZ and to significantly lesser degree welded joint itself. It should be noted that the HAZ width has a decisive impact on further angenesis in the welded joint.

There are several patents [3–7] on welding instrument using measurement of electrode temperature by thermocouples for control and automatic regulation of welding process. This method, the same as for resistance spot welding of metals, did not find practical application due

to complexity and unreliability of instrument and, principally, because of low correlation of temperature of electrode contact surface with temperature of contact in welding.

Temperature probe. Thickness of tissue in welded joint can be less than millimeter, that results in necessity of application of tiny temperature probes. The optimum solution is application of small diameter thermocouples. The industry produces thermocouples with wire diameter up to 4.5 μm [8]. Diameter of seam bead of such a thermocouple equals approximately three diameters of its wires, i.e. 15 μm. Widespread thermocouples of *J-(iron–constantan) or K*-type (chromel–alumel) suit well for 40–200 °C temperature range appearing in welding of biological tissues. Thermocouples of *K*-type of 70 μm diameter (0.0031″) were taken.

Welding of biological tissues is carried out using overlapping or along the flanged edges. The thermocouples are placed between the tissues to be welded along the electrode axis. As a result, part of welding current passes through it. Let's estimate heating of thermocouple by current passing through it. The heat, emitting in the thermocouple, is proportional to specific resistance of thermocouple material ρ. Specific resistances of wire material of used *K*-type thermocouple (chromel and alumel) equal 0.66 and 0.33 μOhm·m, respectively. Specific resistance of the most electro-conductive substance of human body — blood plasma — is 0.66 Ohm·m, i.e. 6 orders higher of specific resistance of thermocouple material. Therefore, welding current, passing through thermocouple seam, can not provide for additional heating and, thus, distort measurement results.

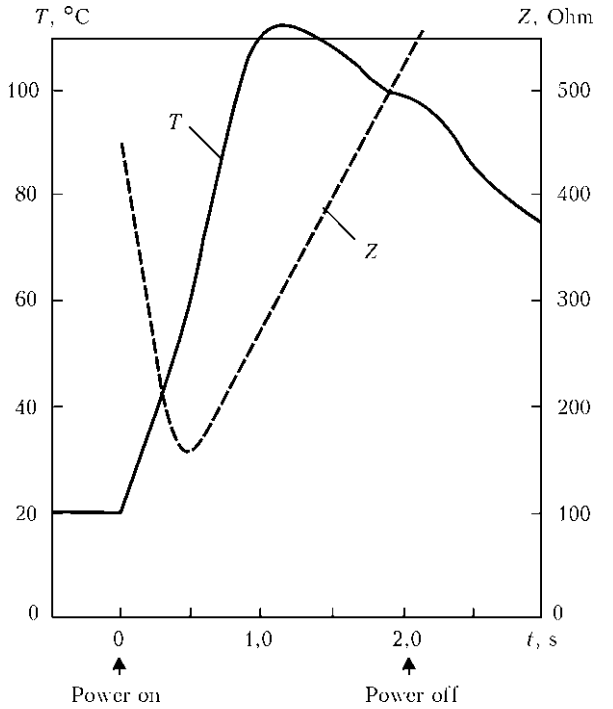

Figure 1. Change of temperature *T* and impendence *Z* of artery in heating by HF current [1]

High electric conductivity of thermocouple material provides for distortion of electric field in the vicinity of seam to be measured. Let's represent thermocouple in form of cylinder. Field density on the surface in external electrostatic field for conductive cylinder of relatively small diameter is proportional to cosine of angle between field density vector and corresponding ra-

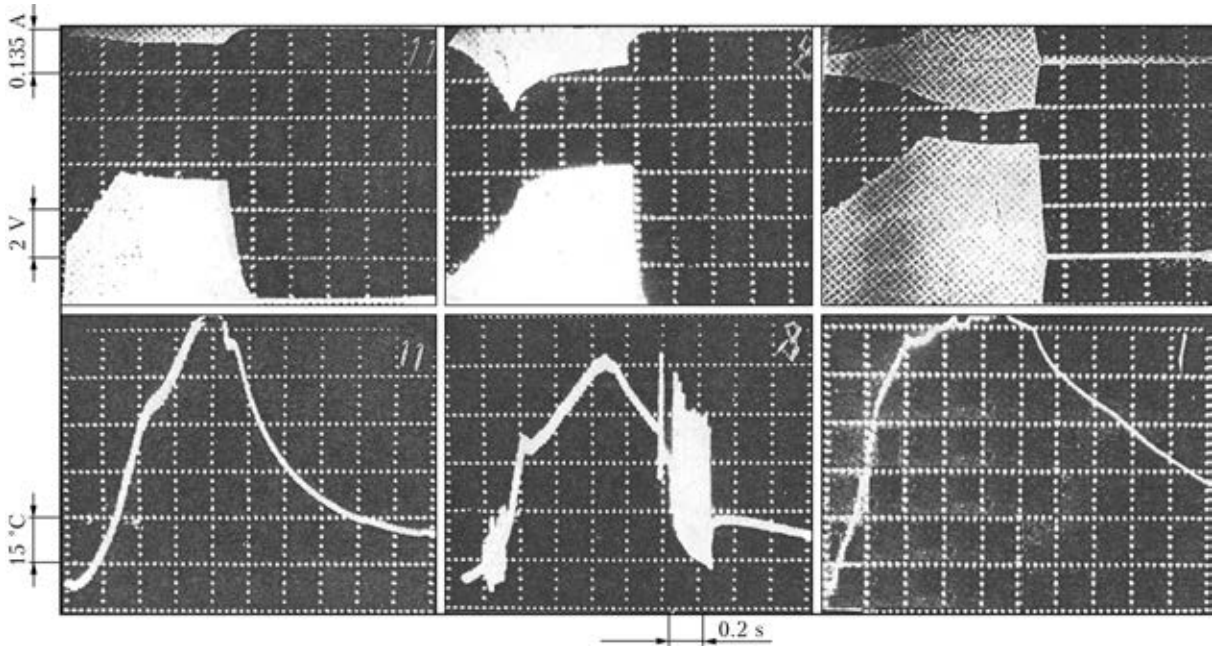

Figure 2. Oscillograms of welding current and voltage, temperature of contact in welding during variation of mode parameters [2]

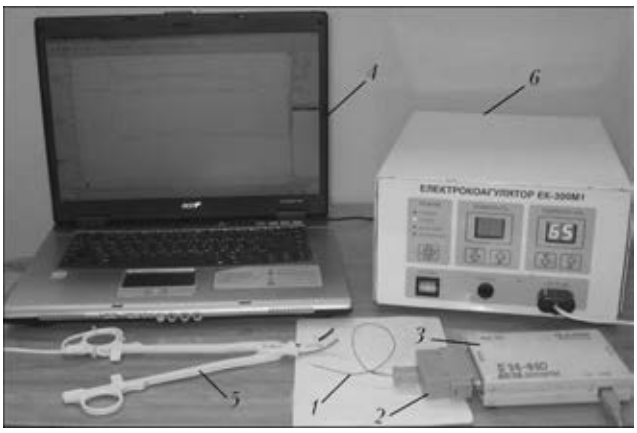

Figure 3. General view of system for temperature measurement in bipolar HF welding of soft biological tissues (for designations see the text)

dius-vector of cylinder [9]. Current density and emitting heat are respectively changed in this area. However, average heat emission on cylinder surface shows small variation and makes only 0.785 part of undisturbed electrostatic field. Since heat conduction of thermocouple material is around 90 W/(m·K) and that of water, determining heat conduction of biological tissues, makes approximately 0.68 W/(m·K), i.e. two orders lower, then the thermocouple temperature in the whole volume is similar and provides for alignment of nonuniformity of temperature in tissue adjacent to the thermocouple. Thus, effect of comparatively small thermocouple on temperature of tissues in welding can be neglected in first approximation.

Dynamic error of thermocouple depends on diameter of its wire. Experimental thermal time constant of iron-constantan thermocouple with wire diameter 0.005″, measured at holding in still water with 93 and 38 °C temperature, equals 0.04 s [8]. Heating time constant, based on theory of similarity, is proportional to square of diameter of thermocouple wire. Respectively, time constant equals 0.015 s for thermocouple of 0.0031″.

Data of *J*-type thermocouple is extrapolated to *K*-type thermocouple. According to homochronous criterion, time constant is inversely proportional to coefficient of thermal conductivity of material. $1.119 \cdot 10^{-5}$ m^2/s was taken as average for iron ($1.626 \cdot 10^{-5}$ m^2/s) and constantan ($0.612 \cdot 10^{-5}$ m^2/s). Material of *K*-type thermocouple consists from nickel by 90 %. Coefficient of thermal conductivity of nickel is $2.29 \cdot 10^{-5}$ m^2/s. Thus, it can be supposed that time constant of used chromel-alumel thermocouple will be 2 times lower than that of *J*-type thermocouple, i.e. around 8 ms.

System for temperature measurement. Figure 3 shows an experimental system of measurement of temperature in welding of biological tissues. The system consists of thermocouple *1*, amplifier of thermoEMF *2*, external ADC modulus E14-440 «L-Card» *3*, laptop with PowerGraph software *4*. Bipolar electrosurgical forceps *5* and HF electrocoagulator EK-300M1 *6* (serially manufactured by International Association «Welding») were used in measurements.

ThermoEMF amplifier was produced based on specialized microscheme AD592 Analog Device (Figure 4). Microscheme transforms thermoEDF of thermocouple into normalized voltage with conversion coefficient 10 mV/°C. Microscheme realizes imbedded compensation of cold seam and linearization of transfer characteristic for *K*-type thermocouple, that guarantees measurement accuracy of 1 °C in all range of measured temperatures.

Receiving *C*1, *R*1, *R*2, *C*2 and output *R*3 and *C*3 filters of lower frequencies were used for hardware filtering of noises of mains voltage and welding source.

The main noises in temperature measurement channel appear in passing of current through tissue being welded (Figure 5, *a*). It can be seen from Figure that level of noises in the output temperature signal is sufficiently high at absence

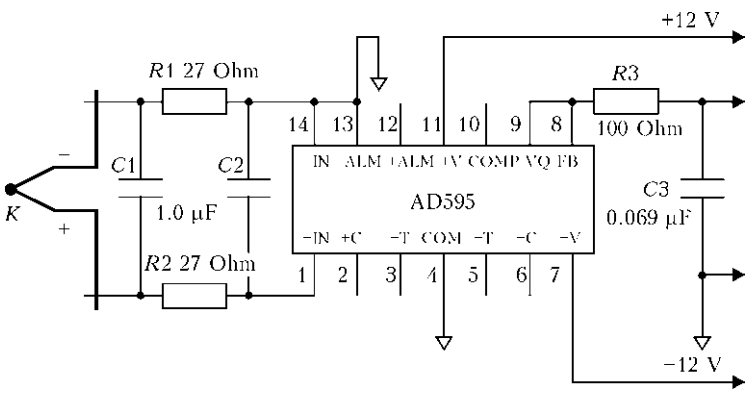

Figure 4. Schematic circuit of thermoEMF amplifier of chromel-alumel thermocouple

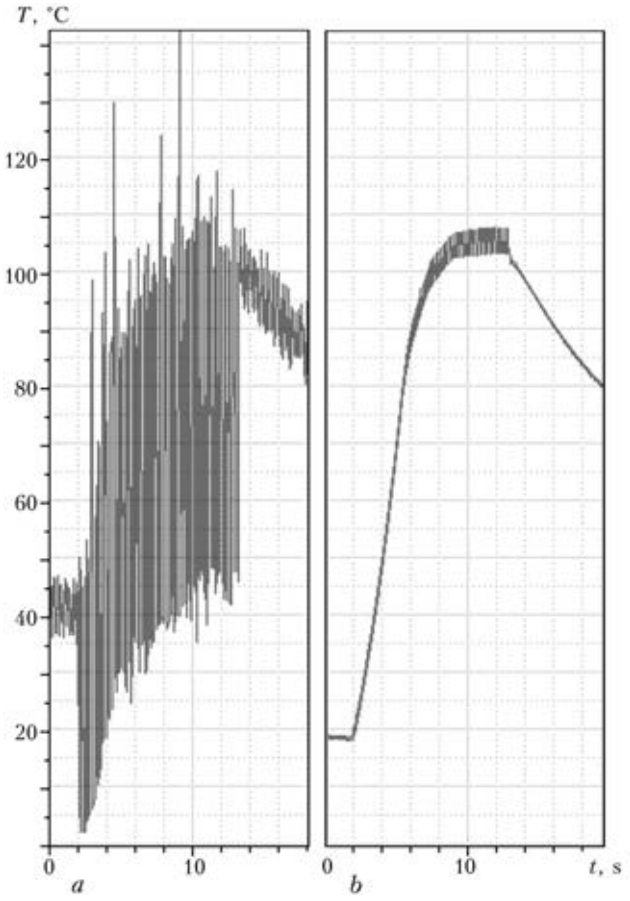

Figure 5. Registration of temperature in welding of pig intestine: *a* — without filtering; *b* — in presence of hardware filters of lower frequency acc. to Figure 4

of filtration. Applied multisection filter promotes almost complete elimination of noises and, at the same time, provides for acceptable pass band of measurement system 25 Hz.

The following experiments were carried out for estimation of response time of thermocouple with nomination amplifier. Specially designed device of spring-release machine type was used for quick positioning of thermocouple in hot water and fixing of curve of its temperature change, namely transient-response curve. Noise filters were removed from amplifier scheme (see Figure 4) for measurement of only thermal time constant of thermocouple. Figure 6 shows one of received transient-response curves. It looks like heating curves typical for real physical bodies, and is usually described by exponent with time constant T and time of pure delay τ. T = 4.3 ms and τ = 1.2 ms were found from Figure 6. In fact τ value is somewhat lower, since it included time of thermocouple heating by vapors during its movement to water surface.

It is supposed that thermo-physical properties of biological tissues to be welded are close to

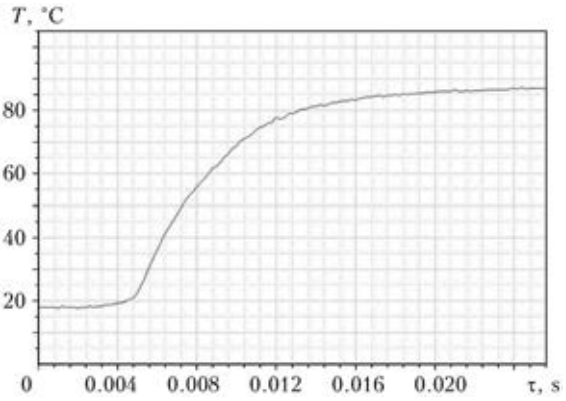

Figure 6. Curve of heating of thermocouple in water

properties of water. Coefficient of thermal conductivity of water in 40–90 °C range equals approximately $16 \cdot 10^{-8}$ m^2/s, that 2 orders lower than the coefficient of thermal conductivity of thermocouple material. Consequently, thermal time constant of the biological tissue is 100 times higher than thermocouple time constant. Therefore, it can be assumed that response time of the thermocouple do not provide for significant dynamic disturbances in measurement of temperature during welding of biological tissues even at welding current modulation. The main response time of temperature measurement system in our case is determined by pass band of electrical noise filter from welding current passing in area of hot thermocouple seam, and noises of supply mains.

It should be noted in the conclusion that the developed system allows measuring the real temperature of contact of biological tissues in HF welding using bipolar electrosurgical instrument without dynamic errors and significant disturbances in tissue temperature field.

1. Bergdahl, B., Vallfors, B. (1991) Studies on coagulation and development of an automatic computerized bipolar coagulator. *J. Neurosurg.*, 75(**8**), 148–151.
2. (1994) *Development of methods for welding of blood vessels*: Report UA 01009046 R. Kiev: PWI.
3. Ensslin, F.H. *Bipolar electrosurgical forseps*. Pat. 4,938,761 US. Publ. 07.1990.
4. Klisek, M.S. *Impedance and temperature generator for control*. Pat. 5,496,312 US. Publ. 03. 1996.
5. Strub, B., Alto, P. *Method and system for radiofrequency ablation of tissue*. Pat. 5,540,681 US. Publ. 07.1996.
6. Hassler, W.L. *Method and apparatus for electrosurgically treating tissue*. Pat. 5,540,684 US. Publ. 07.1996.
7. Baker, J.A. *Method and apparatus for welding blood vessels*. Pat. 6,083,223 US. Publ. 07.2000.
8. (1992) *Omega*: Complete temperature measurement handbook and encyclopedia. Engineering INC, Vol. 28.
9. Govorkov, V.A. (1968) *Electric and magnetic fields*. Moscow: Energiya.

Received 30.04.2014

STATE-OF-THE-ART AND PROSPECTS OF WORLD AND REGIONAL MARKETS OF WELDING MATERIALS (Review)*

A.A. MAZUR, S.V. PUSTOVOJT, O.K. MAKOVETSKAYA, N.S. BROVCHENKO and **V.S. PETRUK**
E.O. Paton Electric Welding Institute, NASU
11 Bozhenko Str., 03680, Kiev, Ukraine. E-mail: office@paton.kiev.ua

Electric arc welding is one of the basic technologies of an industrial economy, by means of which a significant share of GDP of industrialized countries is created. These countries are characterized by a stable development of welding production, which is defined by the growth in consumption of structural materials, emergence of new materials, technologies and equipment for welding to the market. The main structural material for manufacture of welded structures is steel, therefore, the state of the industry for its production defines mainly the dynamics of the welding production development. Economic-statistic information about the development of the world production and consumption of steel, dynamics of the world market of welding materials allows making conclusion about the increase of volumes of welding production in the world in the foreseeable future and growth of demand for the welding materials. At present the cost volume of the world market of welding materials amounts almost to a half of volume of the welding market. The growth in consumption of welding materials in the world is determined by the rates of development of the welding production in China, much more exceeding in this respect the rest countries and regions. Due to reduction in a share of manual arc welding and wider application of the semiautomatic and automatic welding the level of mechanization and automation of arc welding both in separate countries and also all over the world is continuously increased. 12 Ref., 5 Tables, 9 Figures.

Keywords: *welding, welding production, structural and welding materials, technologies, steel production, market, state-of-the-art, prospects*

The electric arc welding, becoming in the XX century as one of the basic technologies of industrial economy, did not also lose its importance today. The welding is a key method of producing the permanent joints of metals and non-metals, providing the creation of a significant share of GDP of the industrialized countries [1–3]. It is impossible to imagine the present civilization without welding and other allied processes. If suddenly all the welded, brazed and other permanent joints are ruined, then the mankind will remain without the majority of machines, mechanisms and other means of production and communication, without transport, electricity, buildings and constructions, habitual household appliances, without space. And even without computers, modern electronics and other material elements of the IT-technologies it is impossible to create the information-oriented society, i.e. the society of future.

Strategies of development of national welding productions for medium-term prospects have no almost the great differences and are oriented to the solution of urgent problems, such as increase in volumes and widening the fields of application of welding and allied technologies, increase in welding efficiency at simultaneous guarantee of high quality of joints, growth of level of mechanization and automation of welding jobs, decrease in energy consumption and expenses for welding and allied technologies; widening of application of new advanced metallic, composite and non-metallic materials in welded structures and constructions.

Stable and effective progress of welding productions in the industrialized countries is based on applying of results of fundamental and applied investigations, high scientific-engineering potential, qualified labor resources and active transfer of high welding technologies and other innovations.

Hence, it results in great attention, which is paid in the whole world to the development of welding science and technology, improvement of technological processes of welding, including the fusion arc welding. In the opinion of national and foreign specialists, it will also remain as the leading method of producing permanent joints in the foreseeable future (Table 1).

Science- and engineering-intensive welding production has an inter-industry nature, and in the metal working industries and construction, this is, as a rule, a self-dependent production and

*From materials of paper presented at the VIII International Conference «Welding Consumables» (Kiev, PWI, 16–18 June, 2014).

Table 1. Development of the European market of welding engineering and technologies (for the nearest 10 years)

Technological sector of market	Without changes or negligible increment	Increment	Significant increment
Arc welding with consumable electrode		×	
Arc welding with non-consumable electrode	×	×	
Submerged arc welding and electroslag welding	×	×	
Plasma-arc welding	×	×	
Laser welding		×	×
Electron beam welding		×	×
Resistance spot and seam welding	×	×	
Flash-butt welding		×	×
Friction welding	×	×	
Ultrasonic welding		×	×
HF welding		×	×
Brazing		×	
Adhesion bonding		×	×
Mechanical joining	×	×	

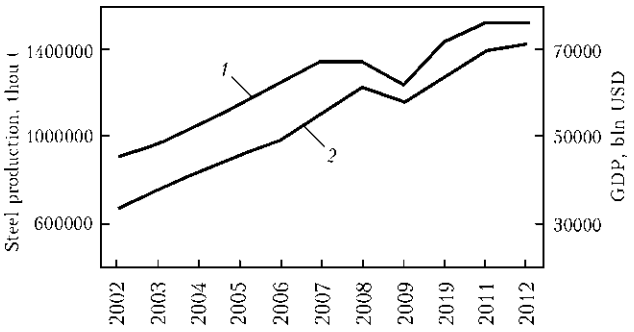

Figure 1. Dynamics of the world indicators of steel production (*1*) and GDP (*2*)

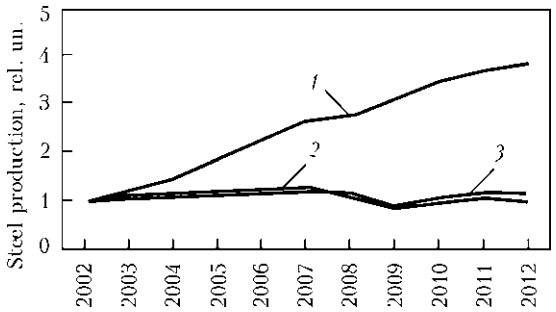

Figure 2. Production of steel in China (*1*), Ukraine (*2*) and world (*3*) (without China) (volume of production in 2002 was taken as unity)

technological sector, closely integrated into the total process of production.

The main structural materials for welded structures are steel (93–95 %), aluminium, titanium and other non-ferrous metals and plastics (5–7 % in total), therefore, the development of steel production industry is one of the most main factors defining the state and dynamics of development of welding production not only today, but also in the foreseeable future.

None of other materials has such a combination of strength, ductility, flexibility and cost, as steel. All the produced steel becomes a resource with unlimited cycle of use and can be remelted.

In the world production of steel more than 4 million employees are engaged and another 4 million — in related industries. Steel production industry is the second one in the world as to the energy consumption in spite of the fact that the power intensity of its production over the recent 30 years reduced by 50 %. It is the mover, which provides the progress of the world industry, and the industry indicators reflect the global economic situation [4, 5]. Figure 1 shows the close interrelation between the world production of steel, steel rolled metal and GDP. During the recent decade the world volume of steel production was increased by 1.7 times and GDP — by more than 2 times. On average, it is necessary to produce 2 kg of steel for each 100 USD of GDP increment.

In 2012, according to data of the World Steel Association (WSA), the steel consumption in the world was amounted to 218 kg per one person, including, kg: China — 500, EU — 340, Russia — 330, the USA — 310, Ukraine — 160, Africa — 30.

Since 1996 China is the world leader in steel production. In 2012 its share was 46 % (731 million tons) of the world volume. The second place

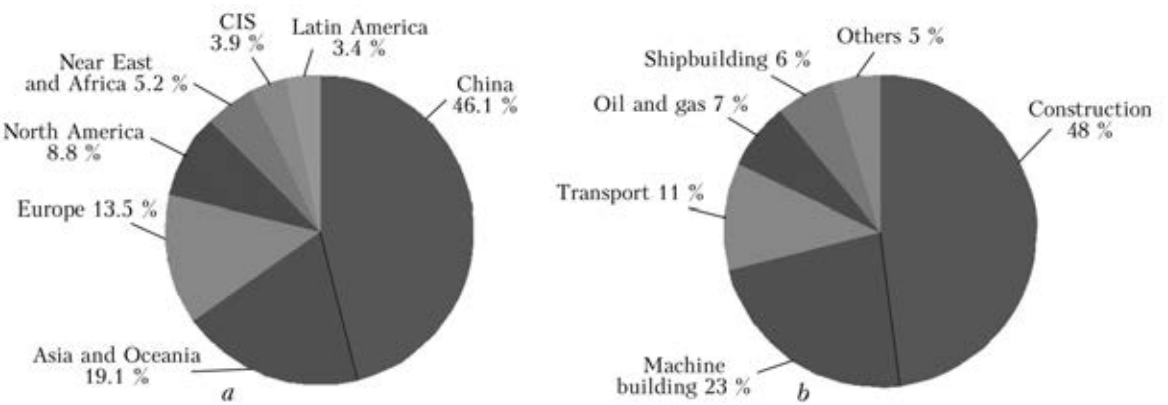

Figure 3. Distribution of world volume of steel consumption by regions (*a*) and industry branches (*b*) in 2012

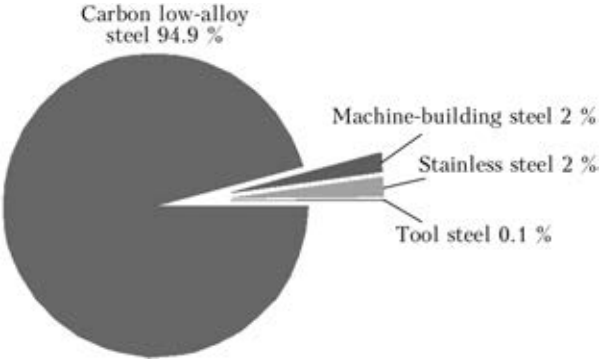

Figure 4. Structure of consumption of rolled metal in 2012

is occupied by Japan, the third one — by the USA. Ukraine in 2012 decreased the steel production by 2.4 million tons as compared to 2011 and lowered in two positions in the rating of the largest producers, occupying 10th position with an indicator of 32.9 million tons [6].

Figure 2 shows the dynamics of growth of steel production in China, Ukraine and world (without China) as compared with 2002.

Tables 2 and Figure 3 show the distribution of the world volume of steel consumption by regions and industry branches.

Structure of consumption of steel rolled metal by steel grades, given in Figure 4, proves that 94.9 % of rolled metal are produced by using carbon and low-carbon steel, the main structural material used in welding.

In spite of the fact that steel production industry encounters a large amount of obstacles, such as excess capacities, volatility of raw materials and energy markets, risks of protectionist policy, steel will remain also in future as one of the most important materials for the advanced economy.

From the estimates of the WSA experts, as well as experts of the International Iron and Steel Institute, the demand for steel will increase up to 2.3 billion tons per year by 2025. Average annual rates of growth in 2014–2025 will amount

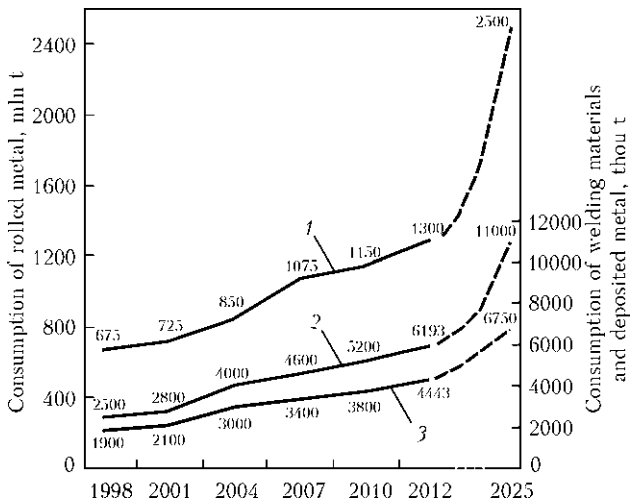

Figure 5. World consumption of rolled metal (*1*), welding materials (*2*) and deposited metal (*3*)

Table 2. Distribution of steel consumption by industry branches in the world, China and EU (%)

Industry branch	World	China	EU
Construction	48	50	38
Machine building	23	19.2	24
Transport	11	7.1	12
Shipbuilding	6	4.3	2
Oil and gas	7	7.1	12
Others	5	7.1	8

to 3.7 %. The construction sector will have 64 % of steel consumption, automobile industry — 17 %, manufacture of technological machines and equipment (machine building) — 15 %.

By 2025, 90 % of expected increase in steel consumption will meet the requirements of the following branches:

- civil building, infrastructural projects in countries with the developing economy (68 % of growth);
- technological machine building (13 %);
- oil-gas and other pipes (9 %).

The above-given information about the state and prospects of development of steel production industry makes it possible to state that the volumes of welding production in the foreseeable future will grow and, respectively, the market of welding materials will increase.

It can be expected that by 2025 the volumes of consumption of rolled metal can reach 2500 million tons, welding consumables — up to 11 million tons. This statement can be based on data, given in Figure 5, about the world consumption of rolled metal, welding materials and mass of metal being deposited, for 1998–2002, and also above-given data about the growth in demand for steel by 2025.

The brightest example, confirming the general tendency of relationship between the growth of steel consumption and total economic level of countries, characterized by high rate of GDP growth, is China (see Figure 2), which has during recent years the highest and stable rate of GDP increment (8–10 %) and occupies the first place in the world as to the volume and rates of steel consumption increment [7]. The share of this country in the world steel consumption increased from 20.1 % in 2002 up to 46 % in 2012.

The EU countries can be given as the second example, the steel consumption increment of which is 1–3 %. Such moderate development of consumer's market of steel corresponds to the moderate growth of GDP in these countries, 2–3 % per year on average.

In the world scientific and technical literature two conceptions are sometimes confused: «welding materials» (consumables) and «materials for welding» (suppliers), that leads to misunderstandings in comparison of statistic indicators.

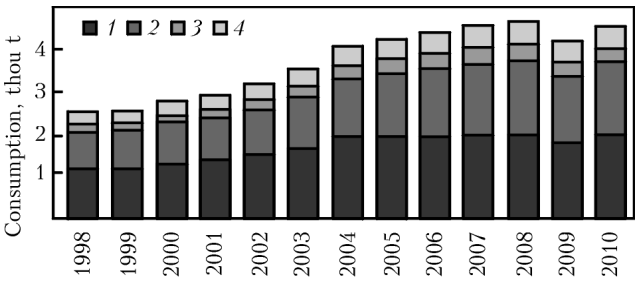

Figure 6. Dynamics of consumption by main types of welding materials: *1* — electrodes; *2* — solid wire; *3* — wire for submerged arc welding; *4* — flux-cored wire

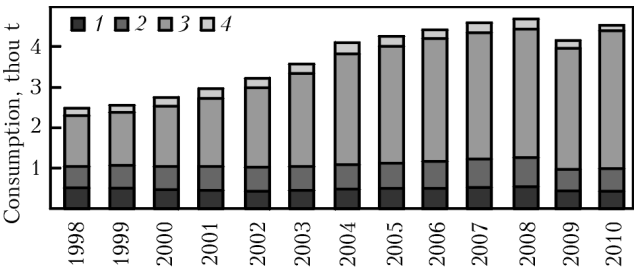

Figure 7. Dynamics of consumption of welding materials by main regions: *1* — North America; *2* — Europe; *3* — Asia; *4* — other regions

The first conception refers to materials, the most part of which transfers in the process of welding to the composition of weld metal (for arc welding these are solid and flux-cored wires, coated and other consumable electrodes, fluxes), and the second one refers to shielding active and inert gases and other materials, including auxiliary ones, which take part in fulfillment of welding processes. It is a disputable question whether the welding flux is referred to welding materials, but it is considered so in practice. Therefore, we shall use further this interpretation of the term «welding materials», though in some countries the national statistics means namely the «materials for welding», that it is necessary to take into account at international comparisons of appropriate indicators.

In cost volume of the world market of welding industry from the estimation of specialists of ESAB company, the welding materials amounted to 70 % in 1996, welding equipment — to 30 %. By 2006 the ratio of these indicators was, respectively, 45 and 55 %. At the present time, it can be considered that the cost volume of the world market of welding materials is about a half of all the volume of welding industry market.

Figures 6 and 7 give the data of ESAB about the volumes of consumption according to main types of welding materials and regions [8, 9].

We periodically selectively compare our data with data of ESAB and Japanese data, published annually in «The Japan Welding News For The World» [10, 11] to be convinced in their validity.

The data of ESAB are close to the greater degree to those results, which we obtain in the course of our investigations. We can say also the same about the Japanese data (Table 3 and Figure 8). The advantage of the latter consists in the wider covering of regions and, the most important, in regularity and timeliness of their publication.

The world volume of consumption of welding materials, which amounted to 5946 thous tons in 2011, was increased by 4.2 % and reached 6193 thous tons in 2012. The growth of world volume of consumption of welding materials was determined by the rates of development of welding production of China, much surpassing in this aspect the rest regions. In 2012 China had 51.7 % of all the world consumption of welding materials (3200 thous tons). Far behind were countries of EU: 8.9 % (550 thous tons), and North America (the USA, Canada, Mexico): 6.9 % (430 thous tons).

From 300 to 200 thous tons of welding materials per year are consumed by Japan (283 thous tons), ASEAN (280 thous tons), India (270 thous tons), Korea (240 thous tons), CIS countries (230 thous tons), Latin America (210 thous tons), the Near and Middle East (190 thous tons), Africa (150 thous tons). This list is finalized by the regions of Taiwan (80 thous tons) and other smaller countries with total consumption of 70 thous tons.

The presence of valid and full information about the volumes of consumption of welding materials allows defining the generic structure of methods of arc fusion welding used in the world, regions and in definite country. Usually, as a criterion the mass of deposited metal is used, by means of which a percent share of manual arc welding with covered electrodes (MAW), shielded-gas solid wire welding (CO_2), flux-cored wire welding (FCW) and automatic submerged arc welding (ASAW) is determined.

Since its foundation in 1965 the PWI Department of Economic Research is carrying out the continuous research of technological structure of

Table 3. Consumption of welding materials in the world, regions, countries [10, 11]

Country, region	Consumption of welding materials, thou t	
	2011	2012
World	5945.6	6193
China	3000	3200
EU	570	550
North America	430	430
Japan	285	283
India	260	270
Korea	230	240
Russia, CIS	220	230
including Ukraine	69	63
Latin America	210	220
Near and Middle East	180	190
Africa	140	150
Taiwan	80	80
ASEAN	270	280
Others	70	70

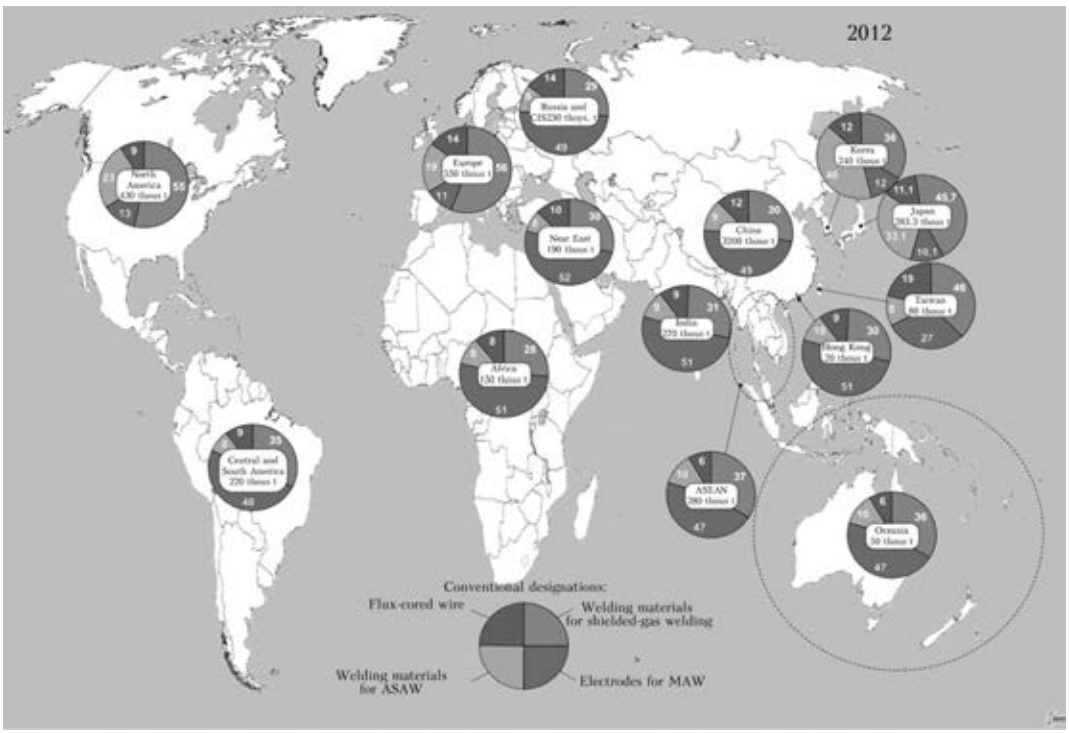

Figure 8. Consumption of welding materials in the world and regions in 2012

arc welding methods in a number of countries, the results of which are given in Table 4 and Figure 9.

The presence of the most complete Japanese data about the world and regional consumption of welding materials (see Figure 8) allowed defining the structure of application of arc welding methods in leading countries, regions and in the world as a whole (Table 5).

Application of data of «The Japan News For The World» for 2012 (see Table 5) shows that they are quite accurately integrated into dynamics of indicators of the PWI data, that proves the rather high degree of validity of information of both sources.

Information, given in Figure 9, confirms that the MAW share, amounting to 80–90 % in leading countries in 1965, was twice decreased for 25 years and was at the level of 35–45 % in 1990. Super optimists of the technical progress in welding production insisted at that period that the next 25 years the MAW share would be equal to zero or a little higher. We considered in our predictions that this method of welding would have the right for existence in the foreseeable future and its share would be about 20 %. As we see, not only super optimists and also we were mistaken, because today the MAW share in Japan is 7.3 %, in EU — 8.9 %, in the South Korea — 9.6 % and in the North America (the USA, Can-

Table 4. Technological structure of methods of arc welding in the world (% by deposited metal)

Country	Method of welding	Years						
		1965	1975	1985	1995	2000	2005	2012*
West Europe	MAW	74	58	34	18	15	12	8.9
	CO_2		31	56	70	71	75	63.9
	FCW		2	3	6	6.5	6.5	19.1
	ASAW		9	7	6	7.5	6.5	8.1
the USA	MAW	71	53	42	25	19.5	15	10.3
	CO_2		25	38	54	54	58.5	61.4
	FCW		13	13	19	19	19.5	22.1
	ASAW		9	7	7	7.5	7	6.2
Japan	MAW	85	67	44	22	14	12	7.3
	CO_2		20	39	52	54	54.5	49.5
	FCW		1	11	25	25	27	35.9
	ASAW		9	10	7	7	6.5	7.3
Ukraine	MAW	65.6	52.4	44.9	65.1	66.6	64.8	48.9
	CO_2	9.5	23.7	35	26.5	23.3	16.1	32.5
	FCW	0.5	3.2	3.4	0.9	0.5	3.2	1.4
	ASAW	27	20.7	16.7	7.5	9.6	15.9	17.2

*Data from «The Japan Welding News For The World» and PWI data.

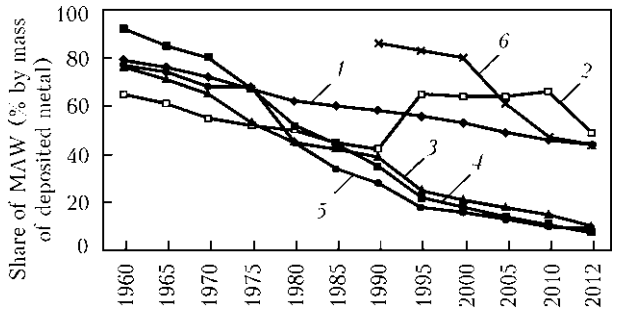

Figure 9. Share of MAW in the world: *1* — Russia; *2* — Ukraine; *3* — USA; *4* — Japan; *5* — West Europe; *6* — China (2012 — from data of «The Japan Welding News For The World» and PWI)

ada and Mexico) — 10.3 %. As a whole, the MAW share in the world is continuously decreased and amounted to 33.7 % in 2012, mainly due to China (47.3 %), India (45 %), CIS (44 %) and the rest countries, where it is 22–52 %.

The share of shielded-gas welding as a whole in the world is amounted to 44 %. Leaders in application of this method of welding are EU (63.9 %), the USA (61.4 %), Taiwan (54.8 %) and Japan (49.5 %). Leaders in FCW application are the South Korea (40 %), Japan (35.9 %) and the USA (22.1 %). As a whole, the FCW in the world amounted to 14 % in 2012.

The ASAW, which amounts only to 7.9 % of deposited metal in welding in the world as a whole, is mostly widely used in Ukraine (17.2 %), Russia (10.3 %), China (8.7 %) and in EU (8.1 %). Over the recent 40 years the ASAW share is almost stable, its fluctuations are as follows: in EU from 6 up to 8.1 %; in the USA from 9 to 6.2 %; in Japan from 9 to 7.3 %; in Ukraine from 20.7 to 17.2 %.

In conclusion, it can be noted that welding is the basic technology in many branches of industry and construction. The industrialized countries are characterized by a rather stable dynamics of development of welding production and welding market, which is defined by a stable growth of consumption of structural materials and widening of their assortment, as well as appearance of the new challenging materials, technologies and equipment for welding and related processes at the welding market.

Economical-statistic information about state-of-the-art and prospects of development of the world production and consumption of steel, the main structural material in manufacture of welded metal structures, as well as the dynamics of the world market of welding materials makes it possible to prove that the volumes of the world welding production will grow in the nearest future. Accordingly, the demand for welding materials will grow in spite of temporary crisis phenomena in separate regional markets.

The level of mechanization and automation of welding jobs, which is mainly defined by the volume of application of manual arc welding, is continuously increased by reduction of its share and growth of mass of deposited metal in use of semiautomatic and automatic welding in shielding gases and also by the flux-cored wire.

Table 5. Structure of methods of arc welding in the world, regions and countries in 2012 (% by mass of deposited metal)

Country	Method of welding			
	MAW	CO_2	FCW	ASAW
World	33.7	44.4	14	7.9
China	43.7	38.4	9.3	8.7
EU	8.9	63.9	19.1	8.1
North America	10.3	61.4	22.1	6.2
Japan	7.3	49.5	35.9	7.3
India	45	39.4	9.2	6.5
Korea	9.6	43	40	7.5
Russia, CIS	44	38.7	7.1	10.3
Ukraine	48.9	32.5	1.4	17.2
Latin America	41.8	30.9	8	6.4
Near and Middle East	46.5	38.5	8.2	7.3
Africa	51.2	36.2	7.1	5.9
Taiwan	21.6	54.8	18.8	5.2
ASEAN	40.3	45.8	10.1	4.2
Others	44.4	42.5	7.7	6.8

1. Bernadsky, V.N., Mazur, A.A. (1999) State-of-the-art and prospects of world welding market. *Avtomatich. Svarka*, **11**, 49–55.
2. Bernadsky, V.N., Makovetskaya, O.K. (2004) About contribution of welding to economics of the USA. *Ibid.*, **3**, 32–38.
3. Bernadsky, V.N., Makovetskaya, O.K., Mazur, A.A. (2008) Welding production and market of welding technique in modern economics. In: *Proc. of 7th Int. Symp. on Welding and Related Technologies* (Minsk, 26 March 2008), 5–9.
4. World Steel Association. Steel Statistical Yearbook 2013. *http*://www.worldsteel.org/dms/internetDocumentList/statistics-archive/yearbook-archive/Steel-Statistical-Yearbook-2013/document/Steel-Statistical-Yearbook-2012.pdf
5. SVESTA-2010. *http*://paton.kiev.ua/images/stories/svesta/pdf/swesta-2010.pdf
6. World Steel Association. World steel in figures 2014. *http*://www.worldsteel.org/dms/internetDocumentList/bookshop/World-Steel-in-Figures-2014/document/World %20Steel %20in %20Figures %202014 %20Final.pdf
7. Ma Pin. Investigations of market medium of welding production technologies: world tendencies and experience of China. *http*://old.nuwm.rv.ua/metods/asp/vd/v39ek24.doc
8. Pekkari, B. (2006) The welding world in changing. *Lume sudarii*, **2**, 3–12.
9. Middeldorf, K., fon Hofe, D. (2009) Tendencies in development of technologies for material joining. *Mir Tekhniki i Tekhnologij*, **11**, 12–16.
10. (2012) Worldwide demand for welding consumables. *The Japan Welding News For The World,* Spring, 16(**59**), 5.
11. (2013) Worldwide demand for welding consumables. *Ibid.*, 17(**63**), 6.

Received 02.09.2014

EFFECTIVENESS OF STRENGTHENING BUTT WELDED JOINTS AFTER LONG-TERM SERVICE BY HIGH-FREQUENCY MECHANICAL PEENING

V.V. KNYSH, S.A. SOLOVEJ and **A.Z. KUZMENKO**
E.O. Paton Electric Welding Institute, NASU
11 Bozhenko Str., 03680, Kiev, Ukraine. E-mail: office@paton.kiev.ua

Cyclic fatigue life of butt welded joints of low-alloyed steel 09G2S, strengthened by the technology of high-frequency mechanical peening (HFMP) at different stages of fatigue fracture: in as-welded state, after accumulation of 70 % of fatigue damage, at formation of surface fatigue cracks, was studied. The objective of these studies is establishing the effectiveness of application of HFMP treatment of butt welded joints after long-term service at alternating loading. It is shown that strengthening of butt welded joints by HFMP right after welding increases the endurance limit (2 mln cycle base) by 50 % — from 180 up to 270 MPa, and cyclic fatigue life — by 5 to 10 times. It is experimentally confirmed that the effectiveness of strengthening welded joints with 70 % accumulated fatigue damage depends on the levels of applied maximum stresses before strengthening. So, residual cyclic fatigue life of samples, tested in the range of maximum 240–260 MPa stresses, falls within the scatter band of experimental data for welded joints in unstrengthened condition, and for those tested in the range of maximum stresses of 280–300 MPa it is within the scatter band of experimental data for welded joints strengthened by HFMP technology in as-welded condition. It is established that application of HFMP technology improves the residual cyclic fatigue life of welded joints with surface fatigue cracks (down to 2 mm deep) 2.5 times compared to fatigue life before crack formation. 11 Ref., 5 Figures.

Keyword: *high-frequency mechanical peening, increase of cyclic fatigue life, fatigue, welded joint, accumulated fatigue damage*

Application of methods of surface plastic deformation of metals allows considerable increase of characteristics of welded joint fatigue resistance. High-frequency mechanical peening (HFMP) is an effective method of strengthening welded structures operating under the conditions of alternating loading. Application of this method of welded joint treatment at the stage of structure fabrication is quite well studied: main regularities of increase of cyclic fatigue life and endurance limits of welded joints, depending on steel strength class, joint type, and alternating loading cycle characteristics are established; its advantages compared to other processes of surface plastic deformation of metal are determined [1–6]. In this research package a number of studies are devoted to evaluation of the effectiveness of strengthening welded components and elements of metal structures in service, joined by fillet welds [7–11]. It is shown that increase of residual fatigue life of welded joints with accumulated fatigue damage after strengthening by HFMP technology essentially depends on the level and duration of the applied maximum stresses before strengthening. As regards experimental data on effectiveness of application of HFMP technology to improve fatigue resistance characteristics of butt welded joints of structures in service, such data are lacking in known publications.

The objective of this work is to establish the effectiveness of strengthening by HFMP the butt welded joints after long-term operation at alternating loading.

Material and experimental procedure. Experimental studies were conducted on samples of butt joints of low-alloyed steel 09G2S (σ_y = = 373 MPa, σ_t = 510 MPa) 12 mm thick. Blanks for samples of 600 × 180 mm size were cut out of hot-rolled sheets of gauge 12. Automatic square-edge submerged-arc welding from two sides with OK Flux 10.71 was performed with 4 mm 08GA wire. Welding parameters were as follows: current of 590–620 A, voltage of 30–32 V, speed of 28.2 m/h. After welding 8 samples were cut out of each plate. Figure 1 shows sample shape and geometrical dimensions. Sample thickness is due to wide acceptance of 12 mm rolled stock in welded structures, and sample gauge width was selected proceeding from test equipment capacity. Four series of samples were prepared for fatigue testing: as-welded condition (first series); HFPM in as-welded condition (second series); HFMP after 70 % fatigue damage accumulation (third series) and HFMP after for-

mation of surface fatigue cracks of specified length (fourth series). At joint strengthening by HFMP technology a narrow zone of weld metal transition to base metal was subjected to surface plastic deformation. Strengthening was performed with manual impact tool with piezoceramic converter connected to ultrasonic generator of output power of 500 W. Single-row four-striker attachment with 3 mm striker diameter was used as strengthening device. HFMP speed was 3 mm/s, oscillation amplitude of manual impact tool wave guide edge was 25 μm. Fatigue testing of samples was performed in URS 20 testing machine at uniaxial alternating loading with cycle asymmetry $R_\sigma = 0$. Complete fracture of the sample and exceeding test base of $2 \cdot 10^6$ stress alternation cycles were taken as the criteria of test completion.

Experimental results. First fatigue curves of butt welded joints of 09G2S steel in as-welded condition and in the condition after HFMP strengthening of as-welded samples, respectively, were established from the results of testing samples of the first and second series. HFMP strengthening increases the endurance limit (base of 2 mln cycles) of butt welded joints by 50 % from 180 up to 270 MPa, and cyclic fatigue life by 5–10 times. Experimental data scatter decreases essentially.

Third series samples were subjected to preliminary cyclic loading up to achievement of 70 % fatigue life by the established fatigue curve of welded joints in unstrengthened condition, and then were treated by HFMP technology. After strengthening by HFMP technology fatigue testing was carried on at the same loading levels as before strengthening. Figure 2 gives fatigue testing results. HFMP strengthening of butt welded joints with 70 % accumulated fatigue damage increases endurance limit (2 mln cycle base) by 22 % — from 180 up to 220 MPa. Here residual cyclic fatigue life of samples, tested in the range of maximum stresses of 240–260 MPa, is within the scatter band of experimental data for welded joints in unstrengthened condition, that of samples tested in maximum stress range of 280 to 300 MPa is within the scatter band of experimental data for welded joints strengthened by HFMP technology in as-welded condition. Note that the majority of third series samples failed through base metal at a distance from fusion line (Figure 3).

Similar improvement of fatigue resistance characteristics of welded joints was obtained when studying the influence of preliminary cyclic

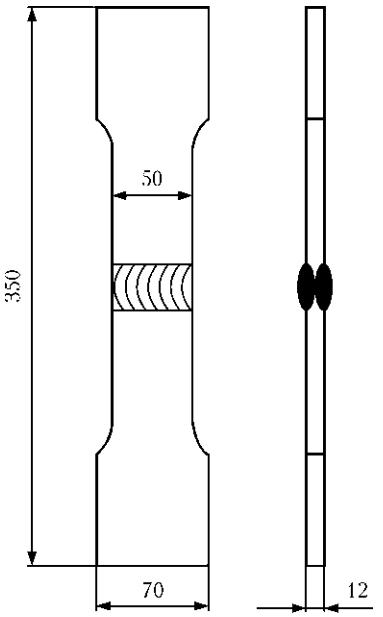

Figure 1. Shape and dimensions of sample of 09G2S steel butt welded joint

loading on effectiveness of strengthening tee welded joints by HFMP technology [8, 10].

Obtained experimental data for butt welded joints confirm that at cyclic preloading of welded joints with maximum cycle stresses corresponding to ratio $\sigma_y > \sigma_y/\alpha_\sigma$ (where σ_y is the material yield point, α_σ is the coefficient of stress concentration), subsequent strengthening by HFMP technology leads to greater increase of fatigue resistance characteristics compared to strengthening in as-welded condition.

This is due to the fact that at maximum stress levels corresponding to the above-given inequality, complete relaxation of residual tensile welding stresses takes place in concentrator zones of welded joints. Method of increasing fatigue resistance characteristics of welded joints by preloading by higher stress levels was called «overloading» in scientific publications. Obtained re-

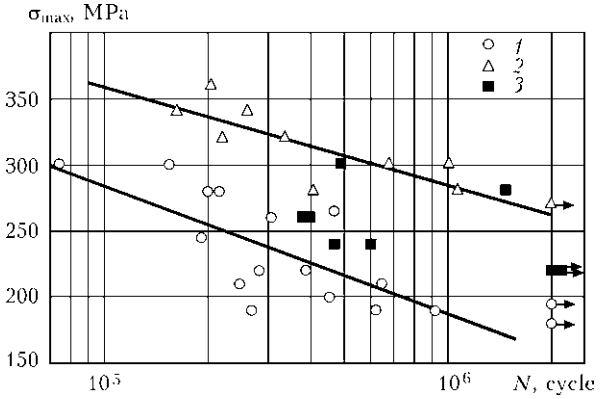

Figure 2. Results of fatigue testing of butt welded joints of 09G2S steel in as-welded condition (*1*), condition of HFMP strengthening after welding (*2*) and HFMP strengthening after accumulation of 70 % fatigue damage (*3*)

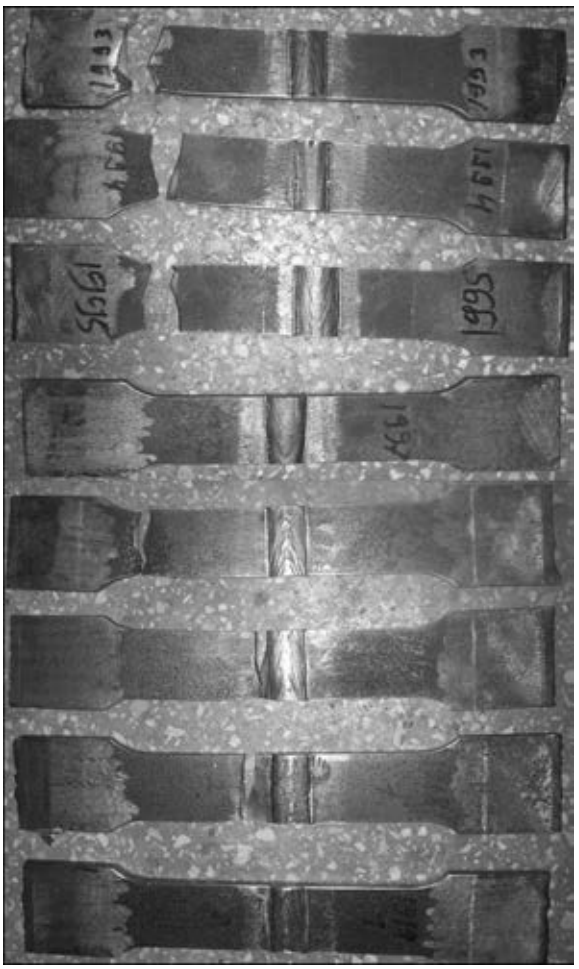

Figure 3. Appearance of 09G2S steel samples, strengthened at accumulation of 70 % fatigue damage, after fatigue testing

sults show the high effectiveness of application of HFMP technology to increase cyclic fatigue life of butt welded joints after long-term service.

The fourth series of samples were strengthened by HFMP technology after formation of surface fatigue cracks of 5 (2 samples), 20 (2 samples) and 50 mm (2 samples) length. To reveal the crack front the welded joint in as-welded condition was lubricated by indicator liquid consisting of kerosene and toner. After formation of a crack of specified length (all cracks formed on the line of weld to base metal transition) remains of indicator liquid were removed by blowing with compressed air. HFMP strengthening was applied not only to the fusion line, containing a crack, but also to all the four lines of weld to base metal transition. No indicator liquid was used after HFMP strengthening. Thus, on sample fractures after fatigue testing the crack front is clearly visible, which was treated by HFMP technology. Figure 4 gives the results of fatigue testing, and Figure 5 shows photographs of broken samples.

HFMP treatment of welded joint samples with cracks of 50 mm length (up to 5 mm depth) did not result in higher cyclic fatigue life. Samples failed within the scatter band of experimental data for unstrengthened welded joints. Strengthening of welded joints with fatigue cracks of 5 mm length (up to 0.5 mm depth) and 20 mm length (up to 2 mm depth) increased their residual fatigue life 2.5 times compared to fatigue life before crack formation. Here, one of the samples with 5 mm long crack after strengthening by HFMP technology did not fail within the range of test base of $2 \cdot 10^6$ cycles of stress alternation (increase of residual cyclic life by more than 10 times compared to fatigue life before crack formation).

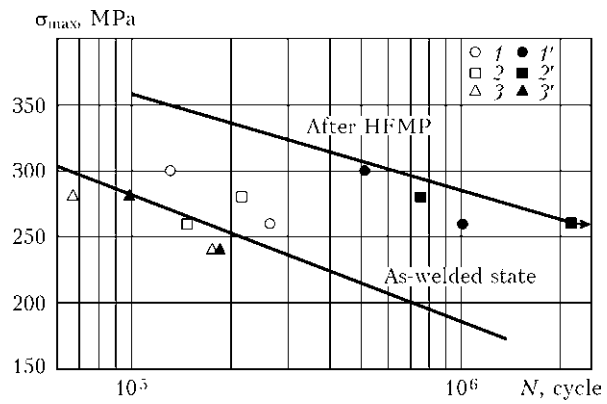

Figure 4. Fatigue curves of butt joints of 09G2S steel in as-welded and HFMP strengthened conditions, as well as results of fatigue testing of samples: *1–3* — up to formation of 5, 20 and 50 mm long crack, respectively; *1′–3′* — after HFMP strengthening of 5, 20 and 50 mm long cracks, respectively

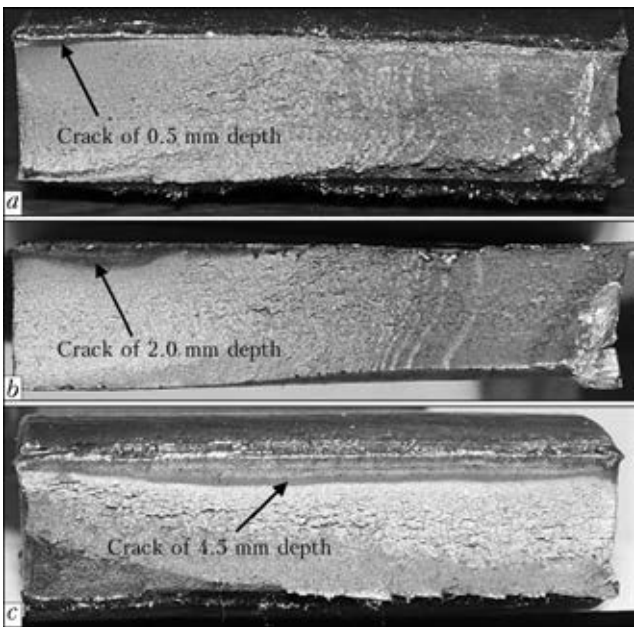

Figure 5. Fatigue fractures of samples of 09G2S steel butt joint strengthened at formation of fatigue cracks of 5 (*a*), 20 (*b*) and 50 (*c*) mm length

Similar improvement of residual fatigue life of welded joints with shallow surface fatigue cracks by HFMP treatment was obtained on tee welded joints [11]. Thus, a high effectiveness of HFMP technology application for increasing cyclic fatigue life of welded joints with up to 2 mm fatigue cracks was confirmed.

Conclusions

1. It is established that HFMP strengthening of butt welded joints of 09G2S steel with 70 % accumulated fatigue damage (fatigue cracks were absent) increases the endurance limit (2 mln cycle base) by 22 % from 180 to 220 MPa. Cyclic fatigue life of samples tested in maximum stress range of 240 to 260 MPa is within the scatter band of experimental data for welded joints in unstrengthened condition, and that of samples tested in maximum stress range of 280 to 300 MPa is within the scatter band of experimental data for welded joints strengthened by HFMP in as-welded condition.

2. It is shown that HFMP strengthening of all the four near-weld zones of butt welded joints with surface fatigue cracks of 5–20 mm length (depth from 0.5 to 2.0 mm) increases their residual fatigue life 2.5 times compared to fatigue life before crack formation.

1. Kuhlmann, U., Duerr, A., Guenter, P. et al. (2005) Verlaengerung der Lebensdauer von Schweisskonstruktion aus hoeher festen Baustaehlen durch Anwendung der UIT-Technologie. *Schweissen und Schneiden*, 57(**8**), 384–391.
2. Lobanov, L.M., Kirian, V.I., Knysh, V.V. et al. (2006) Improvement of fatigue resistance of welded joints in metal structures by high-frequency mechanical peening (Review). *The Paton Welding J.*, **9**, 2–8.
3. Yin, D., Wang, D., Jing, H. et al. (2010) The effects of ultrasonic peening treatment on the ultra-long life fatigue behavior of welded joints. *Materials & Design*, 31(**7**), 3299–3307.
4. Martines, L.L. (2010) Fatigue life extension procedure by ultrasonic peening. *IIW Doc. XIII-2316–10*.
5. Yildirim, H.C., Marquis, G.B. (2011) Overview of fatigue data for high frequency treated welded joints. *IIW Doc. XIII-2362r1–11*.
6. Abdullah, A., Malaki, M., Eskandari, A. (2012) Strength enhancement of the welded structures by ultrasonic peening. *Materials & Design*, 38, 7–18.
7. Garf, E.F., Litvinenko, A.E., Smirnov, A.Kh. (2001) Assessment of fatigue life of tubular connections subjected to ultrasonic peening treatment. *The Paton Welding J.*, **2**, 12–15.
8. Kudryavtsev, Y., Kleiman, J., Lugovskoy, A. et al. (2006) Fatigue life improvement of tubular welded joints by ultrasonic peening. *IIW Doc. XIII-2117–06*.
9. Zhao, X., Wang, D., Huo, L. (2011) Analysis of the S–N curves of welded joints enhanced by ultrasonic peening treatment. *Materials & Design*, 32(**1**), 88–96.
10. Knysh, V.V., Solovej, S.A., Kuzmenko, A.Z. (2011) Influence of preliminary cyclic loading on effectiveness of welded joint strengthening by high-frequency peening. *The Paton Welding J.*, **10**, 36–39.
11. Knysh, V.V., Kuzmenko, A.Z., Solovej, S.A. (2009) Increase of cyclic fatigue life of tee welded joints with surface cracks. *Ibid.*, **1**, 29–33.

Received 04.04.2014

ELECTRON BEAM WELDING OF SHEET COMMERCIAL TITANIUM VT1-0, HARDENED BY NITROGEN IN THE PROCESS OF ARC-SLAG REMELTING, AND PROPERTIES OF PRODUCED JOINTS*

V.Ya. SAENKO, A.A. POLISHKO, V.A. RYABININ and **S.N. STEPANYUK**
E.O. Paton Electric Welding Institute, NASU
11 Bozhenko Str., 03680, Kiev, Ukraine. E-mail: office@paton.kiev.ua

Shown is the efficiency of application of electron beam welding (EBW) for producing full-strength welded joint of commercial titanium rolled metal of 35 mm thickness, hardened by nitrogen of up to 0.1 wt.% in the process of arc-slag remelting (ASR). Data of X-ray spectral analysis prove the uniform distribution of nitrogen, aluminium, titanium, iron, oxygen both in the ASR rolled metal and also in the welded joint. Metallographic examinations confirmed the producing of quality welded joint without cracks, pores and other defects. Weld metal and base metal are characterized by a homogeneous structure. The uniform distribution of hardness *HB* and microhardness *HV* was observed both in the sheet commercial titanium and also in the welded joint. At content of nitrogen of up to 0.1 wt.% in titanium the hard inclusions of titanium nitride are absent both in the sheet ASR rolled metal and also in the weld metal made by the EBW. 13 Ref., 5 Figures.

Keywords: *commercial titanium, arc-slag remelting, titanium hardening with nitrogen from gas phase, sheet rolled metal, electron beam welding, macro- and microstructure, mechanical properties of welded joint*

The new method of remelting of consumable electrode by electric arc, burning between the electrode tip and surface of molten slag pool in a copper water-cooled mould was, developed at the E.O. Paton Electric Welding Institute (PWI) in the beginning of the 1970s and patented in 1982 under the name of the arc-slag remelting (ASR) [1]. Later, the carried out investigations, including those under the plant conditions, showed that in comparison with a traditional electroslag remelting the new method of ASR is economically profitable and allows producing metal, not being inferior to the ESR metal as to the quality.

Figure 1. Macrosections of fillet and butt joints of sheet commercial titanium made by EBW

The first results of investigations of ASR of titanium and its alloys, carried out at the PWI under laboratory and plant conditions, showed [2–4] the challenging future of this method in the solution of problems of reducing the prices in manufacture of semi-products of titanium and its alloys, fist of all, of commercially pure titanium. The feasibility of producing the large-tonnage ASR ingots of rectangular section with a good surface, not requiring the machining for the direct rolling, allows reducing greatly the loss of metal in manufacture of titanium semi-products and decreasing the cost of finished products.

The main factor for reduction of prices of titanium products is also the feasibility of realization of a single-stage ASR process of spongy pressed electrodes [5–7].

Titanium and its alloys are characterized by the better combination of high mechanical prop-

*The work was carried out under supervision of Profs O.K. Nazarenko and V.M. Nesterenkov, Corresponding members of the NASU.

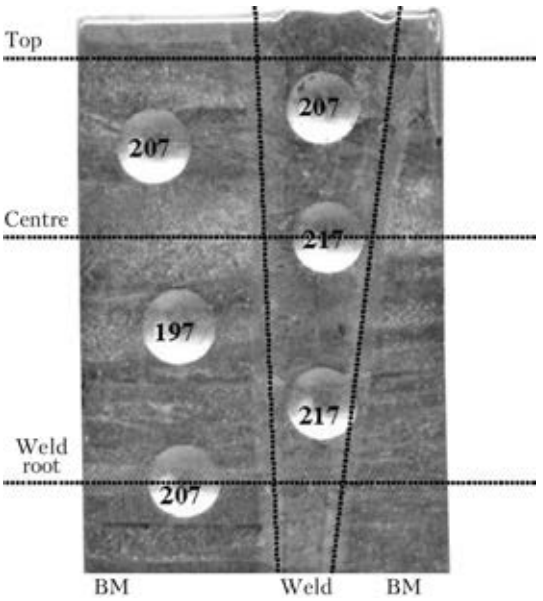

Figure 2. Appearance of specimen of welded joint of sheet commercial titanium and values of Brinell hardness obtained in longitudinal section

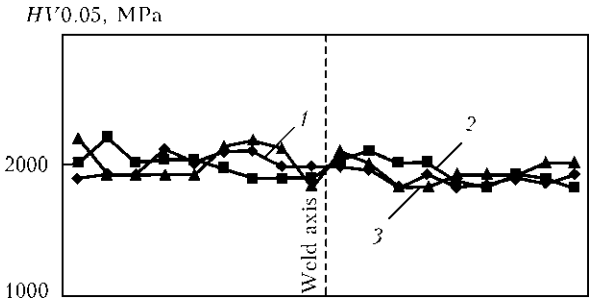

Figure 3. Distribution of microhardness across the EB-welded joint on sheet commercial titanium: *1* — top; *2* — centre; *3* — weld root

erties and low density as compared to other structural materials. Commercial titanium VT1-0 at significant corrosion resistance in different aggressive media has comparatively low strength properties ($\sigma_t \leq 400$ MPa). However, the problem is solved successfully by alloying of titanium with aluminium, vanadium, manganese, molybdenum and other elements, moreover, without noticeable decrease in its ductile properties. As is known, the strength and ductile properties of the commercial titanium are greatly affected by content of oxygen and nitrogen in it [8, 9]. Complex of investigations, carried out at PWI, showed the possibility of increasing the strength characteristics of commercial titanium VT1-0 by its alloying with nitrogen from gas phase in the ASR process [10]. As a result, the commercial ASR titanium was produced, having the strength characteristics at the level or higher than the values of GOST 23755–79 [11].

The next stage of investigations was the evaluation of possibility for producing a full-strength welded joint of 35 mm thickness on sheet rolled metal of commercial titanium VT1-0, hardened with nitrogen of up to 0.1 % from the gas phase in the ASR process (further, the sheet commercial titanium), made by EBW.

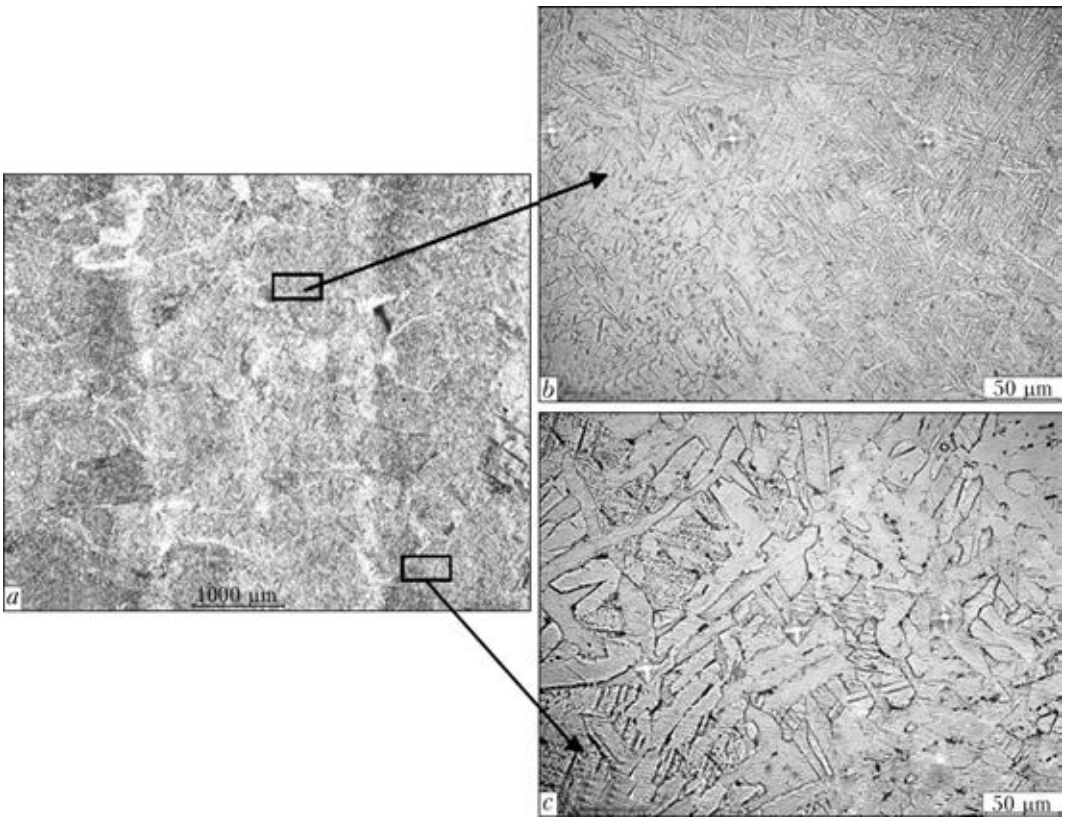

Figure 4. Microstructure of joint zone (*a* — ×25), weld (*b* — ×400) and base metal (*c* — ×400)

It is known that when the titanium is alloyed with nitrogen from the solid phase, the nitrides of different chemical composition are formed, in particular, in the process of remelting of titanium sponge and next producing of titanium alloys. Alongside with titanium nitrides the hard inclusions, enriched with nitrogen, can form. Therefore, one of the tasks consisted of evaluation of the probability of formation of hard inclusions of titanium nitride in sheet commercial titanium and its welded joint in EBW. The possibility of dissolution of hard particles of titanium nitride in molten titanium was also studied [12].

The fillet and butt joints of the sheet commercial titanium were made, the appearance of which is shown in Figure 1. In both cases a good formation of weld and the absence of any defects in weld metal and near-weld zone were noted.

The level of Brinell hardness was evaluated in the specimen longitudinal section. Measurements were carried out at 3000 kg load by a ball of 10 mm diameter. Weld metal had *HB* 207–217, base metal — *HB* 197–207 (Figure 2). Microhardness was measured in LECO hardness meter M-400 at 50 g load and 100 μm pitch in different zones of the welded joint. As the measurements showed (Figure 3), the values are rather uni-

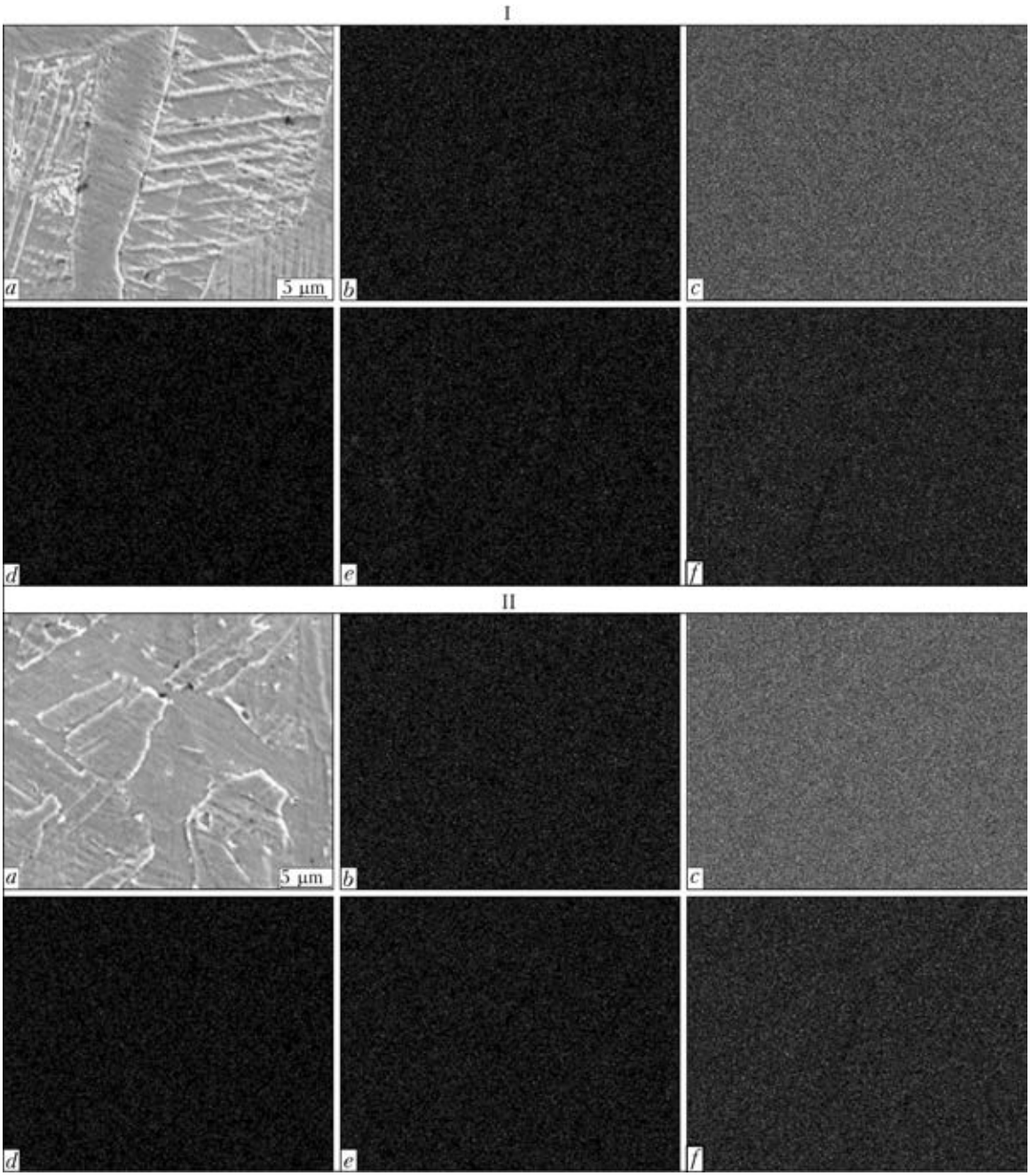

Figure 5. Microstructure (×2000) of base metal (I, *a*), weld metal (II, *a*) and concentration maps of distribution of aluminium (I, II, *b*), titanium (*c*), iron (*d*), oxygen (*e*) and nitrogen (*f*)

formly distributed in the entire volume of the welded joint and amount in the weld upper part to *HV* 1830–2120, in the center — to *HV* 1830–2210 and in the root — to *HV* 1830–2200 MPa.

To examine the microstructure of specimens of welded joints, the chemical etching by reagent $HCl + HNO_3 + H_2O$ was applied and microscope Neophot-32 was used. Structure of the zone of joint, weld and base metal is given in Figure 4. Metallographic examinations* showed that the quality defectless welded joint with a homogeneous structure was produced. Weld of about 3 mm width has an acicular structure with needles of different length (15–40 μm), located at 60° angle. The base metal contains a coarser grain (50–100 μm), the main structural component is α′-phase.

The analytic complex for X-ray spectral examinations was used, which consists of a scanning electron microscope JSM-35CF (JEOL, Japan) and system for energy-dispersed microanalyzer INCA Energy-350 (Oxford Instruments, Great Britain). Experiments were carried out at accelerating voltage of 20 kV, 200- – 10000-fold magnification, element analysis was made in the range from boron to uranium.

Data of X-ray spectral analysis prove the uniform nature of distribution of elements (nitrogen, oxygen, aluminium, iron) in the structure of base metal, hardened with nitrogen of up to 0.1 %, and weld metal, made by EBW (Figure 5). At clearly revealed relief of the structure (Figure 5, I, II, *a*) the chemical non-homogeneity by main elements is not observed. Results of examinations confirm also that at content of up to 0.1 % of nitrogen in titanium the hard inclusions of titanium nitride are absent.

In conclusion, it is necessary to outline the urgency of the carried out works for the updating the technological processes of producing the commercial titanium [13] and increase of its strength characteristics by a regulated adding of admixtures, in particular, the interstitial elements. To produce the full-strength joint of the sheet commercial titanium 35 mm thick, hardened by nitrogen of up to 0.1 % in the ASR process, the application of EBW is effective. At such concentration of nitrogen the hard inclusions of titanium nitride are absent in all the zones of welded joint. The uniform distribution of nitrogen, aluminium, titanium, iron, oxygen, formation of homogeneous microstructure and rather uniform distribution of hardness and microhardness are noted. It is also important that such hardened commercial titanium can find the wide application in industry and medicine.

1. Paton, B.E., Medovar, B.I., Lakomsky, V.I. et al. *Method of consumable electrode remelting*. USSR author's cert. 520784. Int. Cl. C21C5/56. Fill. 09.08.74. Publ. 30.05.82.
2. Paton, B.E., Medovar, B.I., Saenko, V.Ya. et al. (1992) Arc-slag remelting of titanium and titanium alloys. In: *Proc. of Int. Symp.* (USA, CA, June 29–July 2, 1982), Vol. 3, 2429–2431.
3. Medovar, B.I., Shepelev, V.V., Saenko, V.Ya. et al. (1992) Arc-slag remelting of titanium and titanium alloys. *Problemy Spets. Elektrometallurgii*, **2**, 13–15.
4. Paton, B.E., Medovar, B.I., Saenko, V.Ya. et al. (1994) Remelting of spongy titanium consumable electrodes by ESR and ASR methods. *Ibid*., **3/4**, 7–11.
5. Paton, B.E., Saenko, V.Ya., Pomarin, Yu.M. et al. (2002) Possibilities of arc-slag remelting as one of the methods of special electrometallurgy. In: *Proc. of Int. Sci.-Techn. Conf. on Special Electrometallurgy: Yesterday, Today, Tomorrow* (Kiev, 8–9 Oct. 2002), 123–137. Kyiv: Politekhnika.
6. Medovar, L.B., Saenko, V.Ya., Fedorovsky, B.B. (2007) Arc-slag remelting of titanium and its alloys. In: *Proc. of Int. Conf. on Titanium in CIS* (Yalta, 15–18 April 2007), 177–180.
7. Medovar, L.B., Saenko, V.Ya., Ryabinin, V.A. et al. (2010) Improvement of arc-slag remelting of titanium and its alloys. *Titan*, **3**, 15–19.
8. Kolachev, B.A., Livanov, V.A., Bukhanova, A.A. (1974) *Mechanical properties of titanium and its alloys*. Moscow: Metallurgiya.
9. (1980) *ASM metals handbook*, Vol. 3. Ohio: ASM.
10. Medovar, B.I., Saenko, V.Ya., Kumysh, V.I. et al. (1994) Hardening of titanium by nitrogen alloying from gas phase during arc-slag remelting. *Problemy Spets. Elektrometallurgii*, **3/4**, 12–17.
11. Medovar, B.I., Saenko, V.Ya., Grigorenko, G.M. et al. (1996) *Arc-slag remelting of steel and alloys*. Cambridge: Int. Sci. Publ.
12. Grigorenko, G.M., Pomarin, Yu.M., Orlovsky, V.Yu. et al. (2008) On dissolution of TiN solid particles in molten titanium during melting. *Advances in Electrometallurgy*, **2**, 45–47.
13. Aleksandrov, A.V., Prudkovsky, B.A. (2005) Different aspects of titanium and its alloys. *Titan*, **1**, 64–70.

Received 13.05.2014

*The work was carried out with participation of Dr. A.Yu. Tunik.

FEATURES OF RECONDITIONING STEEL DRILL BIT WATERCOURSE

B.V. STEFANIV, V.F. KHORUNOV, O.M. SABADASH, S.V. MAKSYMOVA and **V.V. VORONOV**
E.O. Paton Electric Welding Institute, NASU
11 Bozhenko Str., 03680, Kiev, Ukraine. E-mail: office@paton.kiev.ua

Peculiarities of defects in worn steel drill bit developing in service at gas well drilling are considered, damage at anomalous wear of water course moving element is described; methods to prepare the worn section for its reconditioning by welding and protective coating deposition are tried out. Special attention is given to analysis of microstructure and chemical inhomogeneity of joint line of steel 40Kh + protective wear-resistant coating, stainless steel 08Kh18N10T + protective wear-resistant coating, stainless steel 08Kh18N10T + steel 40Kh + protective wear-resistant coating; deposited layer microhardness is determined. It is shown that deposition of wear-resistant coating by surfacing provides effective protection from erosive and abrasive wear of bits at drilling of medium and hard rock. Proceeding from the derived data, technology of reconditioning the water course moving element of this drill bit was developed. The drill bit has successfully passed trials at drilling of gas and oil wells in soft, medium-hard and hard rocks in the company «Representative Office USEIS SA» in Poltava region. 2 Ref., 3 Tables, 5 Figures.

Keywords: *drill bits, superhard materials, protective coating, surfacing, wear resistance, welding, microhardness, strength, reconditioning of working elements*

In drilling of gas and oil wells working elements of bodies of steel bits and heads are exposed to intensive abrasive, erosive, corrosive, cavitation, hydroabrasive and impact wear, resulting in the change of the initial shape and lowering of technico-economic characteristics of drill tools, that is why increase of service life of working elements of steel and matrix bodies of local and foreign drill bits and heads in an urgent task for Ukraine. Reconditioning, increasing the effectiveness of drill bit and head application and lowering the cost of development of problem fields, is an important reserve for extension of their service life.

Development of technological processes of drill tool repair is progressing, and at this moment the enterprises and companies in Ukraine and abroad offer different methods of reconditioning the worn working elements. In 2010–2012 studies of the degrees of wear and peculiarities of defects of diamond-insert cutters (DIC) of steel and matrix drill bits, applied in drilling of gas and oil wells in rocks, were performed under «Resours» Program. These studies were the basis to compile tables of DIC wear and defects in keeping with the classification of International Association of Drilling Contractors (IADC), depending on rock physico-mechanical characteristics [1], and develop the technology of repair of steel and matrix drill bits of different typesizes with DIC [2].

The objective of this work is evaluation of the peculiarities of watercourse damage as a result of anomalous wear of steel drill bit body with protective coatings and determination of its repairability criteria for subsequent reconditioning of the working element.

Objects of study are tools for rotation drilling method, namely drill bits and heads. Foreign drilling tools are mainly made of B25 and B35 hard alloys produced by Sandvik Coromat, Sweden (local analogs are VK6 and VK8 alloys) and are fitted with polycrystalline diamond cutters XT, HCR, HOT, SQC, GDC, etc., manufactured by leading world companies, such as Genesis, Smith Bits, Element Six. Drilling tool working elements are protected by surface coatings having high tribological properties under the conditions of hydropabrasive wear.

For reconditioning worn drill bits it was necessary to develop the technological procedure, including:

- drill bit wear analysis by IADC classification;
- defect list of worn drill bit working elements;
- machining of working element defective areas;
- special preparation of areas on damaged defective surfaces;
- process of restoration of initial shape of working elements of drill bit body by welding;
- process of restoration of working element protective coatings with preservation of initial drill bit dimensions.

Features of reconditioning drill bits with anomalous wear of working element are demonstrated in the case of repair of watercourse in steel drill bit of 215.9 mm diameter manufactured by Smith Bits, USA. Working elements of such a drill bit at rotation drilling of the well, being exposed to axial load at rock breaking up, move at different speed along bore hole bottom and are subjected to anomalous wear. In addition, removal of fracture products is performed by drilling water at high pressure (1500 MPa) that creates an additional risk of fracture of drill bit watercourses. Evaluation of drill bit condition after driving through 1000 m revealed significant damage of the opening of steel body watercourse with strengthening protective coating — tearing out of thread bushing made of VK8 alloy (Figure 1), to which the hard alloy nozzle was attached, and considerable distortion of watercourse shape. The cause for tearing out of the bushing with nozzle from drill bit body, in our opinion, was violation of technology of watercourse thread bushing manufacturing. Final evaluation of drill bit body by IADC classification was as follows: 3 7 LN N X (LN, NO) PR — «repairable».

During watercourse reconditioning studies were performed on selection of a material that would correspond to all the physico-chemical properties of drill bit body metal. To achieve this goal, preliminary work results were used to develop a new design of transition bushing with the respective thread from corrosion-resistant steel 08Kh18N10T and technology of restoration of damaged watercourse. Welding and surfacing were optimized on mock-up samples: steel 40Kh + protective wear-resistant coating; stainless steel 08Kh18N10T + protective wear-resistant coating; stainless steel 08Kh18N10T + steel 40Kh + deposited metal.

Nonconsumable-electrode manual argon-arc welding with 1 mm filler wire 12Kh18N10T was selected for experiments. One of the most effective technologies of drill bit reconditioning is the low-cost and technologically acceptable process of arc surfacing. Protective coating was deposited on mock-up samples with application of inverter system «Korall-300» and TeroCote 7888 T filler cord of 5 mm diameter with 1.2 mm core, manufactured by Castolin Eutectic. Surfacing was performed in optimum modes with the lowest heat input: I = 80–100 A, U = 10–12 V. Deposit thickness was 2–3 mm.

Metallographic examination of welded and surfaced samples was performed in optical microscope MIM-8M and scanning electron microscope Tescan Mira 3 LMU. Vickers microhardness of the deposited layer was determined in LECO hardness meter (0.01–2 kg load).

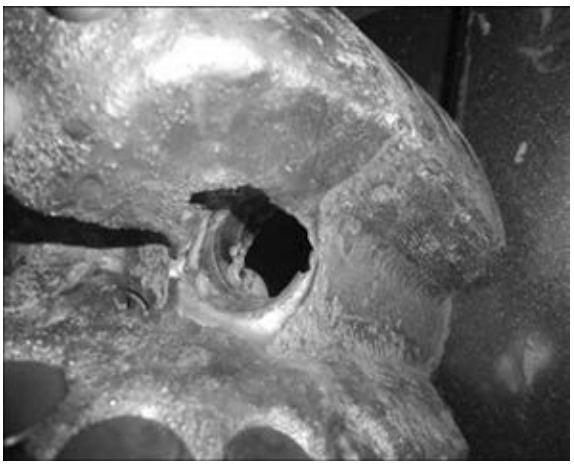

Figure 1. Appearance of wear of working element of steel body watercourse with strengthening protective coating

Microsections with wear-resistant coating TeroCote 7888 T, deposited on plates of steel 40Kh and stainless steel 08Kh18N10T, were used for investigations.

Product wear-resistance is affected by a number of parameters: composition, structural components, deposited metal hardness. For instance, hardness of protective coating surface layer is strongly affected by distribution of hard particles of tungsten carbide in the deposited layer volume. Naturally, functional effectiveness of the deposited coating will rise with increase of the amount of tungsten carbide of high microhardness. TeroCote 7888 T is a highly-effective wear-resistant material in the form of a flexible cord, which consists of nickel-chromium wire core, coated by an elastic binder, containing a mixture of irregular-shaped carbides and a powder-like nickel alloy. TeroCote 7888 T coating is extremely hard and consists of a dense mass of ultrahard tungsten carbide particles, integrated into a viscous nickel-chromium matrix.

TeroCote 7888 T coating, deposited on steel 40Kh, is characterized by cast heterogeneous structure (Figure 2, *a*). Rather coarse carbide particles of up to 500 μm length are concentrated in the deposit lower zone. Needle-like dispersed precipitates of the light phase based on tungsten, which contain chromium, iron and nickel, are revealed in the matrix of the deposit based on nickel (33.7 %), containing iron (26.80 %), tungsten (25.95 %) and other elements (Table 1).

Unlike lower zone structure, metal structure of the deposit upper zone does not contain any coarse carbides (Figure 2, *b*). Microhardness of the deposit upper zone is 4460–4830 MPa that is somewhat lower than that of the lower zone

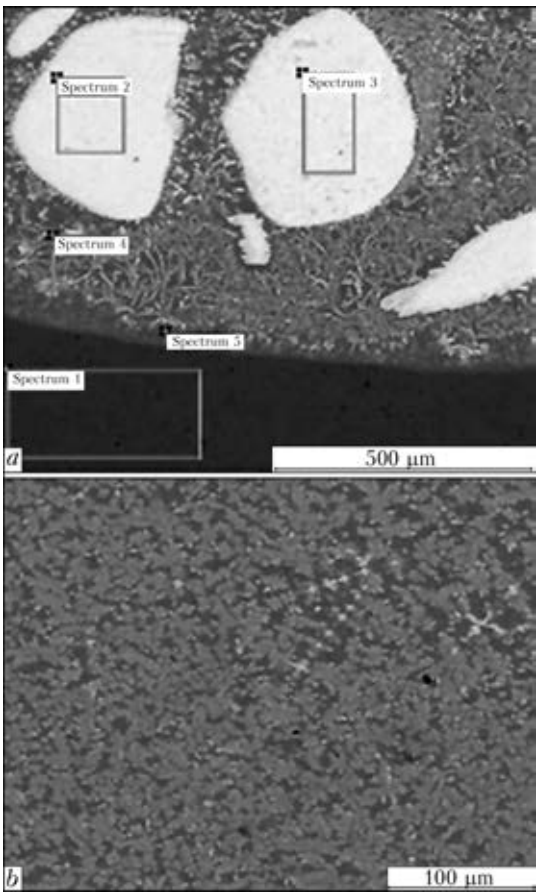

Figure 2. Microstructure of TeroCote 7888 T deposited metal on substrate of steel 40Kh (*a*) and its upper zone (*b*)

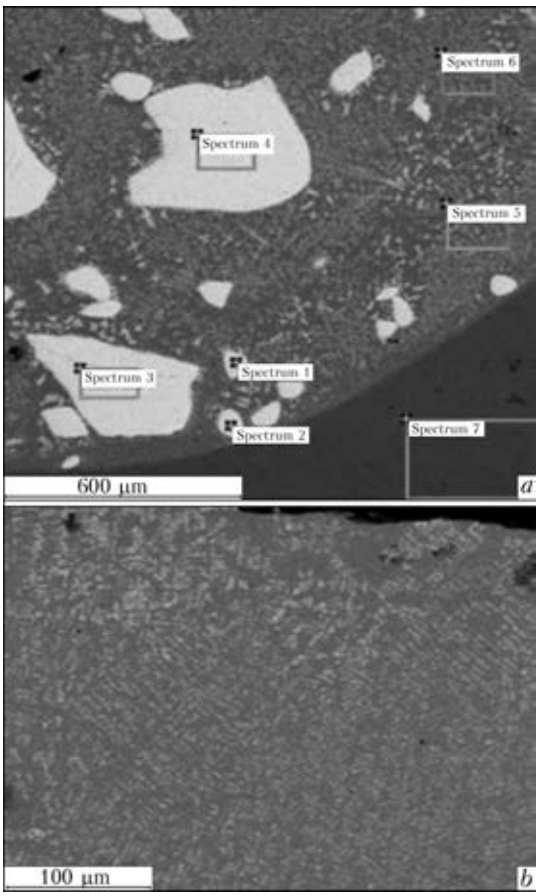

Figure 3. Microstructure of lower (*a*) and upper (*b*) zone of TeroCote 7888 T deposited metal on substrate of 08KN18N10T steel

Table 1. Composition of TeroCote 7888 T deposited metal on 40Kh steel substrate, wt.%

Spectrum number	C	O	Si	Cr	Mn	Fe	Ni	W
1	6.64	–	0.30	3.59	0.51	88.96	–	–
2	12.86	1.15	–	–	–	–	–	85.99
3	11.80	1.03	–	–	–	–	–	87.17
4	6.25	–	–	7.29	–	26.80	33.70	25.95
5	6.47	–	–	9.38	–	41.13	30.99	12.4

Table 2. Composition of TeroCote 7888 T deposited metal on 08Kh18N10T steel substrate, wt.%

Spectrum number	C	O	Si	Ti	Cr	Mn	Fe	Ni	W
1	12.02	0.79	–	–	–	–	–	–	87.18
2	12.31	–	–	–	–	–	–	–	87.69
3	12.18	–	–	–	–	–	–	–	87.82
4	12.72	1.33	–	–	–	–	–	–	85.95
5	6.96	–	–	–	13.91	–	23.25	35.72	20.17
6	6.65	–	–	–	15.25	–	24.01	34.86	19.23
7	5.42	–	0.53	0.37	24.13	0.70	54.35	14.51	–

Table 3. Composition of deposited metal in the joint of 08Kh18N10T + 40Kh + TeroCote 7888 T, wt.%

Spectrum number	C	Si	Cr	Mn	Fe	Ni	W
1	5.51	–	10.23	–	39.12	37.35	7.79
2	6.50	0.33	4.22	0.57	88.38	–	–
3	6.60	–	12.11	–	31.27	35.33	14.69
4	12.16	–	–	–	–	–	87.84
5	11.31	–	–	–	–	–	88.69

(4460–5420 MPa). Note that carbide phase microhardness is stable and is equal to 18540 MPa.

The metal of TeroCote 7888 T deposit on stainless steel 08Kh18N10T steel also contains coarse tungsten carbides in the lower zone (Figure 3, *a*, Table 2).

Metal of deposit upper zone contains less carbides, and in some sections they are completely absent (Figure 3, *b*). Microhardness of the deposit matrix in upper zone decreases to 3510–3760 MPa, and in lower zone — to 3360–4210 MPa.

Metallographic and X-ray microprobe studies of the joint of 08Kh18N10T steel + steel 40Kh + deposited metal showed that a joint of TeroCote 7888 T deposited material + steel 40Kh formed as a result of surfacing. Deposited metal microstructure consists of tungsten carbides and matrix based on nickel of a complex composition (Table 3). As is seen in the previous variants, tungsten carbides are contained predominantly in deposit lower zone (Figure 4, *a*) and are absent in its upper zone (Figure 4, *b*). Slight porosity is observed in all the deposits.

Obtained structure of deposited metal ensures high microhardness of the carbide phase and extremely effective protection from erosive and abrasive wear at drilling of medium and hard rocks. Applied method to improve wear resistance with TeroCote 7888 T filler cord allows a considerable (2–3 times) extension of service life of working elements of drill bit bodies, operating under the conditions of corrosive-abrasive wear.

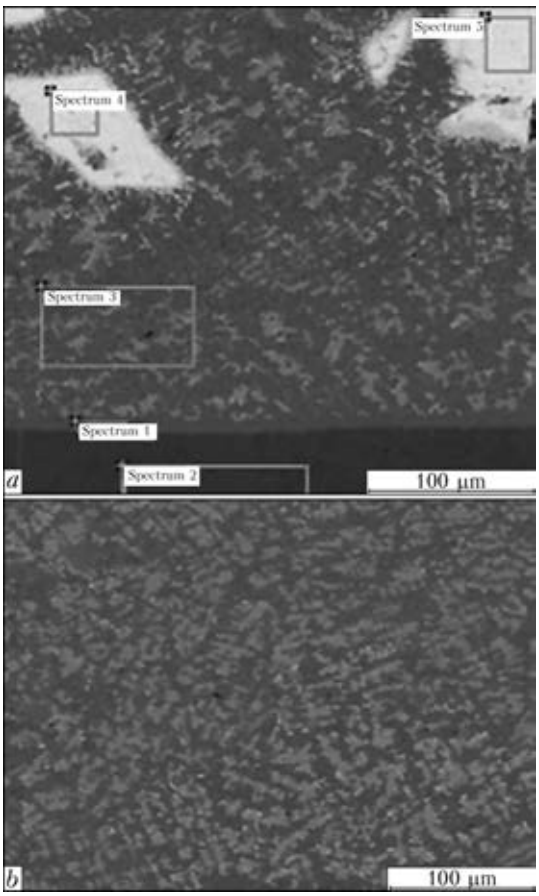

Figure 4. Microstructure of lower (*a*) and upper (*b*) zone of deposited metal in the joint of 08Kh18N10T + 40Kh + TeroCote 7888 T

Obtained results were used at reconditioning of watercourse working element on a worn body of integral steel diamond drill bit of 215.9 mm

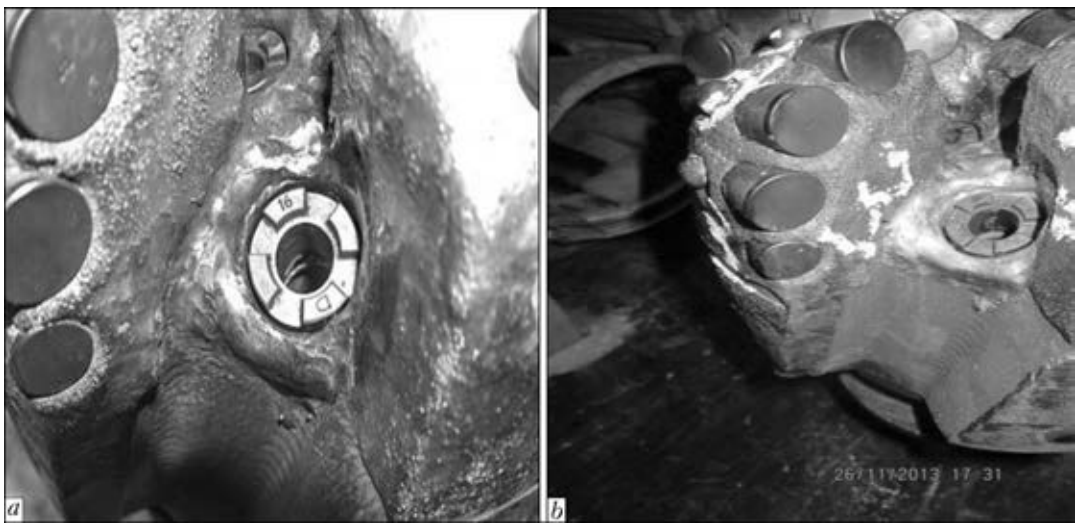

Figure 5. Appearance of reconditioned watercourse before (*a*) and after (*b*) testing

diameter. After machining the damaged opening of the watercourse a bushing from stainless steel 08Kh18N10T was manufactured and mounted in the body opening with the specified angle of inclination. To join the bushing to drill bit body, welding with small heat input was used in the optimum modes of I = 80–120 A, U = 10–12 V, in order to lower the residual stress level in the deposited layers. Welding was performed with 1 mm filler wire 12Kh18N10T. TeroCote 7888 T cord was used for deposition of the protective wear-resistant coating in the following mode: I = 100–120 A, U = 10–12 V.

Drilling of Runovshchina gas wells (Poltava region) was performed for trying out the reconditioned drill bit (Figure 5, *a*). Drill bit $8^{1/2''}$ SI519 BPX SD0502 was tested in well #101 in the ranges of 533–542, 549–734, 744–886 m and in well #110 in the range of 1890–2679 m (Figure 5, *b*). Drilling rigs TW-100 and Skytop Brewster N-75 A were applied for drilling wells #101 and 110, respectively. Drilling was performed at rig rotation speed of 60–90 rpm with 2–12 t force of drilling tool feed. Drilling water (specific weight of 1.12–1.16 g/cm^3, viscosity of 47 sec, pH 10–11.4, water flow rate of 20–25 l/s)) was applied for well flushing-out and drilling tool cooling. Drilling intervals are represented by siltstones, mudstones and abrasive sandstones with up to 120 MPa ultimate strength at uniaxial compression.

Test results were documented by the Act of commercial introduction of this drill bit. Overall driving of the drill bit after reconditioning was 1125 m. Developed reconditioning technology enabled extension of drill bit working life by 112.5 %; after trials the wear of working elements, fitted with DIC, was equal to 10–20 %, and that of reconditioned watercourse was 1–2 %, i.e. it next reconditioning will be possible.

Conclusions

1. Basic technology of reconditioning drill bit steel body corresponds to bit classification by IADC code (watercourse channel) for drilling tools in service.

2. Technology of protective coating deposition by surfacing can be also applied for reconditioning other defective sections of working elements of drill bit steel bodies with protective coatings for uninterrupted drilling.

3. Study results can be used in mining industry of Ukraine and other countries.

1. Khorunov, V.F., Stefaniv, B.E., Sabadash, O.M. et al. (2012) Peculiarities of wear and criteria of repairability of drill bits with diamond-hard-alloy cutters. *The Paton Welding J.*, **10**, 39–43.
2. Khorunov, V.F., Stefaniv, B.E., Sabadash, O.M. et al. (2012) Peculiarities of technologies for repair of drill bits with diamond-hard alloy cutters. In: *Problems of resource and service safety of structures, constructions and machines*, 488–493. Kiev: PWI.

Received 14.05.2014